DEVELOPMENT OF LANDSLIDE-DAM PREDICTION SYSTEM OVER A WIDE AREA CONSIDERING SLIP SHAPES OF EARTHQUAKE-INDUCED LANDSLIDES

范, 亚南

https://doi.org/10.15017/1456010

DEVELOPMENT OF LANDSLIDE DAM PREDICTION SYSTEM OVER A WIDE AREA CONSIDERING SLIP SHAPES OF EARTHQUAKE-INDUCED LANDSLIDES

Yanan Fan

DEVELOPMENT OF LANDSLIDE DAM PREDICTION SYSTEM OVER A WIDE AREA CONSIDERING SLIP SHAPES OF EARTHQUAKE-INDUCED LANDSLIDES

A Thesis Submitted

In Partial Fulfillment of the Requirements

For the Degree of

Doctor of Engineering

By

Yanan Fan

to the

DEPARTMENT OF CIVIL AND STRUCTURAL ENGINEERING

GRADUATE SCHOOL OF ENGINEERING

KYUSHU UNIVERSITY

Fukuoka, Japan

March, 2014

DEPARTMENT OF CIVIL AND STRUCTURAL ENGINEERING
GRADUATE SCHOOL OF ENGINEERING
KYUSHU UNIVERSITY
Fukuoka, Japan

CERTIFICATE

The undersigned hereby certify that they have read and recommended to the Graduate School of Engineering for the acceptance of this thesis entitled, ***"Development of Landslide dam Prediction System over A Wide Area Considering Slip Shapes of Earthquake-Induced Landslides"*** by **Yanan Fan** in partial fulfillment of the requirements for the degree of **Doctor of Engineering**.

Dated: March, 2014

Thesis Supervisor:

_____

Prof. Guangqi CHEN, Dr. Sci.

Examining Committee:

_____

Prof. Noriyuki YASUFUKU, Dr. Eng.

_____

Prof. Takayuki SHIMAOKA, Dr. Eng.

ABSTRACT

A strong earthquake can induce a large number of landslides, and an extensive landslide can create a Landslide dam when debris flows into and stops a river. The water impounded by a landslide dam can create a dam reservoir, which may raise the surrounding groundwater and cause back-flooding (upstream flooding). Because of its loose nature and absence of a controlled spillway, a landslide dam can easily fail catastrophically and lead to debris flows or downstream flooding. Many reports show that the earthquake-induced landslide disaster chain can cause very serious damage. For example, the 2008 Wenchuan Earthquake (Ms8.0) induced approximately 60,000 landslides and created 828 Landslide dams. More than one-third of the total loss (both property and life) from the earthquake damage was due to the disaster chain according to a related report. Moreover, a Landslide dam at Tangjiashan, which has a reservoir volume of 3.16×10^8, threatened more than 1.3 million people in the downstream area. Fortunately the catastrophe was avoided because the dam was detected early so that the countermeasure was taken timely. Therefore, it is important to focus attention on prediction of earthquake induced Landslide dams in order to break the earthquake-induced landslide disaster chain.

In order to realize the prediction of earthquake induced Landslide dams in a wide area, it is necessary to solve the following key issues: how to (1) identify the slope mesh effectively, (2) assess the slope stability accurately, (3) estimate the landslide volume, (4) analyse debris runout path and deposit distribution. There are very few systematic studies on these problems up to now. Therefore, this study aims to develop a prediction system of earthquake induced Landslide dams by (1) proposing a new approach for slope mesh identification; (2) developing a new landslide hazard mapping approach using a more accurate 2-D stability analysis method; (3) developing a new efficient landslide hazards mapping method using 3-D slope stability analysis; and (4) developing an earthquake induced Landslide dam hazard mapping approach based on the newly released ArcGIS technology.

The thesis consists of seven chapters.

Chapter 1 introduces a geo-disaster chain model from earthquake and gives a brief review of previous research on earthquake-induced disasters. It also describes the scope and objectives of the study.

Chapter 2 reviews the existing landslide hazard assessment methods and gives a summary of issues that remain unresolved, such as slope unit identification, 2-D and 3-D slope stability analysis considering failure slip shapes, and Landslide dam prone hazard mapping.

Chapter 3 proposes a new slope unit identification approach. First, the problems of the existing method are analysed. Then, a new approach is proposed to solve the problems by (1) developing a method to detect stream lines and catchment areas instead of detecting valley lines and ridge lines, which is the major reason of mis-identification in the existing method; (2) identifying slope units by cutting catchment areas with stream lines. Finally, the improvement of identification accuracy is shown by using the new approach.

Chapter 4 develops a new hazard mapping method based on the well-known 2-D limit equilibrium analysis with a circular slip mode. The existing hazard mapping method is based on an infinite plane slip model (IPSM) because it is easy to implement in GIS. However, since most failure slip surfaces are not planes, a circular slip mode (CSM) is more popular than IPSM in geotechnical engineering because of its high accuracy and ability to accommodate the complex geometry, stratum and groundwater data. Also, the volume of a landslide can be estimated from CSM, which is necessary in Landslide dam hazard mapping. The issue is that IPSM is not easily incorporated into GIS. Therefore, a new hazard mapping method is developed based on the well-known Swedish Method, a 2-D limit equilibrium analysis method with a CSM. First, a method for automatic extraction of a cross slope section is proposed based on the topography of each slope. Then, a GIS module for evaluating slope safety factors based on the Swedish Method is developed using C#. Finally, practical applications have been made and it has been shown that the accuracy of the slope stability analysis improves and the hazard mapping can be completed quickly and effectively.

Chapter 5 develops a hazard mapping method based on 3-D limit equilibrium analysis. In order to estimate the volume of a landslide, a 3-D slope stability analysis is necessary. A semi-ellipsoid slip model is used in general. The key issue is how to determine the ellipsoid parameters to obtain the minimum slope safety factor. The existing 3-D method applies Monte Carlo simulation to determine the parameters. Because running the 3-D limit equilibrium analysis with Monte Carlo simulation to achieve an acceptable minimum safety factor is extremely time-consuming, the existing method is unadaptable in hazard mapping. Therefore, a new method for determining the parameters of an ellipsoid is proposed based on the 2-D limit equilibrium analysis with the Swedish method. The circular slip determined in 2-D analysis is used to estimate the lengths of two axes of a tri-axial ellipsoid; the other axial length is estimated directly from the slope shape. The GIS module of the 3-D limit equilibrium analysis is developed using the new approach of determining ellipsoid parameters. Practical applications show that the new hazard mapping method based on the new approach for 3-D limit equilibrium analysis can greatly reduce the processing time.

Chapter 6 develops a prediction system of earthquake induced Landslide dams for Landslide dam hazard mapping based on GIS. To date, there have been few studies on Landslide dam hazard mapping, although it is important for breaking the disaster chain. The new approach of Landslide dam hazard mapping includes: (1) identifying the slope units; (2) extracting possible Landslide dam prone slopes (LDPS) using the river buffer filter; (3) excluding impossible LDPS using the aspect filter to exclude slopes that cannot reach a river based on their aspects towards the river; (4) excluding impossible LDPS using the blockage filter, by which a slope that could not reach the river is excluded based on the blockage height along its way to the river; (5) excluding impossible LDPS using the stability filter to exclude stable slopes based on slope stability analysis; (6) excluding impossible LDPS using the volume filter to exclude slopes with a small volume of slide mass. In addition, DDA, a numerical simulation method, is adopted to verify the potential LDPS after filtering. Because we can obtain the run out distance, distribution and volume of debris from the DDA simulation, Landslide dam

formation can be deduced based on river geometry and hydrology data together with the volume of the slide body. The effectiveness of the countermeasure using preventive structures can also be verified by DDA simulation.

Chapter 7 summarizes the results and conclusions of the study. Also, problems are highlighted for future studies.

ACKNOWLEDGEMENTS

I owe a debt of gratitude to many people when the dissertation is finished, and I would like to mention a few of them by name. Without their encouragement, patience, effort and good guidance, this study could have never been finished.

First and foremost, I express my sincere gratitude to my supervisor, Prof. Dr. Guangqi Chen. He is not only strict in study and has a wide range of knowledge, but also integrate and modest. I benefit a lot from each conversation with him and I learned how to behave myself as well as pursing my study and career. Prof. Chen provides me the best scientific research environment, sufficient research data and favorable study atmosphere while I pursuing my PhD in Kyushu University. He provided me many chance to take part in international conferences and field practices, which make me more confident in facing challenges in my later life and work. He not only teaches me professional knowledge, but also scientific thinking mode and basic skills required in doing research. Without his valuable and timely comments, it would be very difficult for me to complete this dissertation.

I would like to express gratefully acknowledgement to Prof. Dr. Kouki Zen for his valuable suggestions on my research. I also deeply appreciate Assoc. Prof. Kiyonobu Kasama, who is so kindly and easy to going that more like a friend. Also, great thanks to Staff Yuichi Yahiro for his enthusiastic and help.

I would like to express my sincerely gratitude to members of my dissertation committee, Prof. Dr. Guangqi Chen, Prof. Dr. Noriyuki Yasufuku and Prof. Dr. Takayuki Shimaoka for their treasure time in review evaluation and valuable comments on my thesis.

I am deeply indebted to Prof. Dr. Guoyun Zhou, my former supervisor in Nishinippon Institute of Technology for recommending me to Prof. Dr. Guangqi Chen. I could not have done this research without his great support.

I would like to express my heartfelt thanks to Prof. Dr. Chuan Tang for his great help and guidance. He provided me precious imagery which helped a lot for my research on Wenchuan earthquake.

I would like to thank all the students whom I have been studying with in Geo-disaster Prevention Laboratory where I really enjoy my studying life in Fukuoka. The special thanks to Postdoctoral Lu Zheng, who gave me valuable idea in my research and taught me DDA simulation. His patience, smartness and kindness contribute too much for my work. Thank my research partner Li Yange, who assisted me in research and helped me a lot in life. There are also special thanks to Mr. Yingbin Zhang, who gave me useful suggestions in thesis writing. Thank all of other friends who always support me and I am proud of to be their elder sister.

Finally, needless to say, I am grateful to my parents who are always confident in my success and support my decisions. I would like to extend my sincerely thanks to all my friends in China, Japan and some other countries. They are always helping, caring about me and encouraging me to keep on this thorny but enjoyable journey.

TABLE OF CONTENTS

TABLE OF FIGURES

TABLE OF TABLES

CHAPTER 1

INTRODUCTION

1.1 THE GEO-DISASTER CHAIN INITIATED FROM EARTHQUAKE

One kind of natural hazard may induce other hazards, which is the so-called "domino or chain effect". For example, a strong earthquake can induce a large number of landslides, and an extensive landslide can create a landslide dam when debris flows into and stops a river. The water impounded by a landslide dam can create a dam reservoir, which may raise the surrounding groundwater and cause back-flooding (i.e., upstream flooding). Because of its loose nature and the absence of a controlled spillway, a landslide dam can easily fail and lead to catastrophic debris flows or downstream flooding. Because these secondary disasters occur in a disaster chain, i.e., "disaster triggering disaster", they can be expressed by a model of a geo-disaster chain initiated by the earthquake (Fig 1.1).

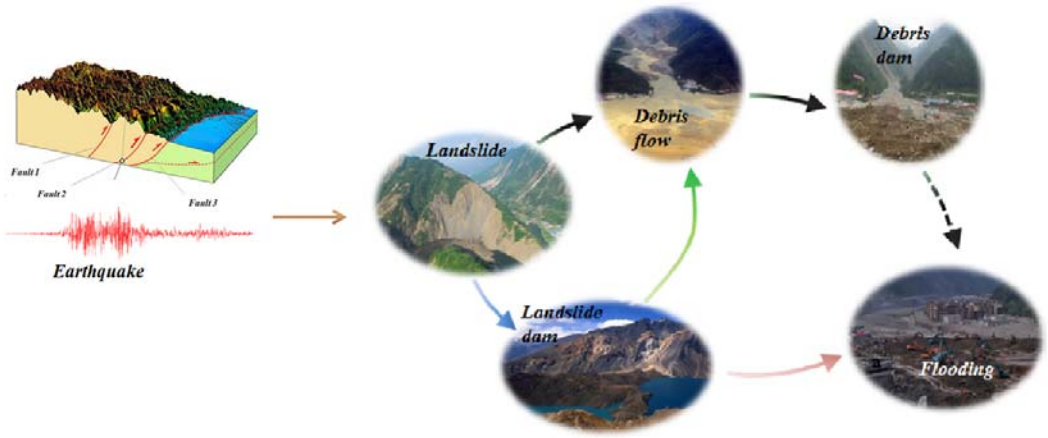

Fig 1.1. The disaster chain model induced by an earthquake (Chen et al., 2011)

The events in a geo-disaster chain consist of an earthquake, landslide, landslide dam, debris flow, debris dam and flood. The relations between each event can be described as follows: 1) a strong earthquake can induce a large number of landslides. These landslides contribute to the accumulation of sediment on a hill slope or in channels (brown arrow); 2) a landslide can create a landslide dam when its debris fills and stops a river (blue arrow); 3) by raising the water level of the impounded lake, a landslide dam can form upstream-flooding (pink arrow); 4) when the water masses of landslide-impounded lakes is catastrophically released, a landslide dam can easily collapse and lead to debris flow or downstream flooding (green arrow); 5) finally, since the landslide debris settles in valleys or ravines when a heavy rainfall occurs, the debris easily transforms to debris flow when it moves down the slope (black arrow) (Chen et al., 2011).

Many reports have shown that the geo-disaster chain initiated from an earthquake can cause very serious damage to both life and property for a long period of time. For example, the 2008 Wenchuan earthquake (Ms8.0) induced approximately 60,000 landslides and created 828 landslide dams. According to a related report, more than one-third of the total loss (in both property and life) from the earthquake damage was caused by the disaster chain. Therefore, it is necessary to understand the occurrence, development, and transformation of hazard chains

and comprehend their mechanism in order to predict secondary hazards (Keefer, 1984; Chen et al., 2011). Effective actions taken to reduce potential losses can break a disaster chain before it expands and transforms.

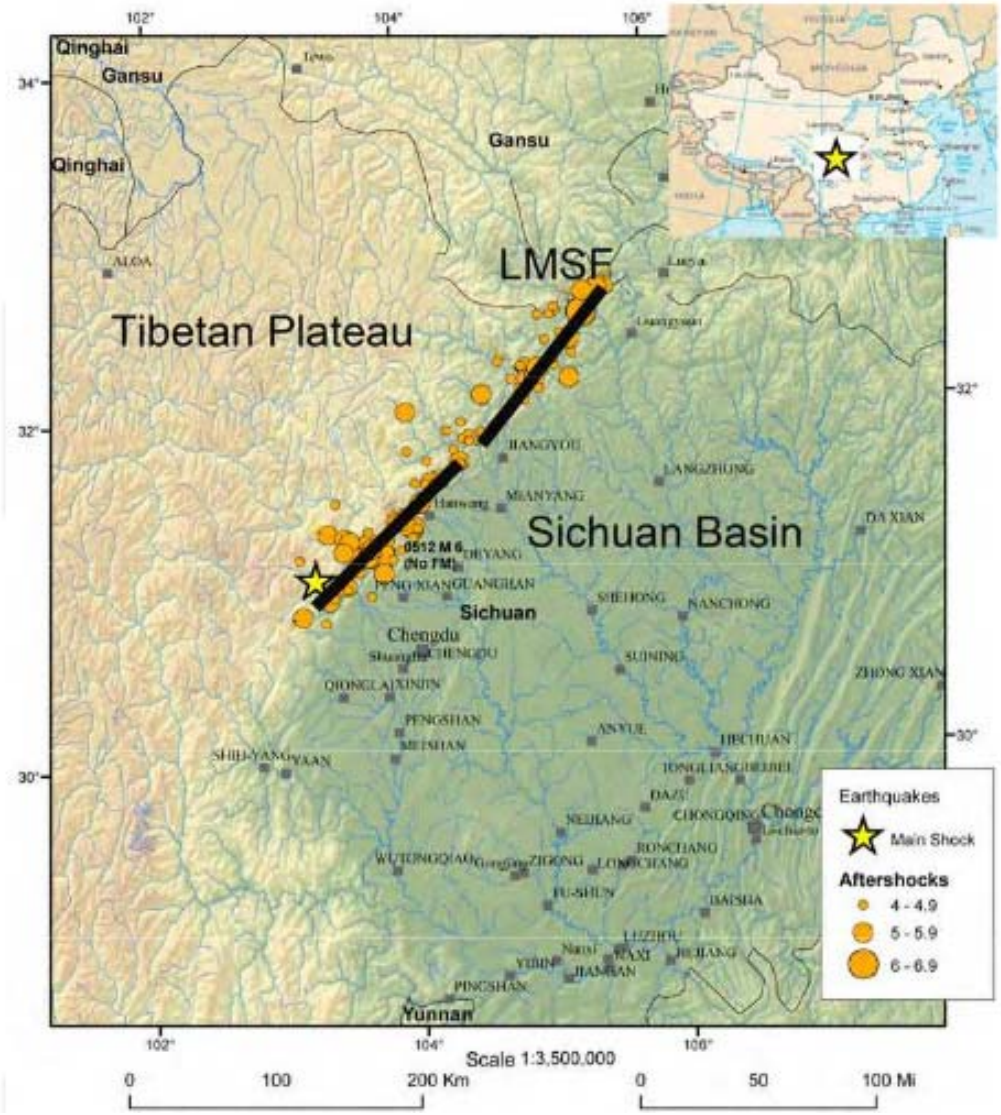

Fig 1.2. The 2008 Wenchuan earthquake, LMSF and aftershocks (modified from United States Geological Survey [USGS], 2008)

Although many geomorphologists have found that earthquake-induced landslides can affect sediment discharge over a long term (Keefer, 1994, 2002; Dadson et al., 2004), most research has concerned earthquake-induced secondary disasters, such as predicting dam-break flooding or debris flow, and has evaluated

the long-term effects of landslide dams on landscape evolution, sediment flux and channel morphology. No study has systematically analyzed the effects of and relations between each event in an earthquake-induced geo-hazard chain.

1.2 SECONDARY GEO-DISASTERS INDUCED BY STRONG EARTHQUAKES

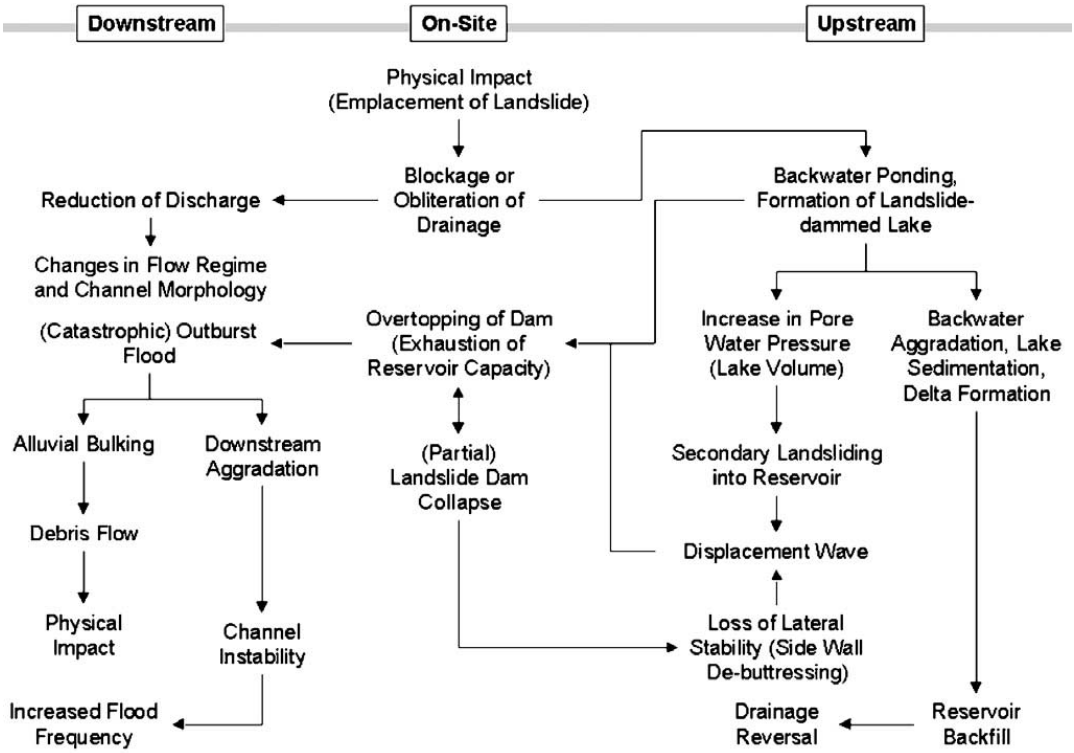

Fig 1.3. Sequential path model of geomorphic processes and hazards associated with the formation and failure of landslide dams (Korup, 2002)

Note: Scale limitations for downstream reaches may range between 10^{-1} and 10^{3} km.

As mentioned above, a strong earthquake can not only cause direct damage to construction, but also lead indirectly to a serious of secondary disasters, which makes research more complex and difficult. A sequential path model of geomorphic processes and hazards associated with the formation and failure of landslide dams was described by Korup (2002) (Fig 1.3). The impact of landslides and landslide dams on fluvial systems was subdivided into on-site and off-site (i.e., upstream

inundation and downstream outburst flooding) components. On-site hazards are the formation of displacement waves caused by secondary landslides into the natural reservoir.

In contrast to conventional landslide/landslide dam hazard assessments, the potential for secondary offsite effects need to be accounted for, particularly the geo-hazard chain effect. Some relative disasters are described as follows:

1.2.1 LANDSLIDE

Fig 1.4. The Beichuan landslides in the 2008 Wenchuang earthquake (Tang, 2011)

When slope-forming materials begin a downward and outward movement, the disaster called a landslide occurs. According the *Glossary of Geology*, The slide materials can be rock, soil, artificial fill, or a combination of these, and they move by a wide variety of processes, including flowing, sliding, toppling, falling or a combination of two or more types of movements (Jackson, 1997; Varnes, 1974; Hutchinson, 1988; WP/WLI, 1990; Cruden and Varnes, 1996; Highland and

Bobrowsky, 2008; Gokceoglu and Sezer, 2009). Landslides can be induced by intense or prolonged rainfall, strong earthquakes, rapid snow melting, or a variety of human activities (Guzzetti, 2006).

Within an earthquake induced disaster chain, a large number of landslides can be induced and cause serious property damage and human casualties. The rapid downward slide mass in the landslide can destroy homes and other structures, block roads, destroy utilities, and block rivers and streams. This phenomenon was first recorded in ancient China in 1789 BCE and in ancient Greece, 2373 years ago (Keefer, 2002). In the last few decades, serious damage caused by earthquake-induced landslides has been reported. For example, 9,272 landslides were induced by the 1999 Chi-Chi earthquake (Ms. 7.6), which caused 2,400 deaths, more than 8000 casualties and over US$10 billion in property losses in Taiwan (Chang et al., 2005); 30% of the total fatalities (officially 87,350) were victims of co-seismic landslides caused by the Kashmiri earthquake (Ms 7.6) (Harp and Crone, 2006; Schneider, 2009). In China, more than 60,000 landslides were induced by the 2008 Wenchuan Earthquake and resulted in more than 50,000 fatalities (Yin, 2009). Fig 1.4 shows a picture taken after the Wenchuan earthquake. As many as 907 children and teachers died in the Beichuan Middle School landslide, and about 1600 people died in the Wangjiayan landslide.

According to US Geological Survey's (USGS) Prompt Assessment of Global Earthquakes for Response (PAGER) system, 18,807 earthquakes occurred from September 1968 to June 2008 (magnitude 5.5 or greater in active tectonic regions and magnitude 4.5 in stable continental regions); 749 events caused fatalities, and 161 events (21.5%) other than earthquake shaking, such as landslides, caused fatalities. Table 1.1 provides data regarding the earthquakes responsible for triggering landslides (Rodríguez et al., 1999).

Table 1.1. Earthquakes responsible for triggering landslides (modified from Rodríguez et al., 1999)

Earthquake	Country	Date	Magnitude		Focal depth	Maximum intensity	Area affected by landslides	Number of slides
		Day/month/year	Ms	Mw	km	MMI	km^2	
Coalinga	USA	02 05 1983	6.7	6.2	7	VIII	650	>10,000
San Salvador	El Salvador	10 10 1986	5.4	5.7	12	VIII	380	1,000-10,000
Spitak	Armenia	07 12 1988	6.8	6.7	5	IV	2200	1,000-10,000
Loma Prieta	USA	17 10 1989	7.1	6.9	8	VIII	14000	1,000-10,000
Manjil	Iran	20 06 1990	7.3	7.4	19	X	1000	100-1,000
Luzon	Philippines	16 07 1990	7.8	7.7	25	VIII	3000	100-1,000
Valle de la Estrella	Costa Rica	22 04 1991	7.6	7.5	21.5	IX	2000	1,000-10,000
Northridge	USA	17 01 1994	6.8	6.7	18	IX	10000	>10,000
Paez	Colombia	06 06 1994	6.6	6.8	12	X	250	1,000-10,000
Hyogu-Ken Nanbu	Japan	17 01 1995	6.8	6.9	22	X	910	100-1,000
Chi-chi	Taiwan, China	21 09 1999	7.3	7.6	8	XI	10000	≈10000
Wenchuan	China	12 05 2008	8.0	7.9	19	XII	>50000	>60,000

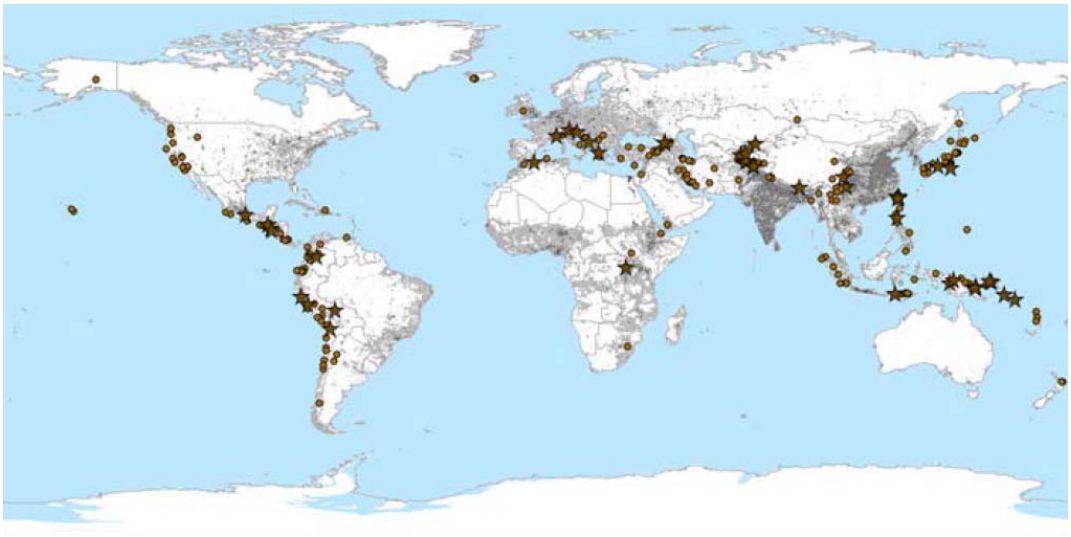

Fig 1.5. Epicenters of earthquake-induced landslides from September 1968 to June 2008 (from Marano et al., 2010)

Therefore, it is very important to assess and mitigate the effects of potential earthquake chain disasters caused by landslides. In recent years, the assessment of landslide hazards and the mitigation of potential landslide disasters have drawn the increasing attention of both geoscientists and engineering professionals, as well as communities and their local administrations in many parts of the world. Fig. 1.5 illustrates the epicenters of earthquakes-induced landslides. The circles represent landslide flags; stars represent deaths caused by earthquake-induced landslides. The figure clearly shows that high-hazard areas are concentrated in tectonically active mountain regions with large topographic relief, such as the Alps, Andes and Himalayas. Consequently, many countries and regions are susceptible to earthquake-induced landslides, such as Mexico, France, Italy, Greece, Georgia, India, China, Japan, Philippines and so on.

Using aerial photographs and field verifications, landslides induced by earthquakes have been mapped and analyzed in California, El Salvador, Taiwan, Japan, Italy and Pakistan (e.g., Wilson and Keefer, 1985; Harp and Keefer, 1990; Harp and Jibson, 1996; Jibson et al., 2000; Parise and Jibson, 2000; Capolongo et al., 2002; Wang et al., 2002, 2003; Chigira et al., 2003; Chigira and Yagi, 2006; Wang et al., 2007; Owen et al., 2008).

1.2.2 LANDSLIDE DAM

Landslide dams can arise in a wide range of geological and geomorphological settings, from high alpine debris avalanches to quick-clay failures in wide valley floors (e.g., Costa and Schuster, 1988; Shang et al., 2003; Kallen et al., 2006; Korup, 2004; Evans et al., 2011). A large number of upstream floods is caused by levels rising in landslide-impounded lakes, as well as by outburst floods and debris flows caused by the catastrophic failure of landslide dams (Mason, 1929; Cenderelli, 2000; Dai et al., 2005). The 27 largest floods during the Quaternary Period, with discharges greater than 100,000 m3/s, were listed by O'Connor and Costa (2004), most of which were caused by breaches of glacier or landslide dams.

In recent years, an increasing number of landslide dams caused by co-seismic landslides has been reported. For example, 828 landslide dams were identified at the Wenchuan earthquake, China (Ms8.0, 2008) (Xu Q et al., 2009; Fan X et al., 2012). There were also landslide dams during the ChiChi earthquake in Taiwan (M7.6, 1999) (Tsuchiya, 2008), the Niigataken Chuetsu-oki earthquake in Japan (M6.8, 2004) (Toyota, 2005), the Hindukush earthquake in Pakistan (M7.6, 2005) (Marui et al., 2005) and the Iwate-Miyagi Nairiku earthquake in Japan (M7.2, 2008) (Uchida et al., 2009).

Fig 1.6 shows a satellite photo taken after Wenchuan earthquake, in which the Donghekou, Shibangou and Hongshihe landslides were catastrophic and responsible for the loss of many lives in Qingchuan County. These three landslides have entombed an estimated 300 families. In particular, the Donghekou landslide dam blocked both the Hongshi River and the Qingzhu River. It was a typical rapid, long run-out compound rockslide with a height difference of 700 m between the toe and main scarp, a sliding distance of 2400 m, and a volume of 10 million m^3. Fig 1.7 shows views from the source area towards the toe of the slide.

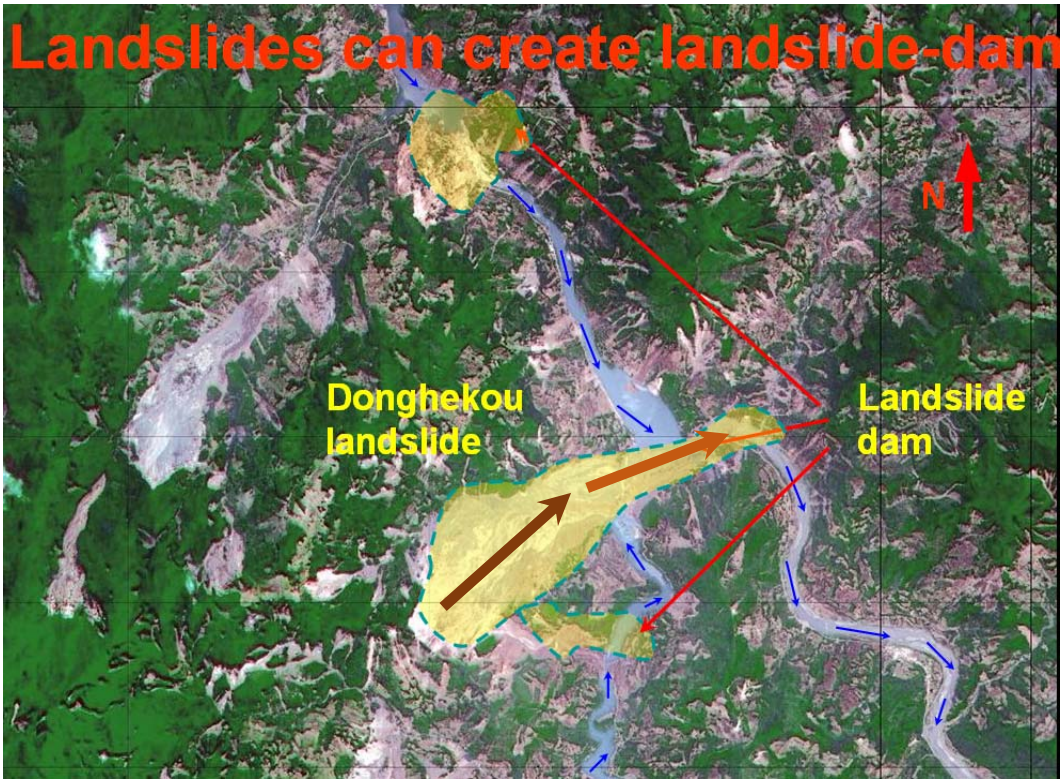

Fig 1.6. Aerial photograph taken on May 18, 2008 shows the location of large landslide dams in the south of Qingchuan County (Tang et al., 2009)

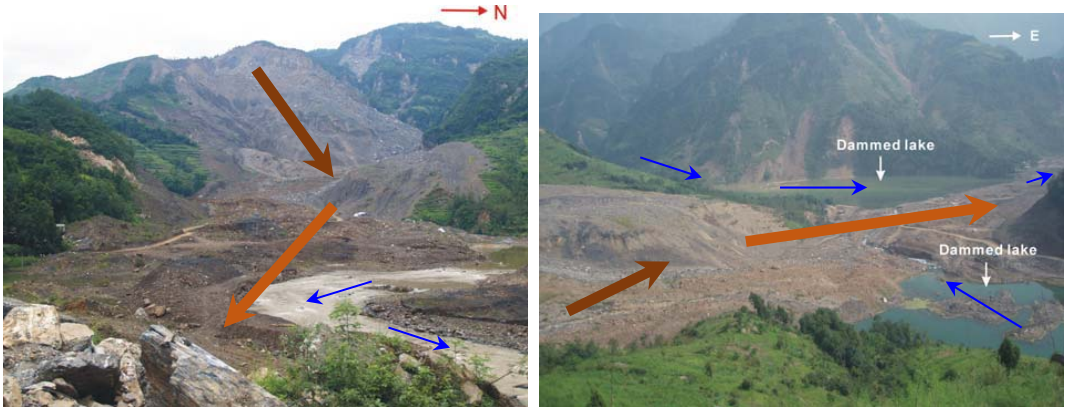

Fig 1.7. Features of Donghekou landslide dam (Sun et al., 2001; Li et al., 2001)

Earthquake-induced landslide dams are a multi-hazard, involving several cascading phenomena. The geo-disaster chain may initiate from an earthquake to coseismal landslides and landslide dams and end with dam-break flooding. It is necessary to analyze the probability of each event in this chain over an enormous

area affected by an earthquake.

Fan (2012) identified 828 landslide dams triggered by the 2008 Wenchuan earthquake in China, which constituted ~1.4% of more than 60,000 coseismal slope failures mapped to this event. While 501 landslides completely blocked the rivers, the rest caused only partial damming or channel changing. Significantly, 32 major lakes in peril, scattered over the disaster area, were identified as posing great threats to the villages and towns.

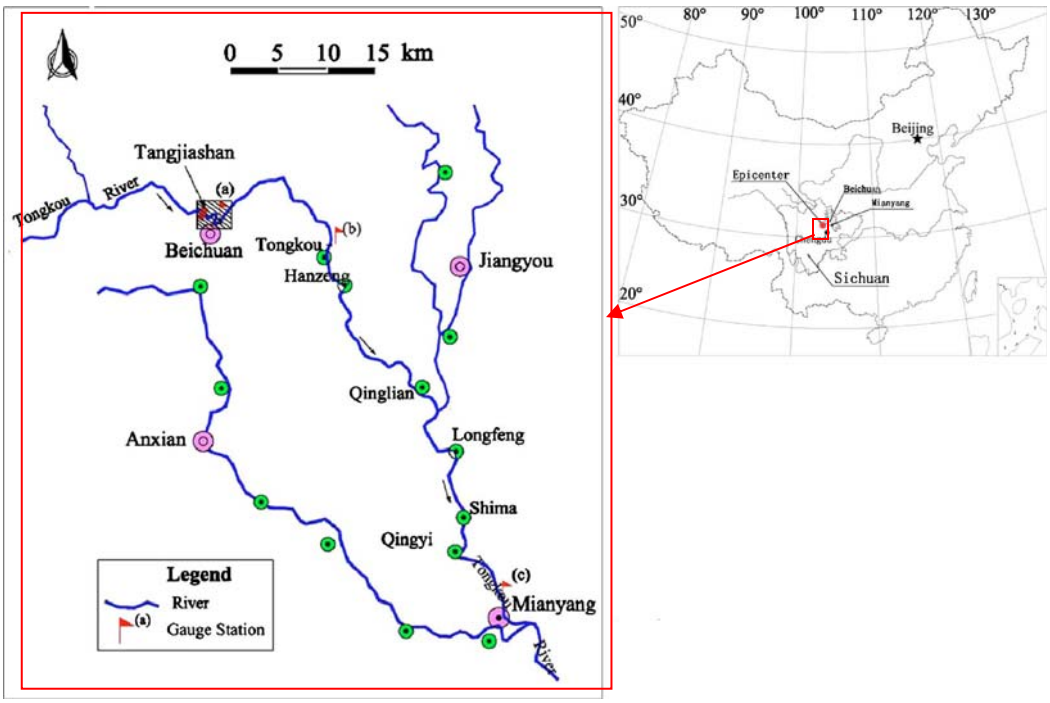

Fig 1.8. Location of Tangjianshan landslide dam and downstream cities and towns threatened by out-bursting (Liu et al., 2010)

Moreover, the debris and upstream flooding caused by a landslide dam at Tangjiashan, which has a reservoir volume of 3.16×10^8 m^3, had the potential to cause several villages to vanish (Fig 1.10). More than 1.3 million people in the downstream cities and towns could be threatened by out-bursting (Fig 1.8). Fortunately, catastrophe was avoided because the dam was detected early and the countermeasures were taken in time (Fig 1.9). Soldiers used digging equipment, explosives, and even missiles to blast channels in the dam in the attempt to relieve

the pressure behind it. Therefore, it is important to focus on the prediction of earthquake-induced landslide dams in order to break the earthquake-induced landslide disaster chain.

Fig 1.9. The Tangjiashan landslide dam and its discharge channel (Tang et al., 2009; Liu et al., 2010; Chen et al., 2011.)

In order to analyze and understand the characteristics, causes, failure mechanisms and effects of landslide dams, some essential landslide dam inventories were collected (Table 1.2), such as the bibliography of 463 landslide dams compiled by Costa and Schuster (1991). Recent research has attempted to establish global and nationwide databases of landslide dams and has made progress in predictive, quantitative and GIS-based modelling (Korup, 2002)

Fig 1.10. Villages vanished by the debris and upstream of Tangjiashan landslide dam (From http://wlypx.blog.sohu.com/88852315.html)

To date, because of the scarcity of direct observational evidence, few studies have focused specifically on landslide dams caused by coseismal landslides (Adams, 1981; Pearce and Watson, 1986; Hancox et al., 1997). Consequently, numerous studies on landslide dams have been conducted in past decades, but most were descriptive and their results were uncertainties. No previous study has systematically analyzed the chain effect initiated by an earthquake, the formation mechanism, or forecasting and hazard mapping of a landslide dam.

Table 1.2. List of the existing landslide dam databases (Fan, 2012)

Region	Number	Description	Reference
Worldwide	463	Including some well-documented cases mainly from the European Alps, North America, China and Japan	Costa and Schuster (1991)
Canadian Cordillera	38	Including 16 existing and 22 historical landslide dams	Clague and Evans (1994)
Northern Apennines	68	Including the characteristics of 68 landslide dams in the northern Apennines	Casagli and Ermini (1999)
New Zealand	38	Including 24 earthquake-induced landslide dams, while the triggering factor of the other 14 is uncertain	Adams (1981)
New Zealand	232	Including detailed dam geomorphometric variables	Korup (2004)
Japan	79	43 of 79 cases have complete records of 16 geomorphic variables	Swanson et al. (1986); Tabata et al. (2002)
China	147	Including the information of the location, formation time, longevity, triggering factor of landslide dams	Chai et al. (1995)

1.3 COUNTERMEASURES TO CUT THE GEO-DISASTER CHAIN

The objective of this study is to determine how to predict the chain disaster of landslide dam and break the next link as early as possible. Because every disaster linked in a geo-disaster chain can cause great damage to both life and property, it is necessary and important to take some measures to disclose the chain in order to prevent disasters or mitigate their effects.

Various approaches to measuring geo-disaster chains are possible, including both “hard” measures (i.e., structural aspects, such as physical infrastructure, equipment, facilities, etc.) and soft measures (i.e., non-structural, non-physical, institutional, operational aspects, etc.). Hard measures use engineering methods to reinforce the geological body, such as retaining walls or anti-sliding piles, to reinforce landslides. Although hard measures are very effective in mitigating disasters, manpower and financial power are limited, and it is impossible to process all disasters in the near future. Thus, the best countermeasures also use soft measures, such as governmental or non-governmental policies, hazard or risk maps, and warning systems.

1.3.1 HAZARD MAP

Regarding earthquake-induced landslides and landslide dams, the most important thing to know is the location of potential slopes, so that hard measures can be carried according to priority, and an emergency response plan can be established and implemented in a controlled fashion. In addition, rescue measures, such as rescue teams, can easily and quickly perform search and rescue operations according to the scale of the landslide. Therefore, hazard mapping and numerical simulation are key issues in preventive measures against earthquake-induced geo-disaster chains in different periods.

A landslide hazard (Varnes, 1984) is defined as “the probability of occurrence within a specified period of time and within a given area of a potentially damaging phenomenon”, which includes the geographical location (where) and the recurrence between events (when) of the landslide. Thus, it is necessary to assess landslide hazards in terms of temporal probability and spatial probability (susceptibility). Although landslide hazard models have been developed to assess landslide susceptibility, they only estimate “where” landslides are expected because in many cases, the temporal factor is difficult to determine. Therefore, a landslide hazard analysis often corresponds to a landslide susceptibility assessment, which determines the degree to which the territory is prone to landslides, according to physical attributes of the terrain.

The process of landslide susceptibility assessment aims at establishing the likelihood that a landslide will occur in a given area, based on factors in the physical terrain. It is an important tool in the land-use planning and special development activity within a given area, which are based on past landslides, geology, topography, hydrology and other pertinent data (Soeters and van Westen, 1996).

1.3.2 GIS IN GEO-DISASTER CHAIN ASSESSMENT

The geographic information system (GIS) is a computer system designed to capture, store, check, and display data related to positions on the Earth's surface. In other words, GIS is a database system with specific capabilities for spatial reference

data, as well as a set of operations for working with data (Star and Estes 1990). Hence, GIS may be thought of as a combination of computer-aided design (CAD), databases, and several spatial analyses. Thus, GIS has functional capabilities for data capture, input, manipulation, transformation, visualization, doubt, analysis, model and output.

In order to mitigate earthquake induced geo-disasters, the assessment needs to evaluate the relationships between various terrain conditions and hazard occurrences. GIS allows the storage and manipulation of information concerning the different terrain factors in distinct data layers and provides many spatial analyses that are effective in landslide analysis. Thus, it is an excellent tool for mapping geo-disasters.

The process of using GIS to analysis landslide hazard involves data preparation and the development of a professional model. The first step in every assessment consists of collecting all available information and data on the study area. The existing functions of GIS are then assembled and specific modules are expanded within GIS, based on the characteristics of the abstracted object.

Recently, a large number of researches have used GIS to analyze landslide hazards. These applications can be either statistical (Ayalew and Yamagishi, 2005; Dai and Lee, 2002) or deterministic (Safaei et al., 2011; Van Westen and Terlien, 1996; Xie et al., 2003). Because GIS enables a more complex analysis of multiple data than can normally be achieved using conventional techniques, it could be used to incorporate a sophisticated engineering model into its system (Qiu, 2007).

1.4 SCOPE AND OBJECTIVES

Hazard mapping is the first and also very important step for predicting landslide and landslide dam since it shows the location, possibility and dangerousness of potential landslides and landslide dams. However, there are very few studies on landslide dam hazard mapping method although several mapping methods have been developed for landslide. In addition, there are following issues unresolved in the existed landslide hazard mapping methods:

(1) How to identify slope mesh with sensed division;

(2) How to apply a higher accurate and effective stability analysis method;

(3) How to estimate the landslide volume;

(4) How to analyze debris runout path and deposit distribution and judge if the river can be blocked.

For these reasons, this study aims at solving the above mentioned problems, and the objectives of this study are as follows:

(1) To propose a new approach for slope mesh identification;

(2) To develop a new landslide hazard mapping approach by using a higher accurate 2-D stability analysis method;

(3) To develop a new efficient landslide hazards mapping method using 3-D slope stability analysis;

(4) To develop a practical hazard mapping method for earthquake induced Landslide dam; and

(5) To verify Landslide dam prone area using DDA simulation.

The organization can be summarized as follows: 1) the new approach of slope mesh identification provides a suitable division of slopes for stability analysis; 2) the new landslide hazard mapping approach using 2-D stability analysis method offers the scale information with accurate safety factors; 3) another new approach using 3-D stability analysis determines the shape of an ellipsoid slide body based on 2-D analysis results and gives a prediction of slide volumes; 4) landslide dam hazard map is produced according to the derived safety factors and slide volumes, together with topography data and river conditions. In addition, discontinuous deformation analysis (DDA), a numerical simulation method, is applied to verify the final results.

The flowchart of scope and objectives are shown in Fig. 1.11.

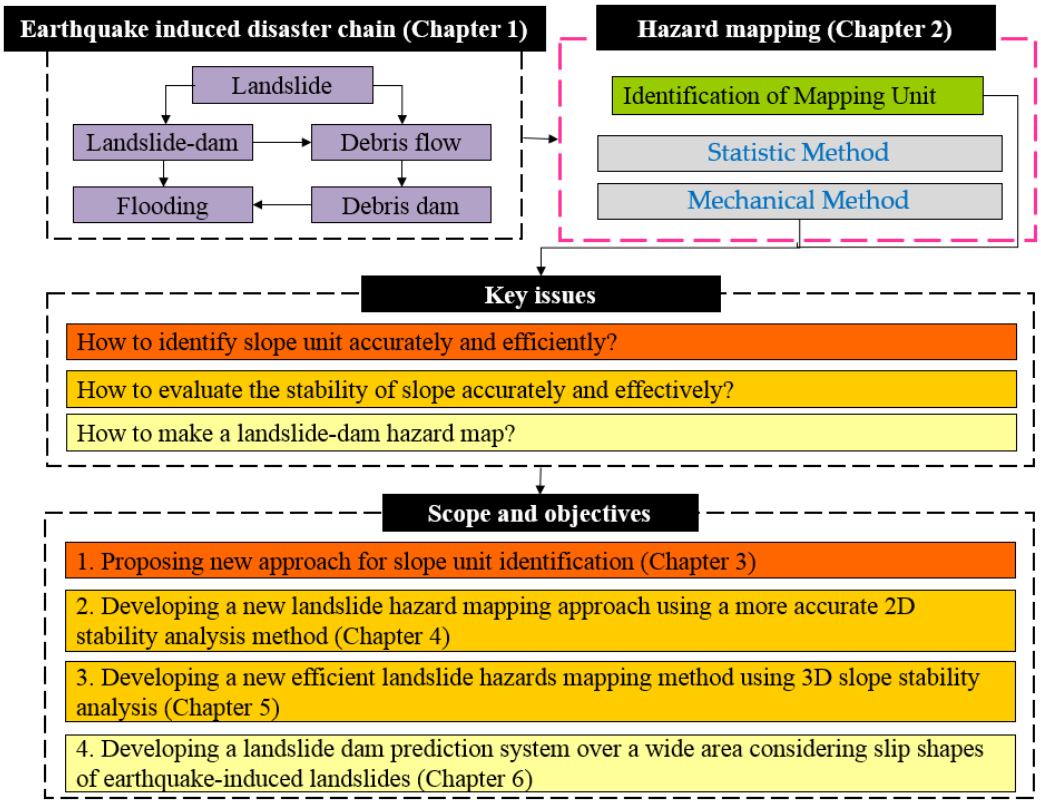

Fig 1.11. Scope and objectives of the dissertation

Based on the results, a hazard system is established for the assessment of landslides and landslide dams, based on the newly released ArcGIS technology.

1.5 THESIS ORGANIZATION

This thesis consists of seven chapters.

Chapter 1 introduces a geo-disaster chain model from earthquake-induced landslides and gives a brief review of researches on earthquake-induced disasters up to now. It also describes the scope and objectives of this study.

Chapter 2 reviews the existed landslide hazard assessment methods and gives a summary of issues that remain unresolved, such as: (1) how to identify slope unit accurately and efficiently; (2) how to assess slope stability with more commonly adaptable 2-D stability analysis method; (3) how to make practical 3-D stability analysis efficiently over a very wide area; and (4) how to make a Landslide dam prone hazard map base on geographic information system (GIS) technique.

Chapter 3 proposes a new slope unit identification approach. At first, the problems and disadvantages of commonly used slope identification method are clarified: (1) slope unit dividing is impossible or inaccurate at hill top area; (2) since the sharp of ridge lines and valley lines are not matched well, hand correction is needed; (3) and it cannot keep the whole catchment of first-degree flow as one slope unit. And then, a new approach is proposed to solve the above problems by using stream lines instead of valley lines to conjoin ridge lines. The new approach can improve the slope identification accuracy.

Chapter 4 develops a new hazard mapping method based on the well-used 2-D limit equilibrium analysis with a circular slip mode. Hazard mapping based on limit equilibrium analysis is very popular and useful. Up to now, an infinite plane slip model (IPSM) is used in limit equilibrium analysis since it is easy to be implemented in GIS and suitable for grid mesh mapping method. However, the volume of landslide cannot be obtained from IPSM, which is necessary in Landslide dam hazard mapping. Moreover, a circular slip mode (CSM) is more popular than IPSM in practical limit equilibrium analysis since it is of high accuracy and can accommodate the complex data of geometry, stratum and groundwater. The problem of that is IPSM is not easy to be incorporated in GIS. For these reasons, a new hazard mapping method is developed based on the well-used Swedish Method, a 2-D limit equilibrium analysis method with a circular slip mode. At first, a method for automatic extraction of cross slope section is proposed base on the topography of each slope. And then, a GIS module for evaluating slope safety factor based on Swedish Method is developed using C# language. Practical applications show that not only the accuracy of slope stability analysis got improved, but also the hazard mapping can be completed quickly and effectively.

Chapter 5 develops a hazard mapping method based on 3-D limit equilibrium analysis. A semi-ellipsoid slip model is generally used for 3-D limit equilibrium analysis. The key issue is how to determine the ellipsoid parameters so as to obtain the minimum slope safety factor. The existed 3-D method applies Monte Carlo simulation to generate a large number of ellipsoids, the safety factor is calculated

for each ellipsoid and the least value is chosen as the final result. Since more than 1000 times of 3-D limit equilibrium analysis in Monte Carlo simulation is extreme time-consuming, it is not efficient to be used in hazard mapping which requires large number of calculations. For this reason, at first, a new method for determining the parameters of an ellipsoid is proposed based on the 2-D limit equilibrium analysis with Swedish Method. The circular slip determined in 2-D analysis is used for estimating the lengths of two axes of a tri-axial ellipsoid, the other axial length is estimated from the slope shape directly. And then, the GIS module of the 3-D limit equilibrium analysis is developed with the new approach of determining ellipsoid parameters. Practical applications show that the new hazard mapping method based on the new approach for 3-D limit equilibrium analysis can reduce the processing time very much.

Chapter 6 develops a Landslide dam hazard mapping method based on GIS technique. Up to now, there are very few papers and reports on Landslide dam hazard mapping although it is very important for cutting the disaster chain. For this reason, a new approach of Landslide dam hazard mapping method is proposed by the following steps. (1) Identifying the slope units in an area. (2) Extract possible Landslide dam prone slopes (LDPS) with so-called River Buffer Filter, by which only those slopes near a river are extracted. (3) Exclude impossible LDPS using so-called Aspect Filter, by which slopes that could not reach to the river are excluded according to their directions to the river. (3) Exclude impossible LDPS using so-called Blockage Filter, by which a slope that could not reach to the river is excluded according to the blockage height along the way to the river. (4) Exclude impossible LDPS using so-called Stability Filter, by which stable slopes are excluded based on slope stability analysis. (5) Exclude impossible LDPS using so-called Volume Filter, by which slopes with small volume of slide mass are excluded. In addition, DDA simulation is applied to verify the potential LDPS after filtering. Since the run out distance, distribution and volume of debris can be obtained from DDA simulation, Landslide dam formation can be judged based on river geometric and hydrologic data together with the volume of slide body. Also, the effectiveness of countermeasure using preventive structures can be verified by

DDA simulation.

Chapter 7 summarizes the results and achievements of the study. Also, problems to be solved in future study are stated.

REFERENCES

Adams J, 1981, Earthquake-dammed lakes in New Zealand. In: Geology, 9(5), p.215-219.

Ayalew L, Yamagishi H, 2005, The application of GIS-based logistic regression for landslide susceptibility mapping in the Kakuda-Yahiko Mountains, central Japan. In: Geomorphology, 65, p.15-31.

Cenderelli D. A, 2000, Floods from natural and artificial dam failures, In: Wohl, E.E. (Ed.), Inland Flood Hazards: Cambridge University Press, New York, p.73-103.

Capolongo D, Refice A, Mankelow J, 2002, Evaluating earthquake-triggered landslide hazard at the basin scale through GIS in the upper Sele river valley. In: Surv Geophys, 23, p.595-625.

Casagli N, Ermini L, Rosati G, 2003, Determining grain size distribution of the material composing landslide dams in the Northern Apennines. In: sampling and processing methods: Engineering Geology, 69(1-2), p.83-97.

Changa K. J, Taboada A, Linb M. L, Chenc R. F, 2005, Analysis of landsliding by earthquake shaking using a block-on-slope thermo-mechanical model: Example of Jiufengershan landslide, central Taiwan. In: Engineering Geology, 80, p.151-163.

Chigira M, Yagi H., 2006, Geological and geomorphological characteristics of landslides triggered by the 2004 Mid Niigta prefecture earthquake in Japan. In: Engineering Geology, 82, p.202-221.

Chigira M, Wang W. N, Furuya T, Kamai T, 2003, Geological causes and geomorphological precursors of the Tsaoling landslide triggered by the 1999 Chi-Chi earthquake, Taiwan. In: Engineering Geology 68, p.259-273.

Chai H, Liu H, Zhang Z, 1995, The catalog of Chinese landslide dam events. In: Journal of Geological Hazards and Environment Preservation, 6(4), p.1-9.

Clague J. J, Evans S. G, 1994, Formation and failure of natural dams in the Canadian Cordillera. In: Geological Survey of Canada Bulletin, 464(35).

Costa J. E, Schuster R. L, 1988, The formation and failure of natural dams. In: Geol Soc Am Bull, 100, p.1054-1068.

Costa J. E, Schuster R. L, 1991, Documented historical landslide dams from around the world. In: U.S. Geological Survey Open-File Report, 486, p.91-239.

Cruden D. M. a. V, D. J, 1996, Landslide types and processes: Landslides, Investigation and Mitigation. In: Transportation Research Board Special Report 247, Washington D.C. p.36-75.

Dadson S. J, Hovious N, Chen H, Dade,W. B, Lin J, Hsu M, Lin C, Horng M, Chen T, Milliman J, Stark C. P, 2004, Earthquake-triggered increase in sediment delivery from an active mountain belt. In: Geology, 32, p.733-736.

Dai F. C, Lee C. F, 2002, Landslide characteristics and slope instability modeling using GIS, Lantau Island, Hong Kong. In: Geomorphology, 42, p.213-228.

Dai F. C, Lee C. F, Deng J. H, Tham L. G, 2005, The 1786 earthquake-triggered landslide dam and subsequent dam-break flood on the Dadu River, southwestern China. In: Geomorphology, 65(3-4), p.205-221.

Evans S, Delaney K, Hermanns R, Strom A, Scarascia-Mugnozza G, 2011, The Formation and Behaviour of Natural and Artificial Rockslide Dams; Implications for Engineering Performance and Hazard Management. In: Natural and Artificial Rockslide Dams, 133, p.1-75.

Fan X, van Westen C. J, Xu Q, Görüm T, Dai F, 2012, Analysis of landslide dams induced by the 2008 Wenchuan earthquake. In: Journal of Asian Earth Sciences, 57, p.25-37.

Chen G, Li L, Zhang Y, Wu J, 2011, Earthquake Induced a Chain Disasters. In: D'Amico S, editor. Earthquake Research and Analysis - Statistical Studies, Observations and Planning: InTech, p.383-416.

Chen X. Q, Cui P, Li Y, Zhao W. Y, 2011, Emergency response to the Tangjiashan landslide-dammed lake resulting from the 2008 Wenchuan Earthquake, China. In: Landslides, 8 (1), p.91-98.

Gokceoglu C, Sezer E, 2009, a statistical assessment on international landslide

literature (1945-2008). In: Landslides, 6(4), p.345-351.

Guzzetti F, 2006. Landslide hazard and risk assement, UniversityBonn, Perugia.

Harp E. L, Crone A. J, 2006, Landslides Triggered by the October 8, 2005, Pakistan Earthquake and Associated Landslide-Dammed Reservoirs. In: U.S. Geological Survey Open-file Report, 2006-1052(13).

Harp E. L, Jibson R. W, 1996, Landslides triggered by the 1994 Northridge, California earthquake. In: Seismological Society of America, Bulletin, 86(1B).

Harp E. L, Keefer D. K, 1990, Landslides triggered by the earthquake. In: Rymer MJ, Ellsworth, WL (eds) The Coalinga, California, earthquake of May 2, 1983, U.S. Geological Survey Professional Paper, 1487, p.335-347.

Hancox G. T, Perrin N. D, Dellow G. D, 1997, Earthquake-induced landsliding in New Zealand and implications for MM intensity and seismic hazard assessment. In: Earthquake studies, Landslips, Seismology & geology, Paper 2276.

Highland L. M, Bobrowsky Peter, 2008, the landslide handbook-A guide to understanding landslides. In: Geological Survey Circular, Reston, Virginia, U.S.

Hutchinson J. N, 1988, General report: Morphological and geotechnical parameters of landslides in relation to geology and hydrology. In: the 5th International Symposium on Landslides, Lausanne, p.3-35.

Jackson J. A, 1997, Glossary of Geology. In: Glossary of Geology, American Geological Institute, Alexandria, Virginia.

Jibson R.W, Harp E. L, Michael J. A, 2000, A method for producing digital probabilistic seismic landslid hazard maps. In: Engineering Geology, 58, p.271-290.

Kallen D, Xiang W, 2006, Landslides at Qingjiang river in the downstream area of Shuibuya dam site, China. In: Journal of China University of Geosciences, 17 (2), p. 158-162.

Keefer D. K, 1984, Landslides caused by earthquakes. In: Geological Society of America Bulletin, 95(4), p.406-421.

Keefer D.K, 1994, the importance of earthquake-induced landslides to long-term

slope erosion and slope-failure hazards in seismically active region. In: Geomorphology, 10, p.265-284.

Keefer D. K, 2002, Investigating Landslides Caused by Earthquakes - A Historical Review. In: Surveys in Geophysics, 23(6), p.473-510.

Korup O, 2004, Geomorphometric characteristics of New Zealand landslide dams. In: Engineering Geology, 73(1-2), p.13-35.

Li X, He S, Lou Y, Wu Y., 2001, Simulation of the sliding process of Donghekou landslide triggered by the Wenchuan earthquake using a distinct element method. In: Environmental Earth Sciences, 65, p.1049-1054.

Liu N, Chen Z, Zhang J, Lin W, Xu W, 2010, Draining the Tangjiashan Barrier Lake. In: Journal of Hydraulic Engineering, 136(11), p.914-923.

Mason K, 1929, Indus floods and Shyok glaciers. In: Himalayan Journal, 1, p.10-29.

Marano K. D, Wald, D. J., Allen, T. I., 2010, Global earthquake casualties due to secondary effects: a quantitative analysis for improving rapid loss analyses. In: Natural Hazards, 52, p.319-328.

Marui H, Miyagi T, Yagi H, Umemura J, 2005, Landslide Disasters Induced by the 2005 Northern Pakistan Earthquake. In: Annual report of the Research Institute for Hazards in Snowy Area, Niigata University, 27, p.57-64.

O'Connor J. E, Costa J. E, 2004, The world's largest floods, past and present—Their causes and magnitudes. In: U.S. Geological Survey Circular, 1254(13).

Owen L. A, Kamp U, Khattak G. A, Harp E. L, Keefer D. K, Bauer M. A, 2008, Landslides triggered by the 8 October 2005 Kashmir earthquake. In: Geomorphology 94, p.1-9.

Parise M, Jibson R. W, 2000, A seismic landslide susceptibility rating of geologic units based on analysis of characteristics of landslides triggered by the 17 January, 1994. Northridge, California earthquake. In: Engineering Geology, 58, p.251-270.

Pearce A. J, Watson A. J, 1986, Effects of earthquake-induced landslides on sediment budget and transport over a 50-yr period. In: Geology, 14(1), p.52-55.

Qiu C, Esaki T, Xie M, Mitani Y, Wang C, 2007, Spatio-temporal estimation of shallow landslide hazard triggered by rainfall using a three-dimensional model. In: Environmental Geology, 52(8), p.1569-1579.

Rodríguez C, Bommer J, Chandler R, 1999. Earthquake induced landslides: 1980-1997. In: Soil Dynamics and Earthquake Engineering, 18, p.325-346

Safaei M, Omar H, Huat B. K, Yousof Z. B. M, Ghiasi V, 2011, Deterministic rainfall induced landslide approaches, advantage and limitation. In: Electronic Journal of Geotechnical Engineering, p.1619-1650.

Schneider J. F, 2009, Seismically reactivated Hattian slide in Kashmir, Northern Pakistan. In: Journal of seismology, 13(3), p.387-398.

Shang Y. J, Yang Z. F, Li L. H, Liu D. A, Liao Q. L, Wang Y. C, 2003, A super-large landslide in Tibet in 2000: background, occurrence, disaster, and origin. In: Geomorphology, 54, p.225-243.

Soeters R, van Westen C. J, 1996, Slope stability recognition, analysis, and zonation application of geographical information system to landslide hazard zonation. In: Turner, A.K., Schuster, R.L., (Eds.), Landslides: Investigation and Mitigation. Sp.-Rep. 247, Transportation Research Board, National Research Council. National Academy Press, Washington, D.C, p.129-177.

Star J, John E, 1990, Geographic information systems: An introduction. In: Bibliography, p.283-295.

Sun P, Zhang Y, Shi J, Chen L, 2011, Analysis on the dynamical process of Donghekou rockslide-debris flow triggered by 5.12 Wenchuan earthquake. In: journal of mountain science, 2011, 8(2), p.140-148.

Swanson F. J, Oyagi N, Tominaga M, Landslide dams in Japan. In: Proceedings Landslide Dams@ sProcesses, Risk, and Mitigation1986, ASCE, p.131-145.

Tang C, Ding J, Qi X, 2010, Remote sensing dynamic analysis of rainstorm landslide activity in Wenchuan high-intensity earthquake area. In: China university of geosciences journal, 35, p.317-323

Tang C, Zhu J, Qi X, Ding J, 2011, Landslides induced by the Wenchuan earthquake and the subsequent strong rainfall event: A case study in the Beichuan area of China. In: Engineering Geology, 122(1-2), p.22-33.

Tsuchiya T, 2008, Sediment disasters caused by earthquake. In: special conference material, flotech anchor Technical Institute, p.1-15.

Toyota H, 2005, Characteristics of landslide blockage of Imo river. In: The Foundation engineering & equipment, 33(10), p.101-104.

Uchida T, A Matsuoka, N Matsumoto, J Matsuda, K Akiyama, K Tamura, K Ichinohe, 2009, Overtopping erosion of landslide dam at Numakura-urasawa, San-hazama river Miyagi Prefecture, Japan. In: Journal of the Japan Society of Erosion Control Engineering 62(3), p.23-29

Varnes D. J, 1974, the logic of geological maps, with special reference to their interpretation and use for engineering purposes. In: U.S. Geol. Survey Prof. Paper, 837, p.48.

Varnes D. J, 1984, Landslide hazard zonation: a review of principles and practice. In: Natural Hazards, 3, p.63.

van Westen C. J, Terlien M. T. J, 1996, An approach towards deterministic landslide hazard analysis in GIS : a case study from Manizales, Colombia. In: Earth surface processes and landforms, 21(9), p.853-868.

WP/WLI, 1990, A suggested method for reporting a landslide. In: International Association Engineering Geology Bulletin, 41, p.5-12.

Wilson R. C, Keefer D. K, 1985, Predicting areal limits of earthquake-induced landsliding. In: Ziony JI (ed) Evaluating earthquake hazards in the Los Angeles region—An earth-science perspective, US Geological Survey Professional Paper 1360, p.316-345.

Wang H. B, Sassa K, Xu W. Y, 2007, Analysis of a spatial distribution of landslides triggered by the 2004 Chuetsu earthquakes of Niigata Prefecture, Japan. In: Natural Hazards 41, p.43-60.

Wang W. N, Nakamura H, Tsuchiya S, Chen C. C, 2002, Distributions of landslides triggered by the Chi-Chi earthquake in Central Taiwan on September 21, 1999. In: Landslide Soc, 38(4), p.318-326

Wang W. N, Wu HL, Nakamura H, Wu S. C, Ouyang S, Yu M. F, 2003, Mass movements caused by recent tectonic activity. In: the 1999 Chi-Chi earthquake in central Taiwan. Isl Arc 12, p.325-334.

Xie M, Esaki T, Zhou G, Mitani Y, 2002, Three-dimensional stability evaluation of landslides and asliding process simulation using a new Geographic Information Systems component. In: Environmental Geology, p.1-24.

Xu Q, Zhang S, Li W. L, van Asch Th. W. J, 2012, The 13 August 2010 catastrophic debris flows after the 2008 Wenchuan earthquake, China. In: Natural Hazards and Earth System Sciences, 12, p.201-216.

Yin Y, Wang, F, Sun P, 2009, Landslide hazards triggered by the 2008 Wenchuan earthquake, Sichuan, China. In: Landslides, 6(2), p.139-151.

CHAPTER 2

OVERVIEW ON HAZARD MAPPING METHOD FOR LANDSLIDE AND LANDSLIDE-DAM

2.1 INTRODUCTION

To produce a hazard map, the slopes in the study area should be first identified by slope susceptibility assessment. Based on the measured data, an appropriate hazard mapping approach is then chosen for the analysis. Finally, verification of accuracy is required before the assessment is applied in practical use.

Many methods have been developed for partitioning terrain. Among them, pixel (or grid) division has been widely used because it can be easily obtained and managed. Slope unit division is recommended for the establishment of logical slope boundaries.

Overviews and classifications of landslide hazard assessment approaches have been provided by Soeters and Van Westen (1996), Aleotti and Chowdhury (1999), Carrara et al.(1999), Guzzetti et al. (1999) and Van Westen et al. (2006). There is a general consensus that a classification involves four different approaches:

- Landslide inventory-based probabilistic approach
- Heuristic approach (direct-geomorphological mapping or indirect-combination of qualitative maps)
- Statistical approach (bivariate or multivariate statistics)
- Deterministic approach

However, some studies have grouped the methods used in GIS applications into two types: mechanical methods and non-mechanical methods (Xie et al., 2003; Zhou et al., 2005). Mechanical methods that use the deterministic approach use the infinite slope model to assess the stabilities of slopes. In many applications, the Monte Carlo simulation is the research target of estimating the possibilities. On the other hand, non-mechanical methods refer to those not related to the mechanical model.

This chapter gives an overview of landslide hazard map processing, including mapping unit divisions, susceptibility assessment approaches, and the Monte Carlo Simulation used in mechanism methods. Although few studies have focused on the prediction of landslide dams, the latest progress in and research status of landslide dam hazard mapping are also summarized.

2.2 OVERVIEW ON MAPPING UNIT

The production of a hazard susceptibility map for a regional hazard analysis requires the selection of appropriate slope mapping units (terrain unit). The term "mapping units" refers to a portion of land surface that contains a set of ground conditions that differ from the adjacent units across definable boundaries (Carrara et al., 1995; van Westen et al., 1997). At the scale of the analysis, a mapping unit represents a domain that maximizes internal homogeneity and between-unit heterogeneity; it should have relatively similar topographic and geological characteristics, respectively (Guzzetti et al., 1999). Some researchers carried out analysis based on tectonics and strata division, soil and vegetation division, administrative and climate division and so on, whereas others used pixel (or grid) division because it can be easily obtained and managed. Several methods have been proposed to partition terrain for landslide susceptibility assessment and hazard mapping (Carrara et al., 1995; Soeters and van Westen, 1996; Xie et al., 2004). These methods include the following:

(i) Grid Cells. A grid is a rectangular array of points. Grids are analogous

to pixels and record regularly spaced samples over an area. The most common technique is to map grid cells onto pixels one-to-one,

(ii) Slope units. A slope unit is partitioned based on terrain gradient, and supposed to represent the shape of a real slope.

(iii) Topographic Units. A topographic unit constitutes the natural spatial frame of a watershed for harnessing and utilizing water, soil and forest resources in a sustainable manner within its

(iv) Unique Condition Units. A unique condition unit is obtained by overlaying spatial-reference data and the intersection of instability factors, such as terrain data, geo-hydrological data, topographic data, political or administrative data and so on.

(v) Terrain Units.

(vi) Geo-Hydrological Units.

(vii) Political or Administrative Units.

The selection of a mapping unit affects uncertainties in the input data, the fitness of the assessment model, and the reliability of the obtained susceptibility zonation (Guzzetti et al., 1999). The main advantages and drawbacks of the different types of mapping units are summarized and examined according to the influence of different terrain subdivisions on susceptibility zonation (van Westen et al., 1993; Carrara et al., 1995; Guzzetti et al., 1999; Guzzetti, 2006). Moreover, the selection can result in considerable differences in the susceptibility assessment (Carrara et al., 2008).

In previous studies using the deterministic approach, grid cell division is widely used with the infinite slope model (Misumi et al., 2008; Hiraoka et al., 2011), whereas for more accurate assessment, slope unit division is employed with the three-dimensional slope model.

2.2.1 GRID CELLS

Many grid-based works are available in slope-stability analysis because the grid mesh can be easily obtained and managed. Grid cells divide the territory into

areas of regular shape (“cells”) and pre-defined size, which then become the mapping unit of reference. They are commonly square, but rarely rectangular. Triangular and hexagonal subdivisions also exist. Each grid cell can be assigned a set value of instability factors from multiple raster layers (e.g., morphological or geological) that are taken into consideration.

This division meets the requirement of the infinite slope mode and can be performed over wide area easily and effectively. However, grid-based objects do not bear any relation to the mechanism of slope failure or geological, geomorphologic, or other environmental boundaries. For example:

- One grid may contain several parts of slopes, or a slope may be divided into several grids (Fig 2.1). It is difficult to determine the grid size.
- Furthermore, a terrain area within a grid mesh is considered a plain surface, which may not represent a real topography in two/three dimensional stability analysis.

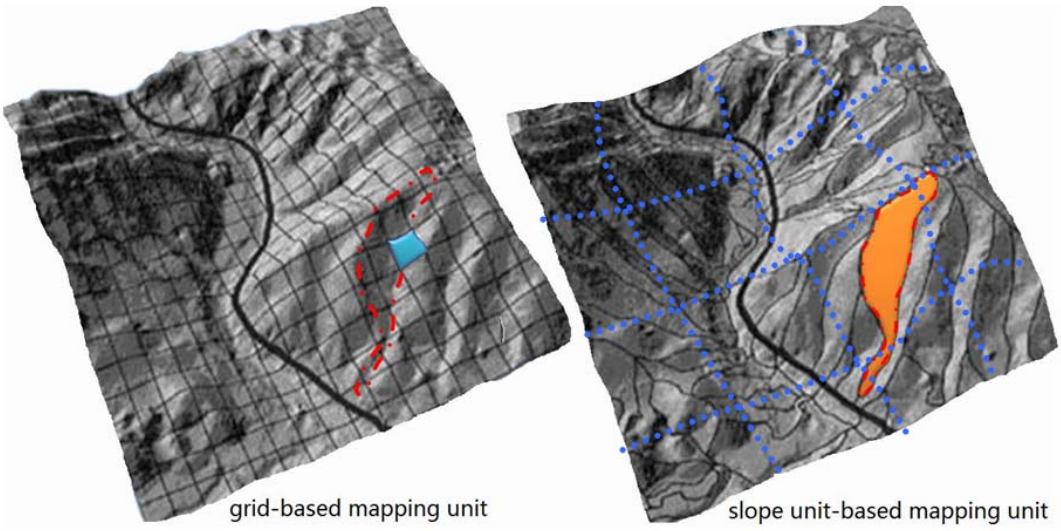

Fig 2.1. Grid-based and slope-based mapping unit

Note: the dotted red line represents a real slope in a grid-based mapping unit; the dotted blue lines represents grid cells in a slope unit-based mapping unit.

2.2.2 SLOPE UNITS

Because landslides occur on slopes, and slope units are digital representations of slopes, slope unit division has recently played an important role in susceptibility analysis. It has more explicit topographical and geological features than other mapping units have (Guzzetti et al., 1999). It shows similar trends related to the possible slide direction and hence can represent the shape of a real slope. Thus, some analysis procedures idealize the landslide of each slope unit as sliding toward one aspect. It is a practical and sensible assumption, so that 2-D/3-D stability analysis can derive and focus on a possible landslide mechanism.

Slope units partition the territory into hydrological zones bounded by drainage and divide lines (Carrara, 1988; Carrara et al., 1991, 1995, 2008; Guzzetti et al., 1999). They can be identified manually from an accurate topographic map. An existing method was provided by Xie (2003), which identifies slope units according to intersecting ridge lines and valley lines (Fig 2.2b).

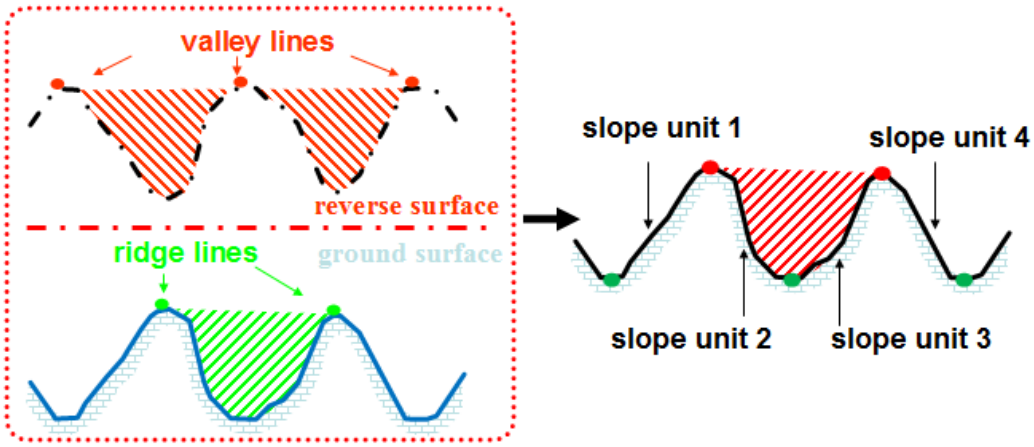

(a) (b)

Fig 2.2. Slope unit identification

This method is employed the Arc Hydro tool module in GIS, a suite of tools that facilitates the creation, manipulation, and display of Arc Hydro features and objects within the ArcMap environment. Through the tools, the catchment polygons and the stream lines of a study area can be obtained easily from the DEM.

Topologically, the outlines of a catchment polygon can be considered the ridge lines and the stream lines can be considered the valley lines in a mountainous area. However, because of the definition, the ridge lines are impossible to conjoin to the stream lines. Instead the valley lines can be assumed to equal the ridge lines of the reversed topography. Thus, the ground surface is reversed to derive the valley lines (Fig 2.2a).

However, some problems occur in the intersection of ridge lines and valley lines: the valley lines are inaccurate in the hill top area and do not match the stream lines; and the division cannot ensure only one possible slide direction of each slope unit. A detailed demonstration will be provided in Chapter 3, and a new mapping method for identifying slope units will be proposed.

2.3 Overview of Landslide Hazard Assessment Approaches

Landslides have considerable and destructive effects on human life, property, infrastructure and the environment. Although a huge amount of money is spent either to mitigate or prevent landslides, the first and probably the most important stage is to assess landslide susceptibility by obtaining data related to landslides.

Among the approaches used in susceptibility assessment are landslide inventories and heuristic methods, which essentially depend on the earth scientist responsible for the analysis. They are considered qualitative methods because human judgment and experience is needed to produce and run such models.

Statistical methods use the relationship between the locations of previous landslides and conditioning factors to predict landslide-prone areas with similar factors. Although they allow a better comprehension of the relationships between landslides and preparatory factors, the landslide inventory and database are not always available in many cases.

Deterministic approaches aim to calculate a safety factor based on slope stability analysis. Their accuracy relies on detailed geotechnical and hydrological data, as well as effective mathematical models. However, the information is not easily acquired, and most mathematical models are extremely time costing.

Although all known methods have advantages and disadvantages, and there

seems to be no agreement on these techniques regarding which is the most effective, the utilization of quantitative methods has become preferred and more commonly used in recent years because it guarantees lower subjectivity levels than qualitative approaches have (Ermini et al., 2005). Because of breakthroughs in computer technology, some traditional methods have disappeared, while new ones, particularly in the GIS software, have become very popular (Murat, 2008).

Thus, some researchers have grouped the methods used in the GIS application into two types: mechanical methods and non-mechanical methods (Xie, 2003; Zhou et al., 2005). Mechanical methods, that is deterministic approaches, mainly use the infinite slope model to assess the stabilities of slopes. In many applications, the Monte Carlo simulation is the research target for estimating the possibilities. On the other hand, non-mechanical models use mainly statistical methods.

2.3.1 STATISTICAL APPROACH

Statistical approaches were developed to overcome the relatively high level of subjectivity in the heuristic approach (Fall et al., 2006). They involve the statistical assessment of combinations of factors that have caused landslides in the past. Quantitative or semi-quantitative estimates are then performed for areas not affected by landslides, but where the same conditions exist (Dai et al., 2002). Statistical methods are generally considered the most appropriate method for landslide susceptibility mapping at regional scales because they are objective, reproducible and easily updatable (Naranjo et al., 1994). They are usually integrated with the GIS platform because most terrain indicator factors can be derived from the DEMs of GIS.

Bivariate statistical analysis involves the idea of comparing a landslide inventory map with maps showing parameters that influence landslides, in order to rank the corresponding classes according to their roles in landslide formation. Ranking is normally carried out using landslide densities (Lee et al., 2002).

The multivariate statistical analysis of important causal factors controlling landslide occurrence may indicate the relative contribution of each factor to the degree of hazard within a defined land unit. Several multivariate statistical

approaches emerged in the 1980s (Baeza, 2001; Carrara, 1983; Santacana, et al., 2003) and are still important, widely used tools (Table 2.1).

Table 2.1. Multivariate statistical analyses

Objective variables		**Explanatory variables**	**Methods**
Exist	**Quantity/Quality**		
yes	Quantity	Quantity	Multiple regression analysis, Logistic regression analysis, Canonical correlation analysis, Neural network analysis
		Quality	Hayashi's quantification method- Ⅰ
	Quality	Quantity	Discriminant analysis
		Quality	Hayashi's quantification method- Ⅱ
no	/	Quantity	Principal component analysis, Factor analysis, Cluster analysis, Multi-dimensional scaling analysis
	/	Quality	Hayashi's quantification method-Ⅲ/Ⅳ

However, statistical approaches have three drawbacks:

- Indicator factors are selected by expert or personal opinion, and in most cases, they are simplified by taking only those that can be relatively easily mapped in an area or derived from a DEM.
- This method assumes that landslides happen under the same combination of conditions throughout the study area and through time, whereas in reality environmental factors change continuously.
- Very few studies have developed separate statistical models for different landslide types, and most merge all active landslides together in one group that is used to generate statistical relations. Statistical landslide susceptibility assessment hardly ever takes triggering factors into account

2.3.2 DETERMINISTIC APPROACH

Deterministic, or physically based, approaches are based on the physical laws of the conservation of mass, energy or momentum. The main physical properties are quantified and applied to specific slope stability models. The input parameters include geometrical data, data on the shear strength parameters (e.g., cohesion and angle of internal friction), and information on pore water pressure. These parameters can be determined in the field or in the laboratory. Deterministic approaches provide the best quantitative information on landslide hazards, which can be used directly in the design of engineering works or in the quantification of risk (Van Westen et al., 2006).

Deterministic approaches are commonly used in small areas and at detailed scales. The reason is that detailed datasets about the spatial variation of parametric values that form the input of the hydrological arid slope stability models cannot be easily acquired.

Slope stability analysis can be carried out by the limit equilibrium method (LEM), the limit analysis method, the finite element method (FEM), or the finite difference method. Compared with other deterministic methods, limit equilibrium formulation is widely employed in geotechnical engineering and engineering geology, and it remains the most popular deterministic method.

The limit equilibrium method requires the division of the soil mass into slices or columns. Some assumptions, such as the side forces and slip surface, have to be made artificially. Despite these inherent limitations, because of its simplicity, fast calculation and easy programming, it remains the most commonly used approach (Hammouri et al., 2008).

Most limit equilibrium models (i.e., one-, two- or three-dimensional models) are based on the limit equilibrium approach. The index of stability is a well-known safety factor and is based on the appropriate geotechnical model (Aleotti and Chowdhury, 1999). The differences among the three models lie in different assumptions and study objects. The choice of a suitable model depends on the capacity to assess the parameters needed for the calculation, whether technical, spatial or financial.

ONE-DIMENSIONAL MODEL (INFINITE SLOPE MODEL)

The infinite slope model (one-dimensional model) assumes that the slope extends infinitely in all directions, and sliding is assumed to occur along a plane parallel to the face of the slope (Taylor, 1948) (Fig 2.3). This model may be justified in the assessment of shallow slope failure and the parts of a study area involving deep-seated failure.

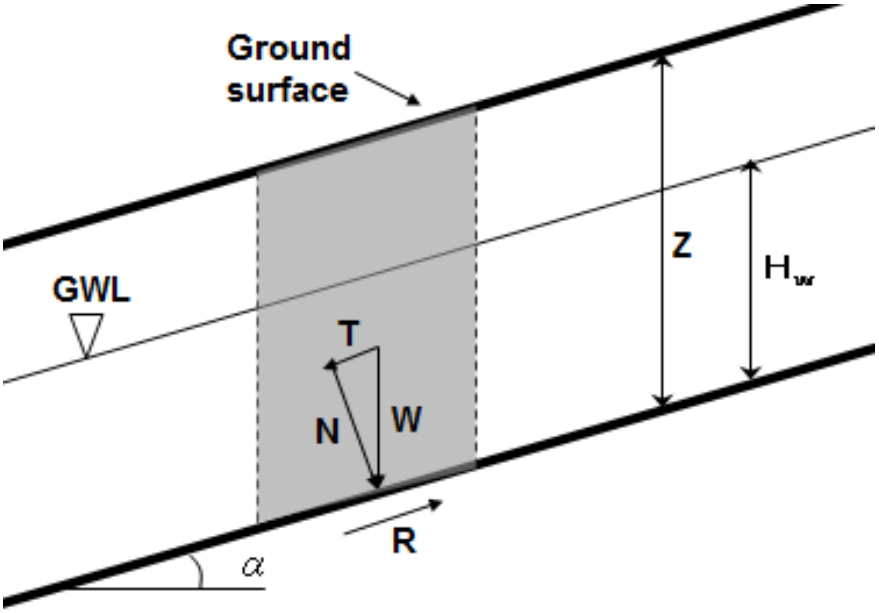

Fig 2.3. Infinite slope and plane failure surface

Such calculations can easily be performed in GIS by calculating the stability of each individual pixel or cell in grid cell division, and ignoring the influence of its neighbors (Van Westen et al., 1997). At present, only the infinity slope model, with the slip plane parallel to the surface, is used efficiently for larger areas in a GIS environment. Previous studies assessed the slope stability under real-time rainfall condition (Misumi et al., 2009; Hiraoka et al., 2012).

However, hazard mapping applications have three drawbacks:

- It is difficult to determine the depth of the slip surface. Circle shaped slip surface assumption in two-dimensional model is more commonly used for

individual slope stability analysis.

- The natural slope is not a plane shape, and the slip surfaces are not always parallel to the slope terrain. Moreover, the infinite slope model can only be used for a plane-shaped landslide.
- It cannot predict the scale of landslides. Knowledge of the latter is essential in studying the domino effect of disasters and predicting landslide-dam hazards.

TWO-DIMENSIONAL MODEL

The two-dimensional model (2-D) is called the method of slices. It studies the stability of the main section along slip direction (Fig 2.4). The soil mass above the slip surface is subdivided into a number of vertical slices. Some methods of slices assume a circular slip surface, whereas others assume an arbitrary (noncircular) slip surface. Methods that assume a circular slip surface consider the equilibrium of moments rotating the center of all slices. In contrast, the procedures that assume an arbitrary shape of the slip surface usually consider equilibrium in terms of individual slices.

In contrast with the infinite slope model, 2-D methods have the ability to accommodate complex geometries and variable soil and water pressure, which provides more sensitivity and more accuracy to satisfy the requirement of precise data. Thus, various 2-D methods have been developed and applied in practice. Among these 2-D models, the ordinary method of slices, the simplified Bishop method, the simplified Janbu method and the Sarma method have been widely adopted and have become the most common methods. However, 2-D methods have the following drawbacks:

- 2-D methods are difficult to integrate with the GIS environment because its study object is a section map, which is different from planar or three-dimensional (3-D) maps of GIS software.
- To search for a critical slip surface, the shape of slip surface shall be assumed several times and seek the minimum safety factor calculation

result. Optimization search schemes have been adopted by commercial software, but they are difficult to integrate within a GIS platform and create a regional assessment tool.

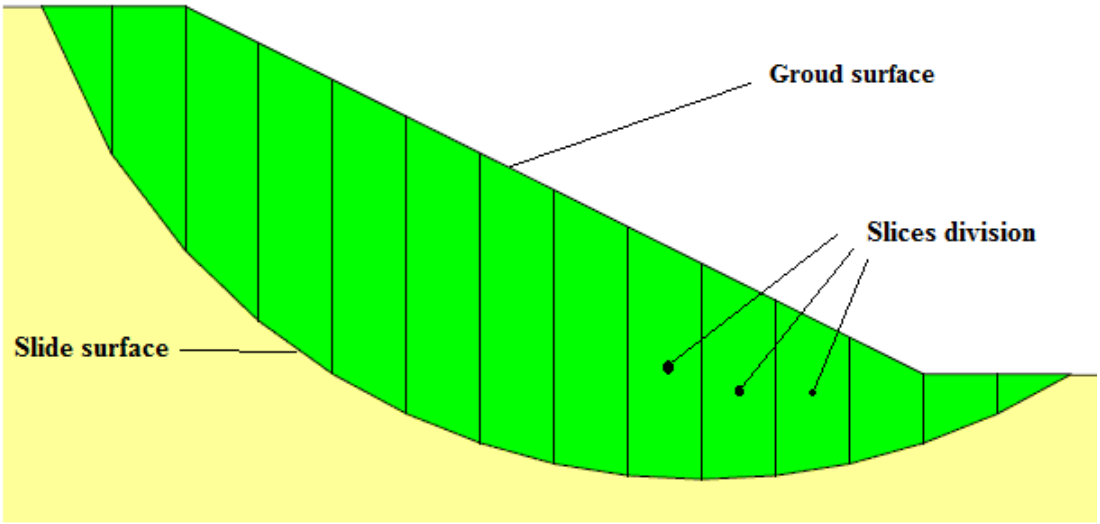

Fig 2.4. Slice division of slide body in the two-dimensional method

For the above reasons, we developed a systematic procedure for extracting slope cross sections from topographic terrains. A new mapping approach using the 2-D limit equilibrium model is also proposed in Chapter 4.

THREE-DIMENSIONAL MODEL

As mentioned above, 2-D methods produce good results, compare with the infinite slope model because 2-D methods can accommodate complex geometries and variable soil and water pressure in the direction of the main section, which means more sensitivity and more accuracy to satisfy the requirement of precise data. Sequentially, 3-D methods accommodate the most complex data of geometry, stratum and groundwater, which vary in space even along a short distance. Moreover, the safety factor in 2-D models is conservative because the shear resistance along the two sides of the slip mass are ignored. The 3-D model is thus recommended for the stability analysis of natural slopes.

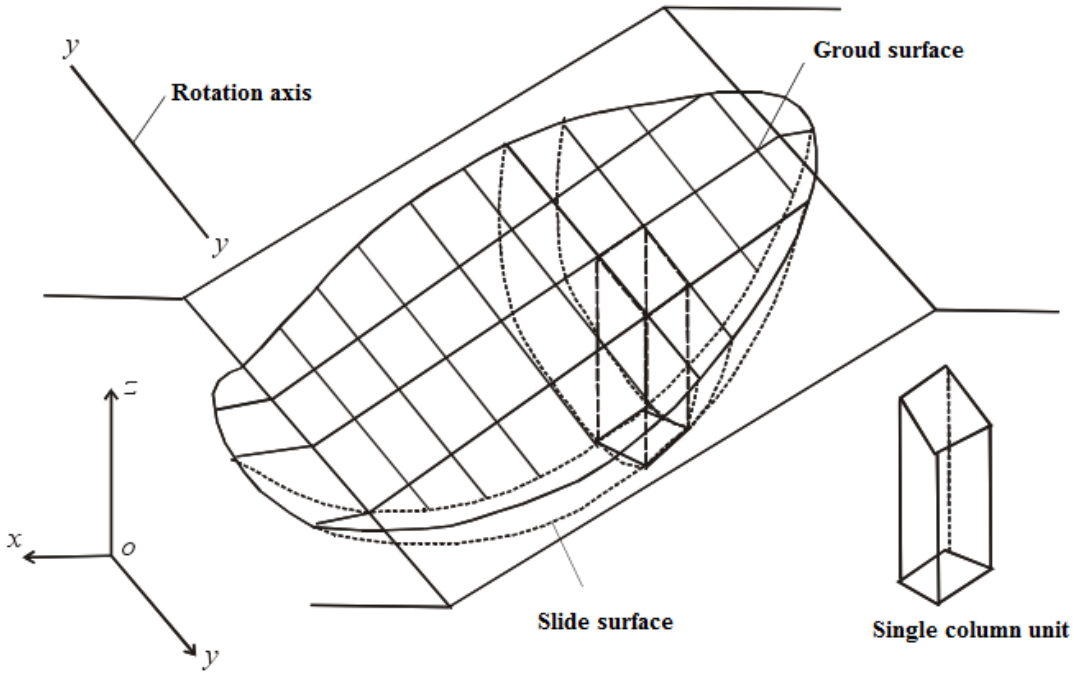

Fig 2.5. A column division example of slide body in the three-dimensional model

Since the late 1960s, a large number of 3-D methods for assessing slope stability have been proposed (Hovland, 1977; Hungr, 1987; Hungr et al., 1989; Lam and Fredlund, 1993; Leshchisky and Huang, 1992). Most 3-D methods are based on the column unit (Fig 2.5) and can be considered direct extensions of corresponding 2-D methods. In general, a semi-ellipsoid slip model is used to cut a slide body from the slope surface. The key issue is determining the ellipsoid parameters to obtain the minimum slope safety factor.

The existing hazard mapping approach was proposed by Xie (2003) using the Hovland method with the Monte Carlo simulation. The parameters used to determine the slide body are applied through the Monte Carlo simulation. However, this approach has the following drawbacks:

- Running the 3-D limit equilibrium analysis with the Monte Carlo simulation to achieve an acceptable minimum safety factor is extremely time-consuming. Xie (2003) emphasized that the calculation must be

repeated 300 times at least and recommended more than 1000 times.

In Chapter 5, column-unit based 3-D methods will be expanded, and the process searching for the slip surface will be improved to increase the effectiveness of the execution. In addition, its integration with GIS will be described in detail.

2.3.3 MONTE CARLO SIMULATION

The accurate assessment of potential landslide hazards early in the planning process is essential. Roth (1983) suggested that a geotechnical stability model of hazard assessment has advantages over subjective or statistical approaches, because it is widely applicable (model-based, not data-based), and because it can be used in sensitivity studies and to predict the effects of managerial actions. However, the application of equilibrium models is limited because of their high dependency on detailed geotechnical and hydrological data, which is scarce in most regions. Thus, in a stability analysis, a probabilistic approach is essential in considering the natural variability and uncertainty of each input variable.

Previous studies (Zhou, 2003; Liu 2008; Yazdani, 2012) have recommended the Monte Carlo simulation to overcome the shortcomings of natural variability and uncertainty of physical properties. Although the model cannot be sampled or measured directly, it can be expressed as a mathematical function of properties that can be sampled.

On the other hand, the Monte Carlo simulation is the option of last resort in gathering uncertain geotechnical and hydrological data, because of the following drawbacks:

- No better than an assured or referenced actual values
- Most engineering Monte Carlo simulations ignore the distinction between parameter values and estimates of parameter values.
- When multiple values are applied through the Monte Carlo simulation, the possibility of a “true” series of parameters is too low, which results in the gross underestimation of “low-probability” events.

- Its application in the assessment of an extensive area is extremely time consuming.

2.4 OVERVIEW ON LANDSLIDE-DAM HAZARD MAPPING APPROACHES

A number of landslide-dam inventories (Costa and Schuster, 1988, 1991; Chai et al., 1995; Casagli and Ermini, 1999; Korup 2004; Hewitt, 2006; Hermanns et al., 2011; Weidinger, 2011) have been created by compiling and reconstructing historic large events. However, little research has focused on earthquake-induced landslide dams (Adams, 1981; Hancox et al., 1997; Evans et al., 2011) because of the scarcity of well-documented inventories. Moreover, little work exists on the systematic analysis of regional distribution patterns and related controlling factors.

Unlike the landslide susceptibility assessment, a few landslide-dam susceptibility assessments use only statistical analysis, but the relationship and chain effect between the landslide and the landslide-dam are not considered (Fan et al., 2012; Yoshimatsu et al., 2012). Numerous studies of landslide dams have been done in the past decades, but most are descriptive and their results are uncertain. Some deterministic approaches have aimed to predict the stability, failure time, and dynamic failure process of landslide dams as well as the hydraulic-dynamic parameters of dam-break floods (Dunning et al., 2006; Harp and Crone, 2006; Nash et al., 2008; Duman, 2009; Schneider, 2009). Because they relied on detailed geotechnical and hydrological data, they can only be applied to small areas at a single slope scale.

In a quantitative study, Hayashi et al. (2012) examined the geomorphology features in the occurrence of landslide dams in a case study of the 2004 Mid-Nigata Prefecture earthquake. The results showed that larger landslides along a larger amount of river discharge have a tendency to induce landslide dams. Accordingly, a zonation map showing landslide dam susceptibility was proposed, based on the ground openness and the catchment area.

During the 2008 Wenchuan earthquake, to reduce the potential for dam-break floods, the Chinese army created artificial spillways at 32 of the most harmful dams by using explosives and heavy machinery. Xu et al. (2009) qualified the hazards of

these 32 dams by considering the dam height, dam composition and maximum capacity of the landslide-dammed lakes. Fan et al. (2012) compiled an inventory (Fig. 2.5) of 828 river-blocking landslides that occurred during the Wenchuan earthquake; 501 (61%) caused the complete damming of rivers, while 327 (39%) only partially dammed the rivers. Partially damming landslides ranged in areas from 768 m^2 to 1.3 × 10^6 m^2, which were slightly smaller than the areas of completely damming landslides, ranging from 1,249 m^2 to 7.1 × 10^6 m^2. Lake areas varied from 217 m^2 to 6.5 × 10^6 m^2. The landslides triggered by the Wenchuan earthquake covered an estimated total area of ~811 km^2 (Dai et al., 2011), and the damming landslides covered an area of ~54 km^2, which is ~7% of the total landslide area. This event-based inventory is unprecedented in both quantity and size, and it provides a unique opportunity to study the immediate post-earthquake dynamics of landslide dams.

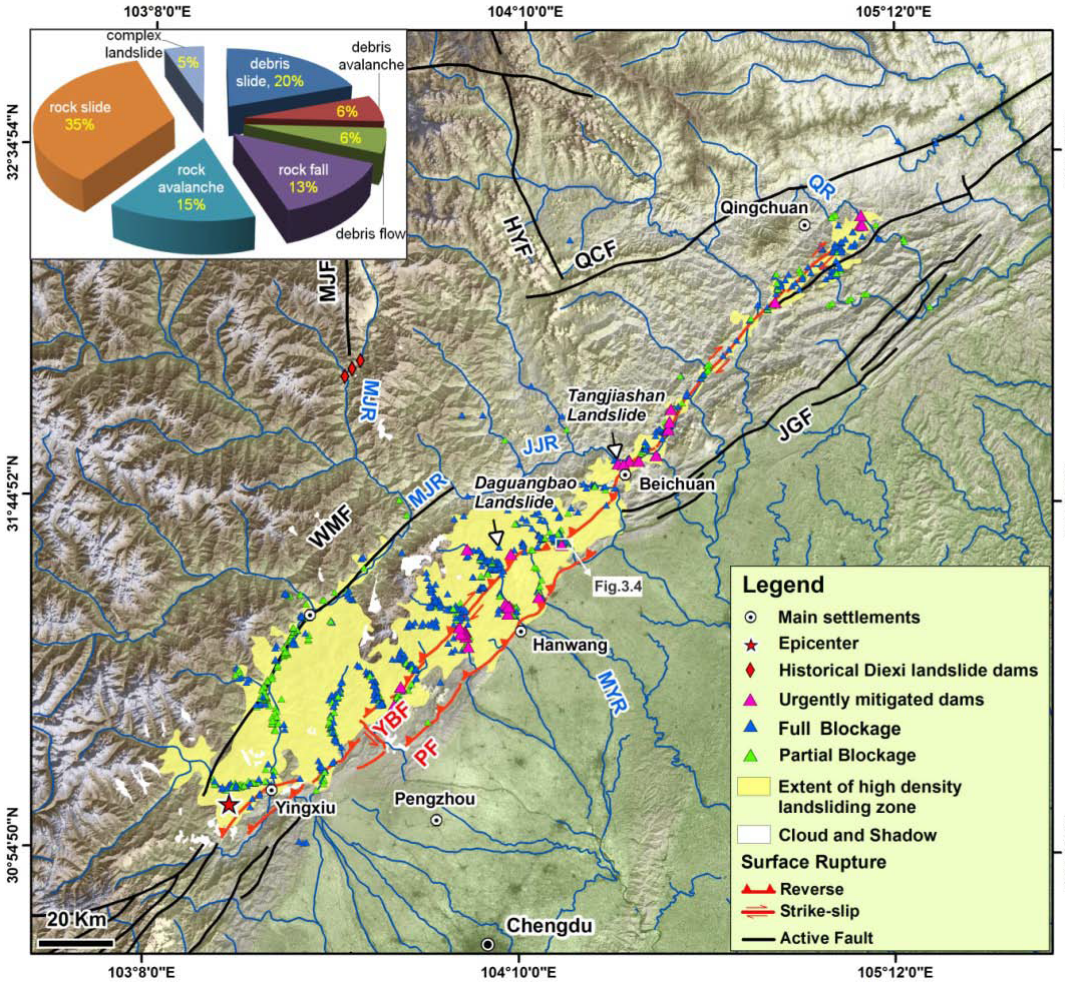

Fig 2.6. Distribution of landslide dams triggered by the Wenchuan earthquake in China

Note: The high landslide density zone is defined by a landslide area density >0.1 km^{-2}; also shown are epicenters of historical earthquakes (USGS, 2008) and historical Diexi landslide dams. Polygons are unmapped because of the presence of clouds and shadows in the post-earthquake imagery (From Fan, 2012).

However, a detailed understanding of the post-earthquake behavior of landslide dams will contribute to a better understanding of landslide dam formation and longevity. In Chapter 6, we propose a new hazard mapping method for earthquake-induced landslide-dam formation, which examines the geomorphology and analyses the susceptibility, using the limit equilibrium method and hydrology conditions.

2.5 SUMMARY

Several mapping units were introduced, and the slope units were recommended. Because some problems exist in the extraction of the slope unit, the present study aims to improve this process.

Next, four approaches to the assessment of landslide susceptibility were introduced. Former trends related to landslide assessment were explained. Quantitative methods, specifically GIS based ones were described. The advantages and disadvantages of statistical approach and deterministic approach were discussed in detail. In addition, Monte Carlo simulation was recommended for dealing with the natural variability and uncertainty of input variables in deterministic analysis. However, because the Monte Carlo simulation is used as the last resort in gathering uncertain geotechnical and hydrological data, many assumptions were considered first to decrease the uncertainty. The following chapters focus on driving accurate safety factors and effective execution.

Finally, previous studies of approaches to the assessment of landslide-dam susceptibility were discussed. An event-based inventory of the Wenchuan Earthquake was introduced because of its unprecedented quantity and size. This inventory provides a unique opportunity to study the immediate post-earthquake dynamics of landslide dams.

REFERENCES

Adams J, 1981, Earthquake-dammed lakes in New Zealand. In: Geology, 9(5), p.215-219.

Aleotti P, Chowdhury R, 1999, Landslide hazard assessment: summary review and new perspectives. In: Bulletin of Engineering Geology and the Environment, 58(1), p.21-44.

Baeza C. C. J, 2001, Assessment of shallow landslide susceptibility by means of multivariate statistical techniques. In: Earth Surface Processes and Landforms, 2, p.1251-1263.

Carrara A, Cardinali M, Detti R, Guzzetti F, Pasqui V, Reichenbach P, 1991, GIS techniques and statistical models in evaluating landslide hazard. In: Earth

Surface Processes and Landforms, 16, p.427-445.

Carrara A, Cardinali M, Guzzetti F, Reichenbach P, 1995, GIS technology in mapping landslide hazard, in: Geographical Information Systems in Assessing Natural Hazards, The Netherlands, p.135-176.

Carrara A, Guzzetti F, Cardinali M, Reichenbach R, 1999, Use of GIS technology in the rediction and monitoring of landslide hazara. In: Natural Hazards, 20(2-3), p.117-135.

Carrara A, Crosta G. B, Frattini P, 2003, Geomorphological and historical data in assessing landslide hazard, Earth Surface Processes and Landforms, 28(10), p.125-1142.

Carrara A, Crosta G. B, Frattini P, 2008, Comparing models of debris-flow susceptibility in the alpine environment, Geomorphology, 94, p.353-378.

Casagli N, Ermini L, 1999, Geomorphic analysis of landslide dams in the Northern Apennine. In: Transactions of the Japanese Geomorphological Union, 20, p.219-249.

Costa J. E, Schuster R.L, 1988, The formation and failure of natural dams. In: Geol. Soc. Am. Bull., 100, p.1054-1068.

Costa J. E, Schuster R.L, 1991, Documented historical landslide dams from around the world. In:: U.S. Geological Survey Open-File Report, 486, p.91-239.

Dai F. C, Lee, C. E, Ngai Y. Y, 2002, Landslide risk assessment and management: an overview. In: Engineering Geology, 64, p.65-87.

Dai F. C, Xu C, Yao X, Xu L, Tu X. B, Gong Q. M, 2011, Spatial distribution of landslides triggered by the 2008 Ms 8.0 Wenchuan earthquake, China. In: Journal of Asian Earth Sciences, 40(4), p.883-895.

Dunning S. A, Rosser N. J, Petley D. N, Massey C. R, 2006, Formation and failure of the Tsatichhu landslide dam, Bhutan. In: Landslides, 3(2), p.107-113.

Duman T. Y, 2009, The largest landslide dam in Turkey. In: Tortum landslide: Engineering Geology, 104(1-2), p.66-79.

Evans S, Delaney K, Hermanns R, Strom A, Scarascia Mugnozza G, 2011, The Formation and Behaviour of Natural and Artificial Rockslide Dams; Implications for Engineering Performance and Hazard Management, in Evans,

S. G., Hermanns, R. L., Strom, A., and Scarascia-Mugnozza, G., eds., Natural and Artificial Rockslide Dams, Volume 133, Springer Berlin Heidelberg, p.1-75.

Ermini L, Catani F, Casagli N, 2005, Artificial Neural Networks applied to landslide susceptibility assessment. In: Geomorphology. 66 (1-4), p. 327-343.

Fall M, Azzam R, Noubactep C, 2006, A multi-method approach to study the stability of natural slopes and landslide susceptibility mapping. In: Engineering Geology, 82(4), p.241-203.

Fan X, van Westen C. J, Xu Q, Görüm, T, Dai, F, 2012, Analysis of landslide dams induced by the 2008 Wenchuan earthquake. In: Journal of Asian Earth Sciences, 57, p.25-37.

Guzzetti F, Carrara A, Cardinali M, Reichenbach P, 1999, Landslide hazard evaluation: a review of current techniques and their application in a multiscale studym, Central Italy. In: Geomorphology, 31(1-4), p.181-216.

Guzzetti F, Galli M, Reichenbach P, Ardizzone F, Cardinali M, 2006, Landslide hazard assessment in the Collazzone area, Umbria, Central Italy. In: Natural Hazards and Earth System Sciences, 6, p.115-131.

Hammouri N. A, Husein Malkawi A. I, Yamin M. M. A, 2008, Stability analysis of slopes using the finite elemnet method and limiting equilibrium approach. In: Bulletin of Engeering Geology and the Environment, 67(4), p.471-478.

Hancox G. T, Perrin N.D, Dellow G.D, 1997, Earthquake-induced landsliding in New Zealand and implications for MM intensity and seismic hazard assessment. In: Lower Hutt: Institute of Geological and Nuclear Sciences Client Report 43601B prepared for Earthquake Commission Research Foundation.

Harp E. L, Jibson R. W, 1995, Inventory of landslides triggered by the 1994 Northridge, Calilbrnia earthquake. In: U. S. Geological Survey.

Harp E. L, Crone A.J, 2006, Landslides Triggered by the October 8, 2005, Pakistan Earthquake and Associated Landslide-Dammed Reservoirs. In: U.S. Geological Survey Open-file Report, 2006-1052(13).

Hayashi K, Wakai A, Tanaka N, Abe S, 2012, Susceptibility zonation for landslide

dams induced by near-field earthquake. In: Journal of the Japan Landslide Society, 49(5), p.259-266.

Hermanns R. L, Hewitt K, Strom A.L, Evans E.G, Dunning S.A, Scarascia Mugnozza G, 2011, The classification of rock slide dams. In: Natural and artificial rockslide dams. Lecture Series in Earth Sciences. Evans SG, Hermanns RL, Strom A, Scarascia Mugnozza, G (eds). Springer: Berlin, p.581-593.

Hiraoka T, Zen K, Chen G, 2012, An Approach Which Forecast the Slope Failure that Happens Because of the Rainfall using Geographical Information System. In: Western Regional Division report of Natural Disaster Research Council, 36, p.13-16.

Hovland H J, 1977, Three-dimensional slope stability analysis method. In: ASCE J Geotech Eng Div, 103(9), p.971-986.

Hungr O, 1987, An extension of bishop's simplified method of slope stability analysis to three dimensions. In: Geotechnique, 37(1), p.113-117.

Hungr O, Salgado F. M, Byrne R. M, 1989, Evaluation of a three-dimensional method of slope stability analysis. In: Can Geotech J, 26, p.679-686.

Korup O, 2004, Geomorphometric characteristics of New Zealand landslide dams. In: Engineering Geology, 73(1-2), p.13-35.

Lam L, Fredlund D. G, 1993, A general limit equilibrium model for three-dimensional slope stability analysis. In: Canadian Geotechnical Journal, 30(6), p.905-919.

Lee S, Choi J, Min K, 2002, Landslide susceptibility analysis and verification using the Bayesian probability model environmental. In: Geology, 43, p.120-131.

Leshchisky D, Huang C. C, 1992, generalized three dimensional slope stability analysis. In: Journal of Geotechnical Engineering, 118(11), p.1748-1763.

Li T, Wang S, 1992, Landslide hazards and their mitigation in China. In: Science Press, Beijing.

Liu C. N, 2008, Landslide Hazard Mapping Using Monte Carlo Simulation- a Case Study in Taiwan. In: Geotechnical Engineering for Disaster Mitigation and Rehabilitation, p.189-194.

Murat E, 2008, An Overview on the Landslide Susceptibility AssessmentTechniques. In: 1st WSEAS International Conference on environmental and geological science and engineering, Malta, September 11-13.

Misumi M, Zen K, Chen G, Kasama K, 2008, Accuracy evaluation of slope disaster risk map at kita-kyushu city using geographical information system, In: Proceedings of the 2nd International Symposium on Climate Change and the Sustainability, p.136-139.

Naranjo J. L, Van Westen C. J, Soeters R, 1994, Evaluating the use of training areas in bivariate statistical landslide hazard analysis: a case study in Colombia. In; ITC Journal, 1994-3, p.292-300.

Nash T, Bell D, Davies T, Nathan S, 2008, Analysis of the formation and failure of Ram Creek landslide dam, South Island, New Zealand. In: New Zealand Journal of Geology and Geophysics, 51(3), p.187-193.

Roth, R. A. 1983. Factors affecting landslide-susceptibility in San Mateo County, CA. In: Bull. of the Assoc. of Eng. Geologists, 10(4), p.353-372.

Santacana N, De Paz A, Baeza B, Corominas J, Marturi J, 2003, A GIS-based multivariate statistical analysis for shallow landslide susceptibility mapping in La Pobla de Lillet area (Eastern Pyrenees, Spain). In: Natural Hazards, 30(3), p.281-295.

Schneider J. F, 2009, Seismically reactivated Hattian slide in Kashmir, Northern Pakistan. In: Journal of seismology, 13(3), p.387-398.

Taylor D. W, 1948, Fundamentals of soil mechanics, Wiley, Hoboken, NJ.

The Japan Landslide Society, 2012, <http://landslide.bosai.go.jp/lsmap/index.html>.

van Westen C. J, van Duren I, Kruse H.M.G, Terlien M.T.J, 1993, training package for geographic information systems in slope instability zonation. In: TEC publ, 15(1&2), Enschede, The Netherlands.

van Westen C. J, Terlien M.T.J, 1996, An approach towards deterministic landslide hazard analysis in GIS : a case study from Manizales, Colombia. In: Earth surface processes and landforms, 21(9), p. 853-868.

van Westen C. J, Rengers N, Terlien M. T. J, Soeters R, 1997, Prediction of the occurrence of slope instability phenomena through GIS-based hazard zonation. In: Geol Rundsch, 86, p.404-414.

van Westen C. J, Van Asch T. W. J, Soeters R, 2006, Landslide hazard and risk zonation - Why is it still so difficult?. In: bulletin of Engineering Geology and the Environment, 65(2), p.167-184.

Weidinger J. T, 2011, Stability and Life Span of Landslide Dams in the Himalayas (India, Nepal) and the Qin Ling Mountains (China), in Evans, S. G., Hermanns, R. L., Strom, A., and Scarascia-Mugnozza, G., eds., Natural and Artificial Rockslide Dams, Volume 133, Springer Berlin Heidelberg, p.243-277.

Xie M, Esaki T, Zhou G, Mitani Y, 2002, Three-dimensional stability evaluation of landslides and asliding process simulation using a new Geographic Information Systems component. In: Environmental Geology, p.1-24.

Xu Q, Fan X. M, Huang R. Q, Westen C, 2009, Landslide dams triggered by the Wenchuan Earthquake, Sichuan Province, south west China. In: Bulletin of Engineering Geology and the Environment, 68(3), p.373-386.

Yazdani A, Shahpari A, Salimi M. R, 2012, the use of monte-carlo simulations in seismic hazard analysis in tehran and surrounding areas. In: IJE TRANSACTIONS C: Aspects, 25(2), p.159-166.

Yoshimatsu H, Abe S, Marui H, Kanno T, 2011, Prediction of landslide dam breach events by pattern classification analysis. In: Journal of the Japan Landslide Society, 48(6), p.22-29.

Zhou G, T Esaki, M Xie, Y Sasaki. 2005. GIS-Based Three-Dimensional Landslide Evaluation System Development and Its Application. Journal of the Japan Society of Engineering Geology, 46(1), p.28-37 in Japanese.

Zhou G, Esaki T, Mitani Y, Xie M, Mori J, 2003, Spatial probabilistic modeling of slope failure by using GIS and Monte Calro method. In: international jarnal of Engineering Geology, 68(3-4), p.373-386.

CHAPTER 3

DEVELOPMENT OF A NEW SLOPE UNIT IDENTIFICATION APPROACH TO LANDSLIDE HAZARD MAPPING

3.1 INTRODUCTION

To produce a hazard map, the first and essential step is to identify the slopes in a wide area. The selection of an appropriate mapping units affects uncertainties in the input data, the fitness of the assessment model, and the reliability of the obtained susceptibility zonation (Guzzetti et al., 1999). Several methods have been proposed to partition terrain for landslide susceptibility assessment and mapping (Carrara et al., 1995; Soeters and van Westen, 1996; Xie et al., 2002). Among them, slope unit division has played an increasingly important role in susceptibility analysis because its topographical and geological features are more explicit than other mapping units are (Guzzetti et al., 1999).

Because a slope unit shows similar trends related to the possible direction of slides and hence can represent the shape of a real slope, this study adopts slope unit division and uses the detection of possible slide directions for the assessment of landslide susceptibility.

To gather geomorphological and hydrological information about a prone slope, a GIS based Arc Hydro tool (David, 2002) provides an effective means to extract

catchments and drainage lines from DEM. Xie (2002) described a slope units identify method using ridge lines and valley lines division. However, existing identification methods have many limitations, which negatively affect the utility and accuracy of the analysis.

This chapter first introduces topography processing in GIS and the existing identification method. The problems encountered in slope units identifying are then classified and discussed in detail. Finally, a new approach is proposed to solve the problems using the GIS technique. The improvements offered by a new identification method are proved by comparing the accuracy of the results with existing method.

3.2 TOPOGRAPHY PROCESSING IN GIS AND EXISTING IDENTIFICATION METHODS

Recently, several studies have analyzed landslide hazards using GIS. These studies were either statistical (Ayalew and Yamagishi, 2005; Dai and Lee, 2002) or deterministic (Safaei et al., 2011; Van Westen and Terlien, 1996; Xie et al., 2002). In the process of every assessment, the first step is to extract a set value of instability factors according to the mapping units. The identification of mapping units affects the data collection and the fitness of the assessment model. Since breakthroughs in computer science, identification methods utilizing the new GIS technology have become very popular (Murat, 2008).

The geographical information system (GIS) is a computer system designed to manage spatial data. The word geographical implies that the locations of the data items are known or can be calculated in terms of geographic coordinates. The word information implies that the data in GIS are organized and easy to utilize interactively. The word system implies that a GIS comprises several interrelated and linked components with different functions. Thus, GIS has functional capabilities for data capture, input, manipulation, transformation, visualization, combination, query, analysis, modelling and output (Bonham Carter, 1994).

There are two types of GIS data: vector or raster GIS. Vector GIS comprises three different types of geometric data: point, line and polygon in an area; raster

GIS is formed by raster layers, as shown in Fig 3.1.

GIS software is unique in its ability to capture, store, and manage spatially referenced data. Simply used as a spatial database, GIS assists in modelling applications through handling a special form of data. GIS also contains facilities for constructing and importing digital elevation models (DEM) and triangulated irregular networks (TIN). Thus, GIS can be easily utilized to overcome difficulties in slope information acquisition and identifying the vector type and the raster type.

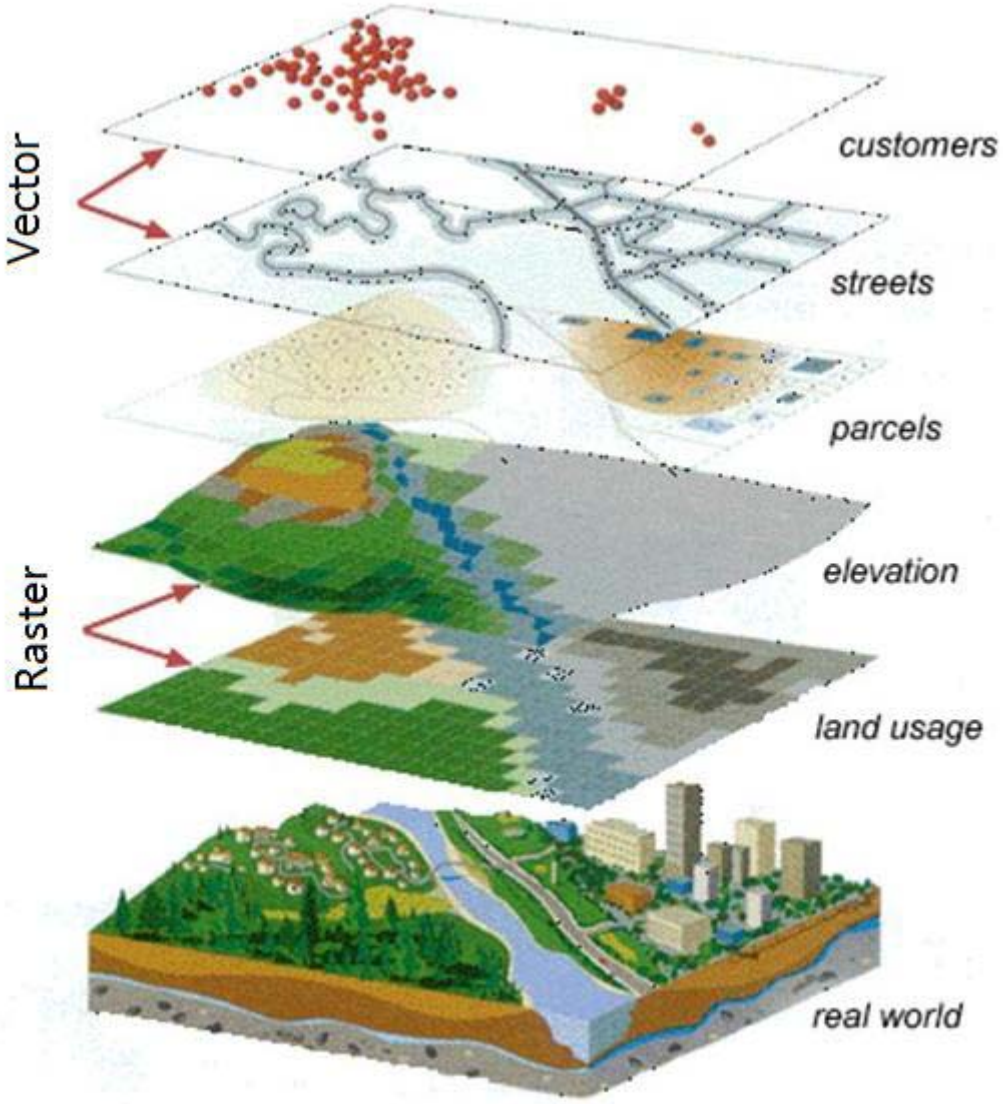

Fig 3.1. Basic concept of GIS (from ESRI)

Because GIS has become a useful and important tool in hydrology studies and

the management of water resources, the Environmental Systems Research Institute (ESRI) has provided a suite of tools called Arc Hydro Tools, which facilitates the creation, manipulation, and display of hydro features and objects within the ArcMap environment. Through these tools, the catchment polygons and the stream polylines of a study area can be obtained easily from the DEM.

As explained in Chapter 2, slope units are bounded by ridge and valley lines (Carrara et al., 1991, 1995, 2008; Guzzetti et al., 1999). The method used to identify existing slope units takes advantage of the outlines of catchment polygons to partition slope units (Fig 3.2b). The outlines are considered the ridge lines and the valley lines are assumed to equal the ridge lines on the reversed topography. The ground surface (DEM) is then used to derive the ridge lines and is reversed to derive valley lines (Fig 3.2a). The slope unit division is obtained by using the intersection of ridge lines and valley lines.

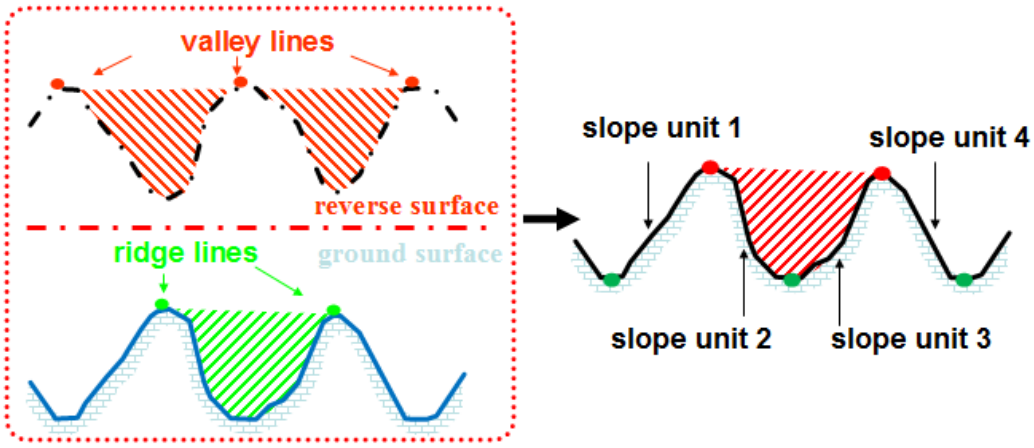

(b) (b)

Fig 3.2. Slope unit identification

3.3 PROBLEMS IN COMMON IDENTIFICATION METHOD

One unit slope (slope unit) is a region bounded by the valley lines and the ridge lines of the mountains. The existing method employs Arc Hydro Tools and identifies slope units by the intersection of ridge lines and valley lines. However, in many applications, the following problems are usually encountered:

3.3.1 INACCURATE DIVISION AT HILL TOP AREAS

Because many streams in reversed topography are concentrated at the hill tops, they serve as impounded lakes in the hydrologic analysis tool. In the "fill sink" step, the hill tops are translated to flat plains. No catchment can be derived here, and slope unit division is impossible or inaccurate in hill top areas. An example is shown in Fig 3.3.

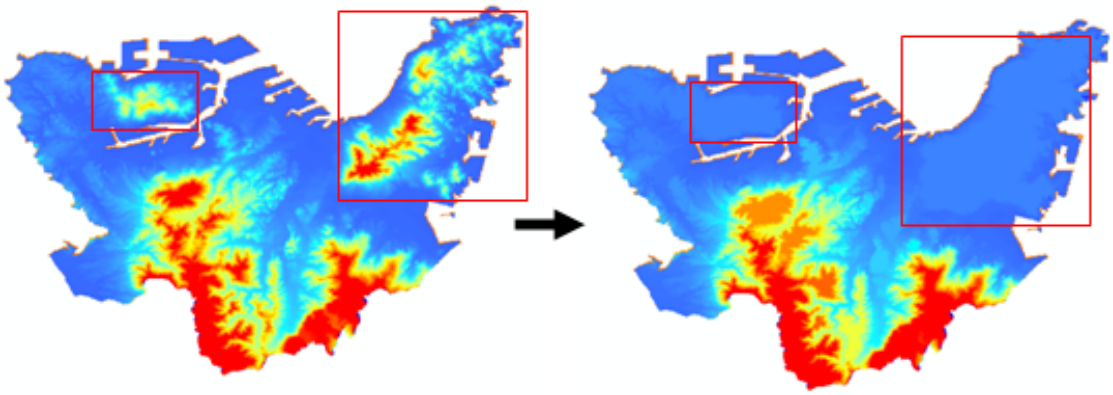

Fig 3.3. The incorrect changes of hill tops through fill sink step shown in DEM

Some researchers suggested skipping the fill sink step in reversed topography to improve the appearance. However, without the fill sink step, reversed topography cannot provide a complete stream network. As shown in Fig 3.4, the disjointed steam network still results in undivided hill tops.

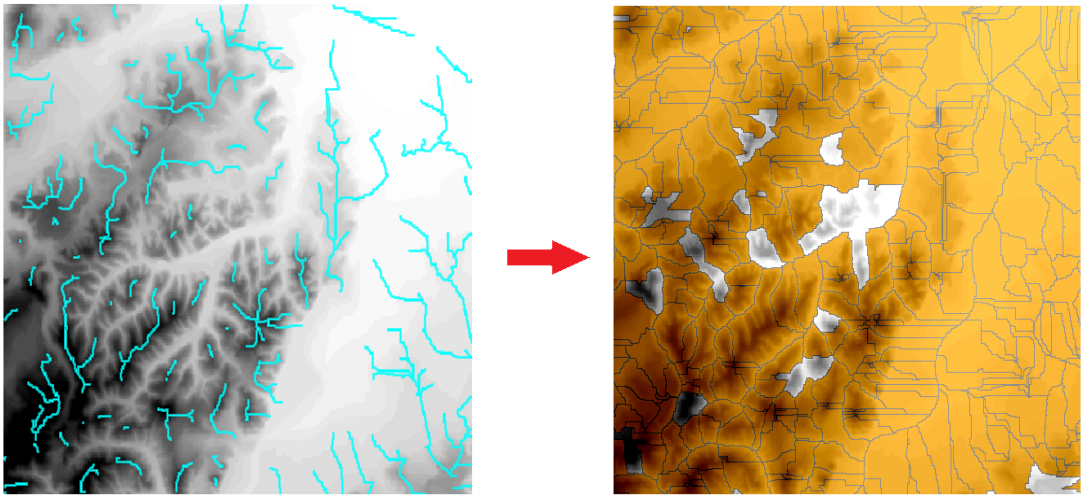

Fig 3.4. The disjointed steam network results in some undivided hill tops

3.3.2 MISMATCHED VALLEY LINES AND RIDGE LINES

Because the process of slope unit identification is carried out in both frontal and reversed topography, the hydrologic analysis was performed twice. Unlike the general assumption, the valley lines in frontal topography do not equal the ridge lines in reversed topography. Furthermore, to get the proper size of slope units, the two thresholds of minimum drainage area to partition catchment are adjusted and distinguished. This causes an intersection problem, in which the sharps of the ridge lines and the valley lines are mismatched, so hand correction is needed. An example is shown in Fig 3.5, in which the formations of numerous small pieces of slope units are useless.

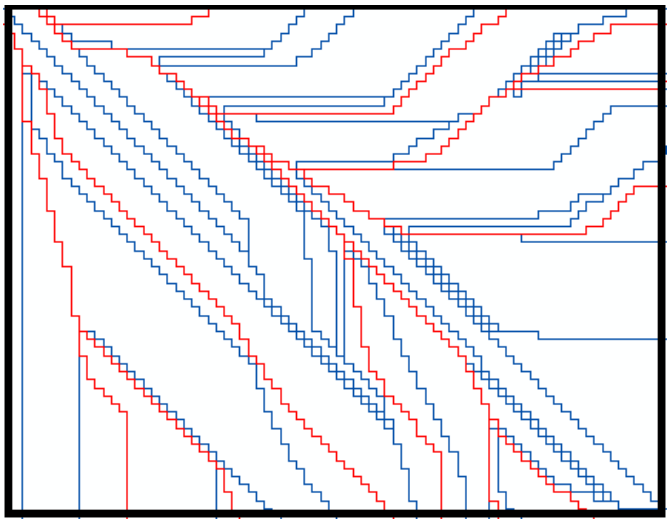

Fig 3.5. An example of numerous, useless slope units of one or two pixels

Note: Obtained by the intersection of ridge lines (red lines) and valley lines (blue lines)

3.3.3 UNDETECTED MULTIPLE POSSIBLE SLIDE DIRECTIONS

Because the stream network is broken in reversed topography, the division of the watershed (valley lines) is smaller than in frontal topography. Furthermore, to minimize the negative influence of the first problem, in practice, the threshold of minimum drainage used in the reversed topography is usually set smaller than in the frontal topography. Consequently, many slope unit divisions are extracted only by the stream lines (i.e., the valley lines in the reversed topography) (Fig 3.6).

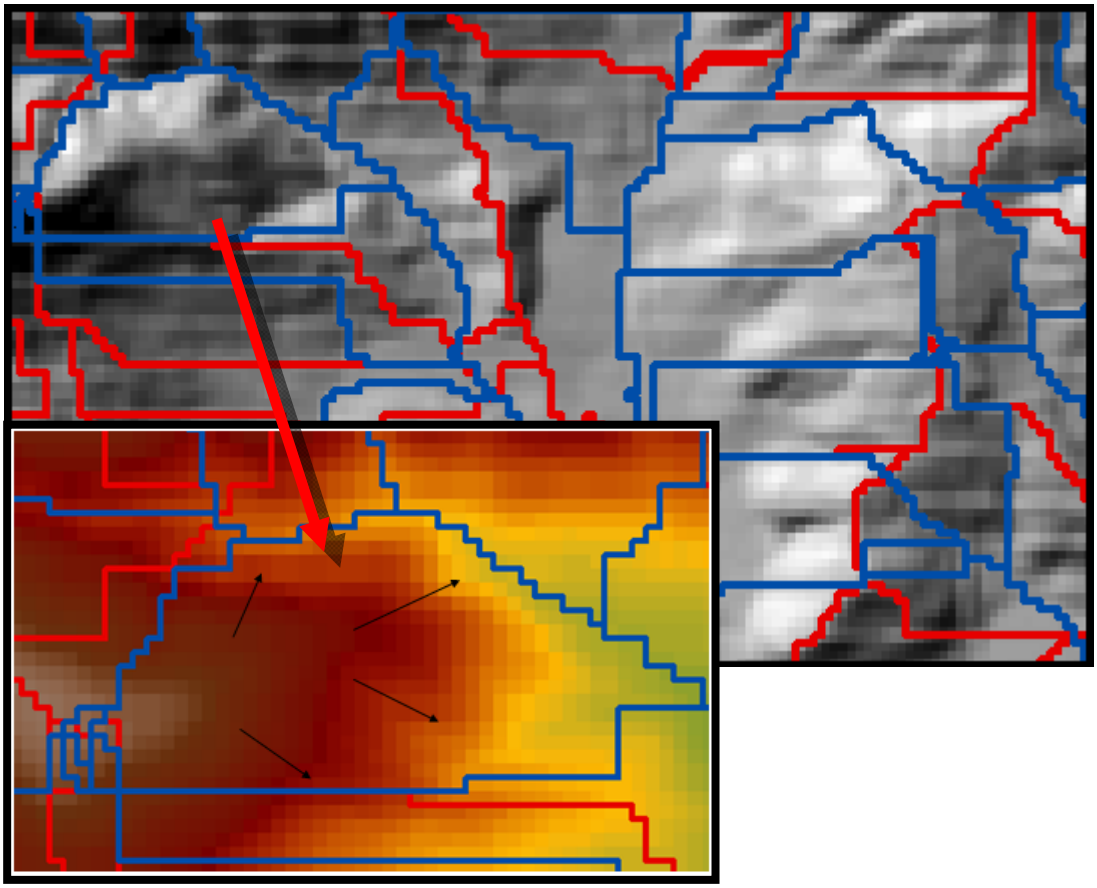

Fig 3.6. An example of slope units divided by stream lines only (blue lines)

Note: The example slope unit has multiple possible slide directions (black arrows)

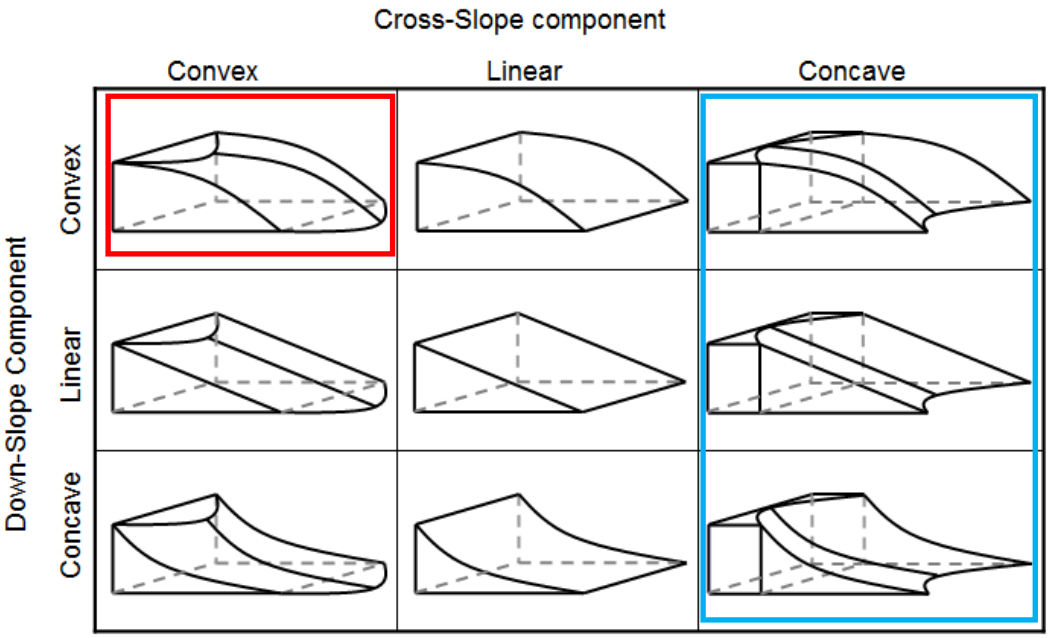

Fig 3.7. The slope type according to curvature

In the topography of one slope, the profile curvature and plan curvature can be used to indicate concave or convex formations in the down-slope and cross-slope components (Fig 3.7). In the water dashing down along the stream lines, the lines have relatively lower elevations than the surrounding pixels show. Thus, the extracted slope units bounded by stream lines are apt to be convex slopes that have multiple possible slide directions (Fig 3.8). The slope type is represented by the red squares (Fig 3.7). It is difficult to determine a possible slide path in such slope units. Some possibilities of landslides will be ignored if a division will further detail is not implemented.

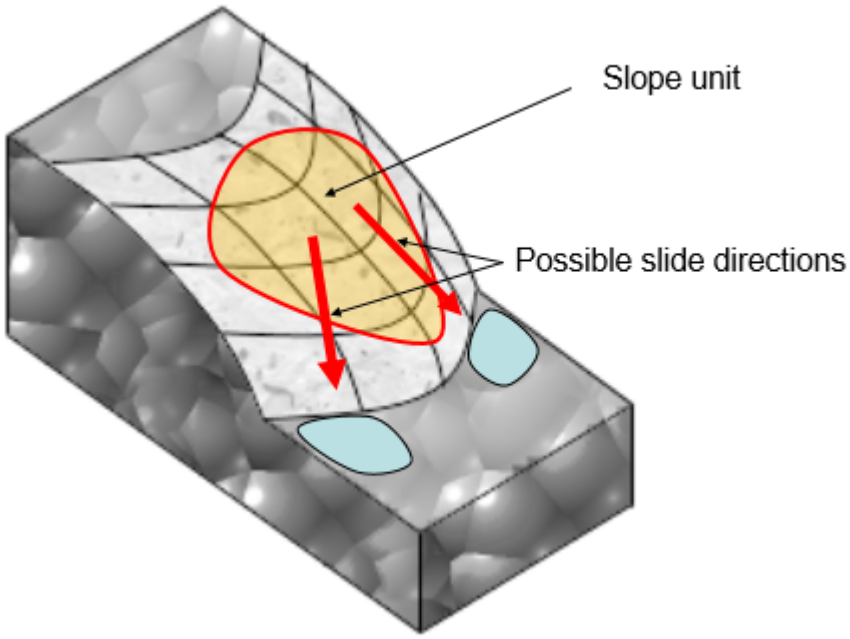

Fig 3.8. A convex slope with multiple possible slide directions

3.3.4 Error division of flow origin area

Because the head flow, also determined as the first-degree flow, is usually in an un-channeled valley, the slope units containing a head flow are concave slopes in the cross-slope component (Fig 3.9) where headward erosion usually takes place. The slope types are represented as blue squares (Fig 3.7). In the existing method, it is difficult to divide the flow origination (flow origin) area. A landslide occurring in this area will run towards the stream direction. It is better to keep the flow origination area as an individual slope unit, but undivided by valley lines, because

only one possible slide direction exists. This is very important in the landslide hazard mapping approach proposed in the next chapter.

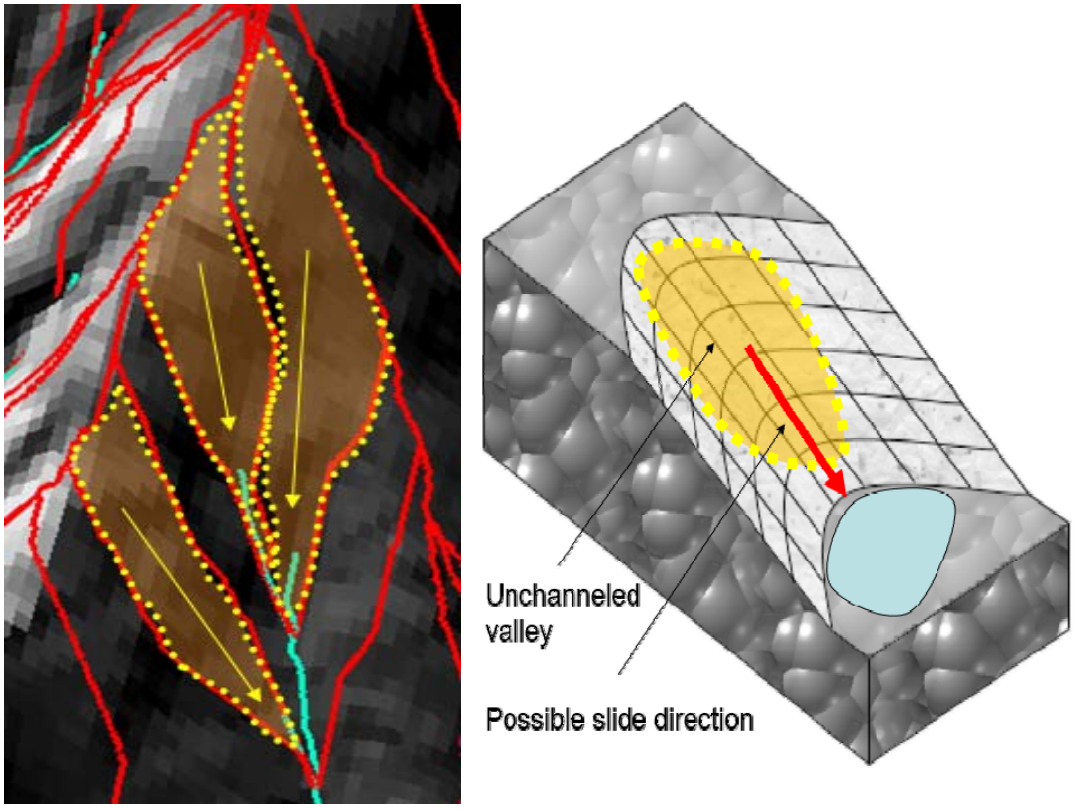

Fig 3.9. Un-channeled valleys (dotted yellow lines) and slide directions

3.4 A NEW SLOPE UNIT IDENTIFICATION METHOD

As mentioned above, several problems occur in the mapping of slope units, and the accuracy of division has challenged researchers. Thus, this study proposes a new method of identifying slope units in order to improve the accuracy of identification and provide a basis for assessing slope stability.

The proposed method uses stream lines instead of valley lines to conjoin ridge lines, which consists of three steps: 1) preparing a topography with ensured delineations of basins and streams; 2) using Arc Hydro tools to detect stream lines instead of valley lines; (3) extracting catchments (ridge lines) based on the previous process; (4) identifying slope units by cutting catchment areas with stream lines.

3.4.1 TOPOGRAPHY DATA PREPARING

The process of preparing topography data is shown in Fig 3.10. In usual conditions, the topography is prepared by a contour map that is composed of extracted polyline files, as shown in Fig 3.11. The polylines are the direct description of the terrain but cannot be used directly in slope stability assessment because they do not intersect and cannot form slope faces. The first step is to transform the polygon files into a triangulated irregular network (TIN) map using the TIN tool feature in GIS. The TIN model shown in Fig. 3.12 has already been applied. Because of the nature of the data storage technique, data analysis is not easy to program or quick to perform. Thus, it is necessary to transform TIN into a raster type (DEM) by using the TIN to Raster tool, as shown in Fig 3.13.

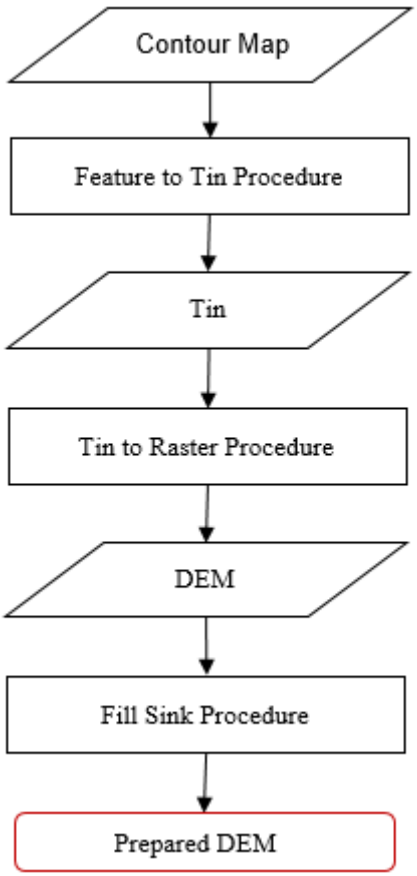

Fig 3.10. Process of preparing elevation data (DEM)

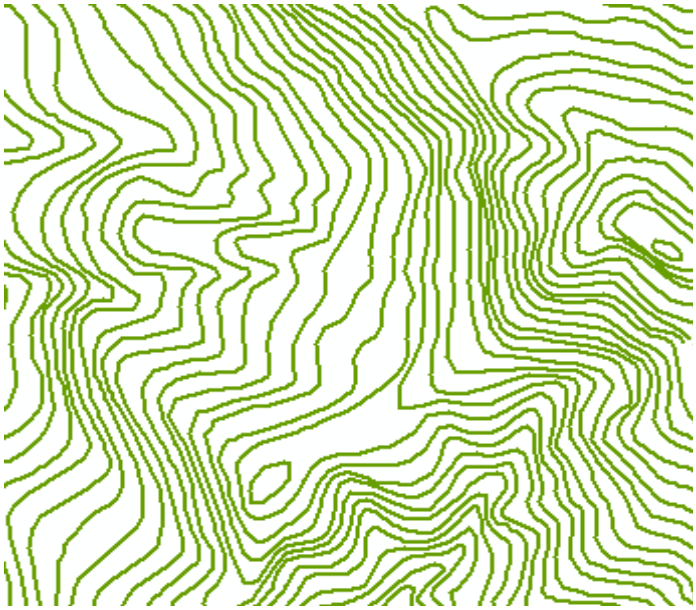

Fig 3.11. Contour map (Extracted polyline file)

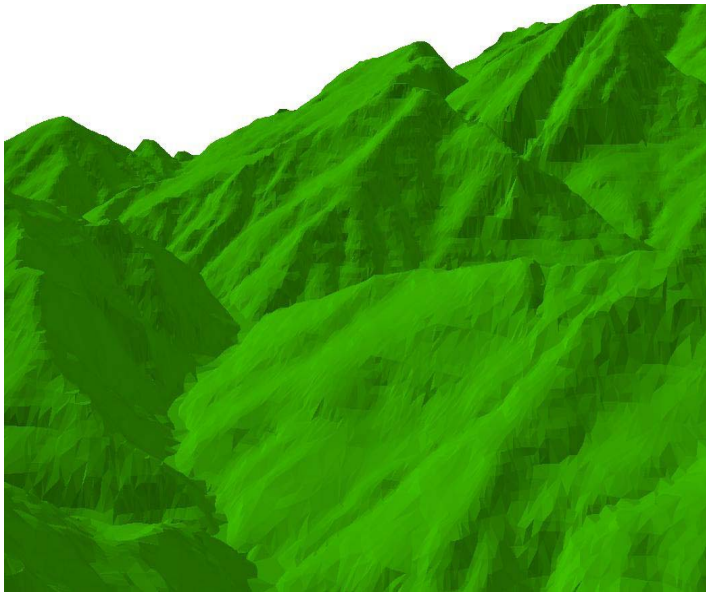

Fig 3.12. Slope presented by the TIN model

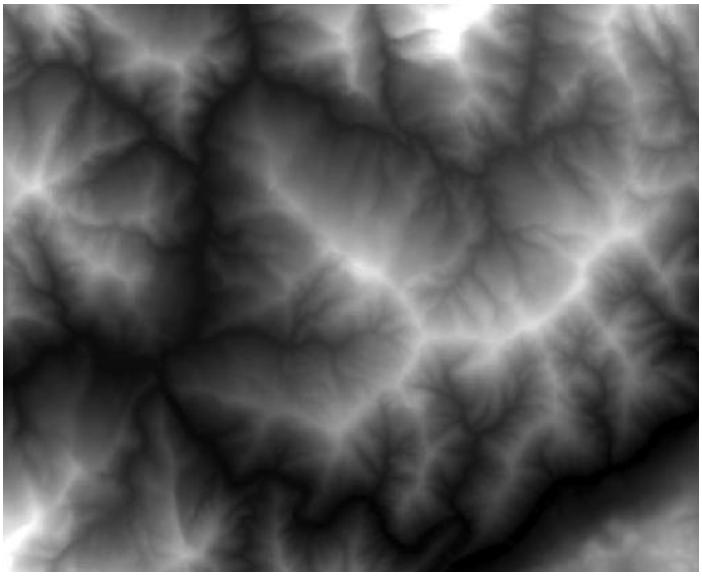

Fig 3.13. Topography of raster data represented by greyscale image

Because random errors may occur in the field investigation or in the interpolation of elevation data, the fill sink procedure is required to ensure the proper delineation of basins and streams in the obtained DEM. For example, a cell elevation may be extremely low among the surrounding topography. Thus, a derived drainage network will be discontinuous without pre-processing (Fig 3.14). Thus, the fill sink procedure resets the illegal pixels according to surrounding elevations.

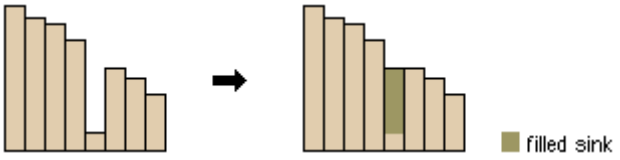

(a) Profile view of a sink before and after running Fill

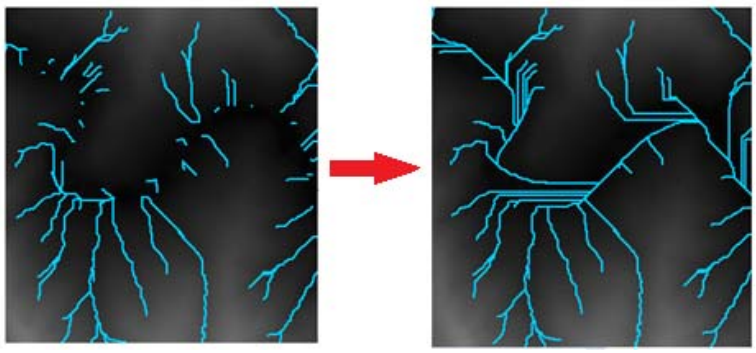

(b) Vertical view of stream link before and after running Fill

Fig 3.14. Views before and after the fill sink process

3.4.2 STREAM LINES DETECTING

The detection of stream lines requires the combination work of GIS-based hydrologic analysis tools, including flow direction, flow accumulation, stream definition, stream definition and raster to polyline procedures. The process is shown in Fig 3.15.

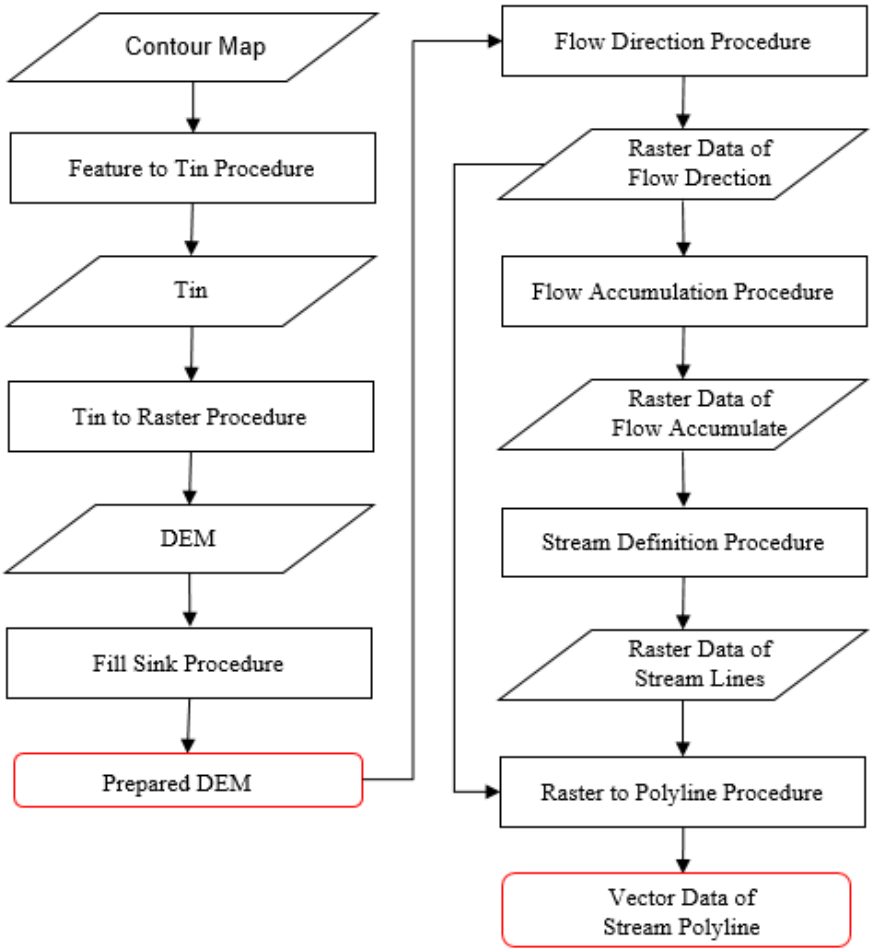

Fig 3.15. Process of stream lines detecting using hydrologic analysis tools

FLOW DIRECTION

To determine the steepest gradient direction (aspect) of a certain cell, the difference in elevations among the surrounding cells to eight altitudes is calculated with the inclination angle. An example of the steepest gradient direction of each cell is shown in Fig 3.16: (a) represents the elevation data from DEM, and (b) shows the values represent the directions of eight aspect. The directions of each cell is stored

as (c), and the impression of steepest gradient direction is shown in (d).

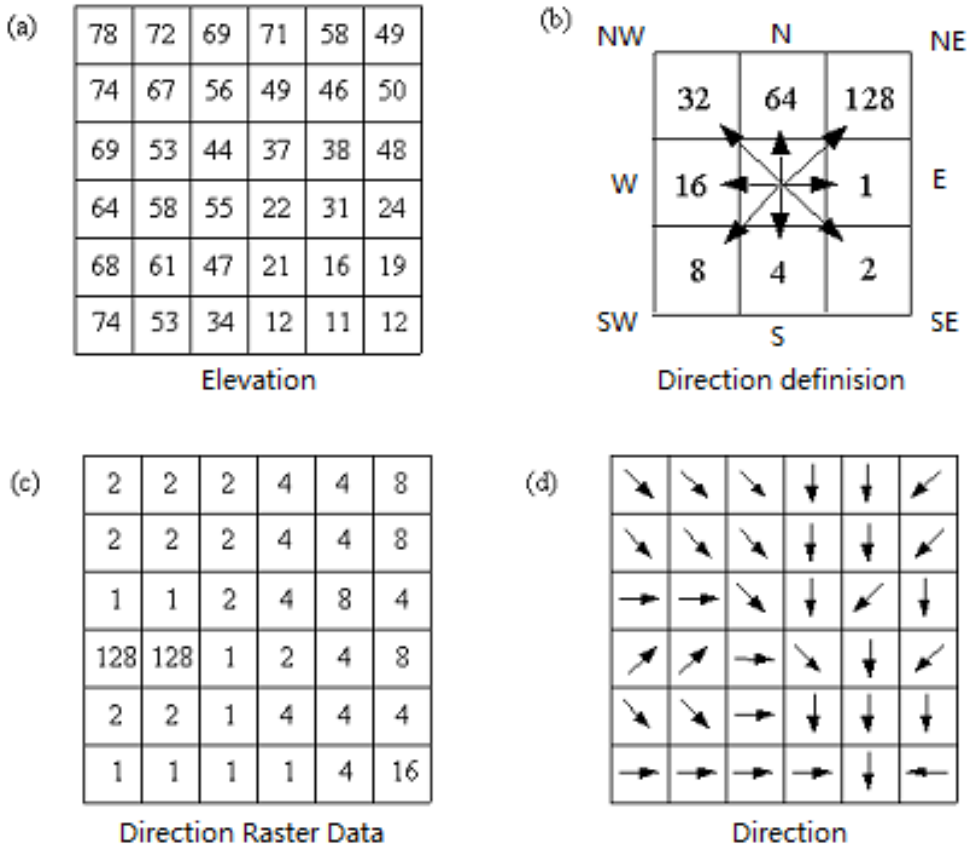

Fig 3.16. Flow direction procedure (from ESRI)

FLOW ACCUMULATION

By linking the direction of each cell, the flow paths of a digital terrain can be derived. For each cell in the input flow direction grid, a flow accumulation grid is then computed to contain the accumulated number of cells upstream of the cell.

It is supposed that in flow accumulation, there is one unit of water in each cell of the raster data, and the accumulated flow of each cell along the flow directions is calculated. Fig 3.17 shows the process of calculating flow accumulation through flow direction. For example, G_{mn} represents the cell at row m, column n. G_{42} has 0 units of water because no cell flows into it, and G_{32} has 3 units of water because it receives water from G_{41}, G_{31}, and G_{21}. G_{22} has 1 unit of water because it receives water from G_{11}. G_{33} receives water from three cells: G_{42}, G_{32} and G_{22}, $3+G_{42}+G_{32}+G_{22}=7$; therefore it has 7 units of water.

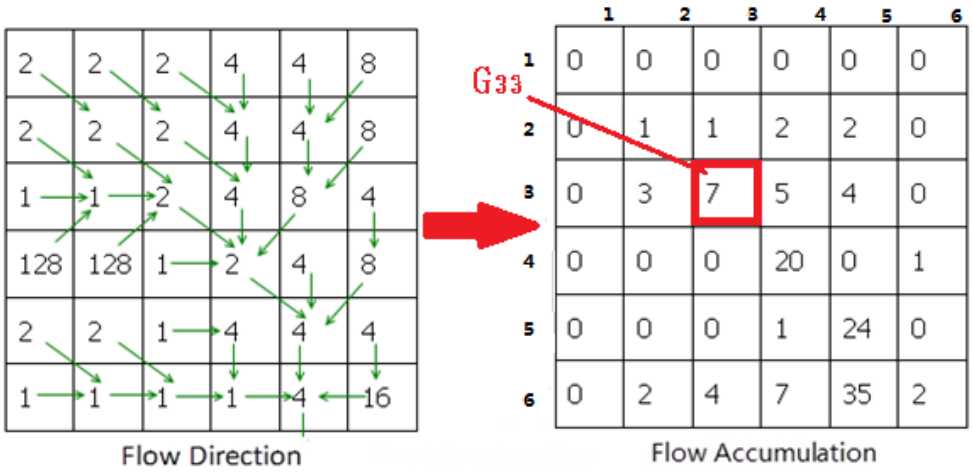

Fig 3.17. Flow accumulation procedure

STREAM DEFINITION

By connecting the center points of cells according to the direction and accumulation results of the water flow, it is possible to extract the drainage line. Because there are a variety of streams at different levels in mountainous area, it is necessary to determine the number of cells to be included, which indicates the stream level obtained. In other words, the minimum number of cells to be included in a stream is represented as the minimum aggregate value of the flow in the drainage line origin. In Fig 3.18, for example, 7 is set as the threshold. All cells larger than 7 are then extracted to indicate the flow links (blue lines), and the results are stored as raster data.

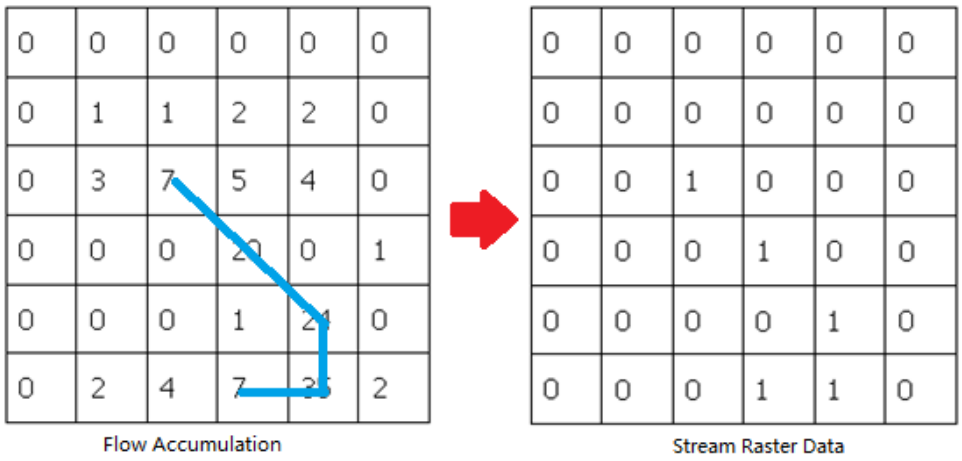

Fig 3.18 Stream definition procedure

RASTER TO POLYLINE

The raster to polyline procedure changes the raster data of stream lines into the vector data of polylines. Thus, the vector data of the stream lines is ready to be used.

3.4.3 CATCHMENTS (RIDGE LINES) DETECTING

The detection of catchments (ridge lines) needs a combination of GIS-based hydrologic analysis tools, including stream segmentation, catchment grid delineation, and raster to polygon procedures. The process is shown in Fig 3.19.

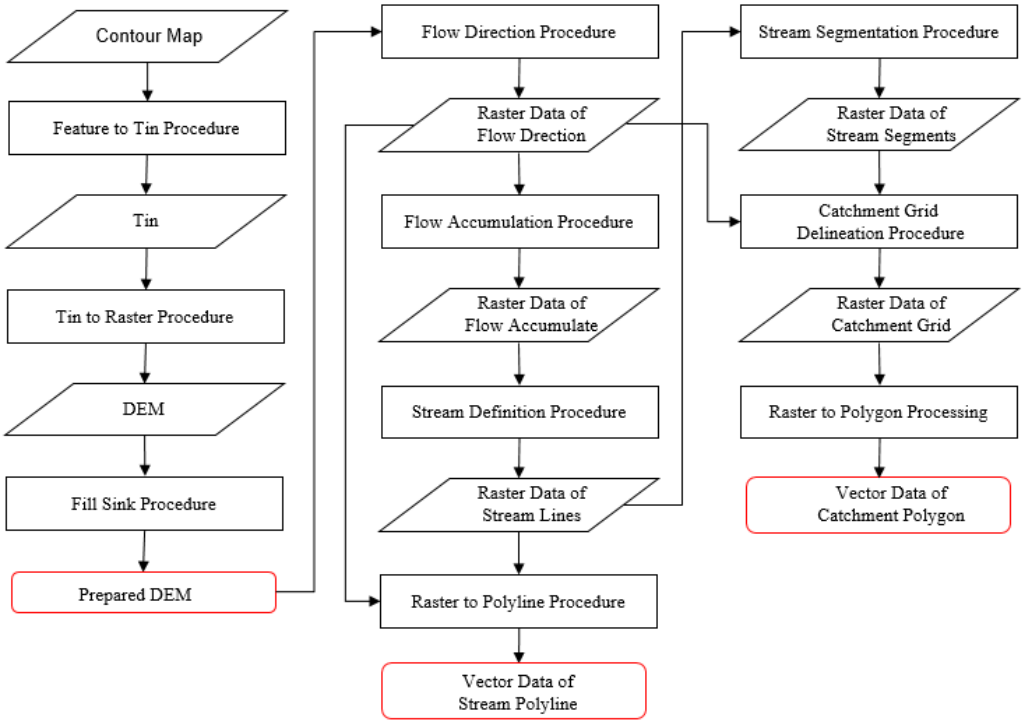

Fig 3.19. Process of catchment detection using hydrologic analysis tools

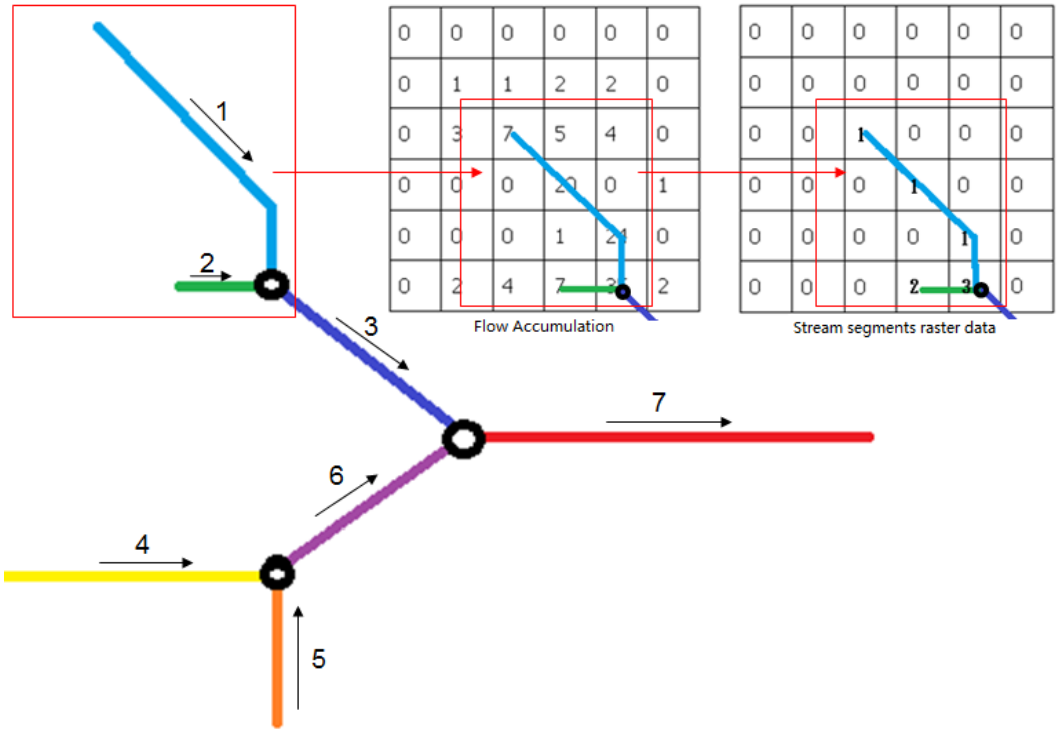

Fig 3.20. Stream segmentation procedure

Note: The colored lines represent stream segments; the black points represent conjoint points.

STREAM SEGMENTATION

When the conjoint point of stream lines is detected, the stream link is divided into stream segments. Two branch streams flow together into one mother stream at a conjoint point, which is represented in Fig 3.20 as a black circle. The stream link is then divided by the number of conjoint points and each segment is assigned an index number (stream code). Finally, raster data are created to store the stream segments using its indexes. Each segment indicates the pooling of a watershed area.

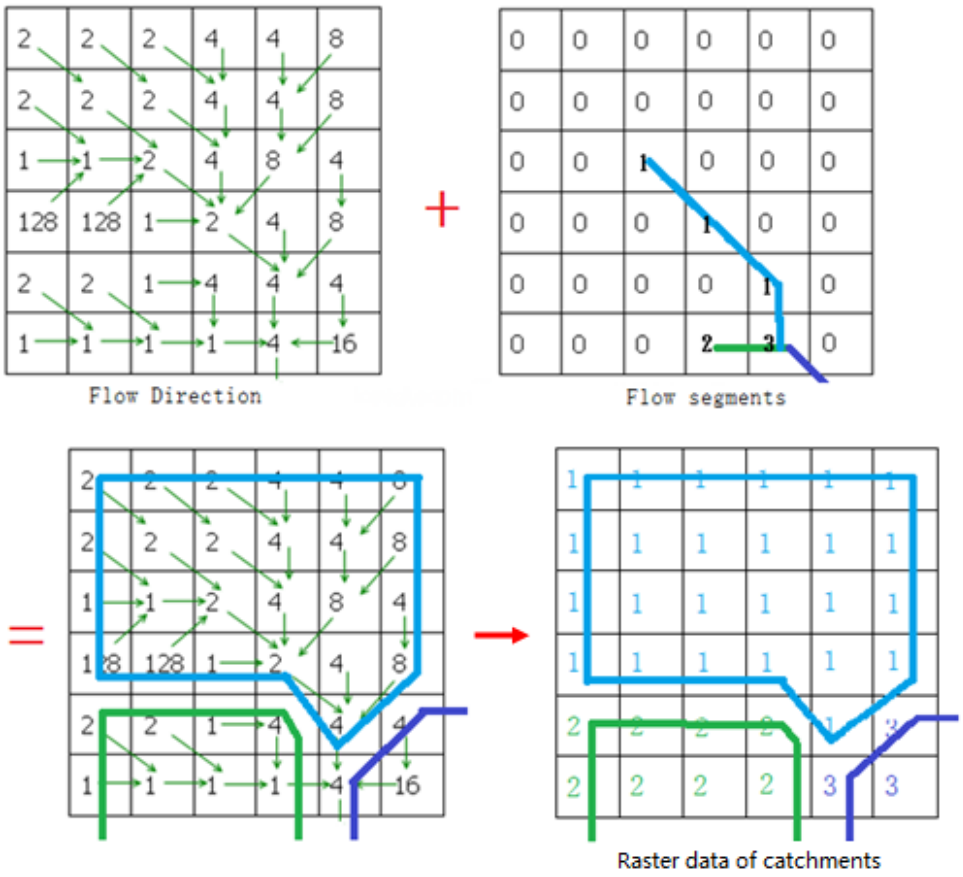

Fig 3.21. Catchment delineation procedure

CATCHMENT GRID DELINEATION

According to the flow direction data, the map is divided into catchment using stream segments. Within one catchment, all the cells flow towards one stream segment, and each cell carries an index value (grid code) indicating to which catchment (watershed area) the cell belongs. The value corresponds to the index carried by the stream segment that drains this catchment. Finally, raster data are created to store the catchment using its indexes (Fig 3.21).

RASTER TO POLYGON

The raster to polygon procedure changes the raster data of catchments into vector data of polygon. Thus, the vector data of catchments are ready to be used. (Fig 3.22). The attributes of each feature in the vector data record an assigned index number and neighbor relations.

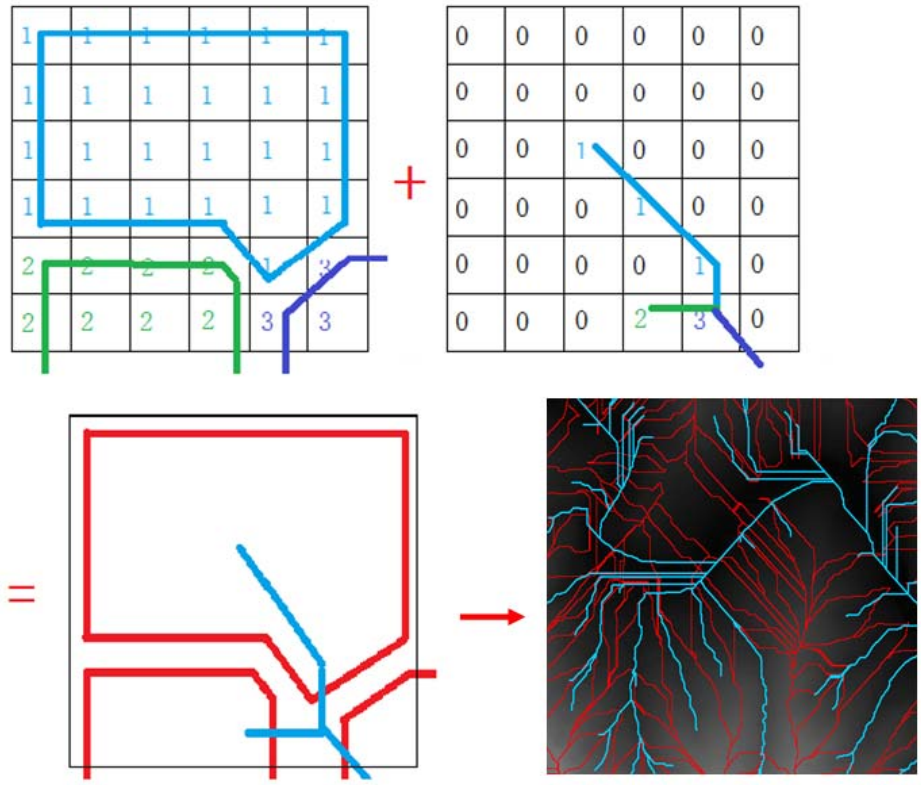

Fig 3.22. Stream lines and catchment areas transformed into vector formation

3.4.4 SLOPE UNIT DIVISION

An example of slope unit division by stream lines is shown in Fig 3.23. By using the union tool within GIS, the catchments corresponding to the first-degree flows (marked with ①, ②, ③) are left as slope units, and the catchments corresponding to the subsequence-degree flows (marked with ④, ⑤) are split by stream flows and saved as slope unit pairs.

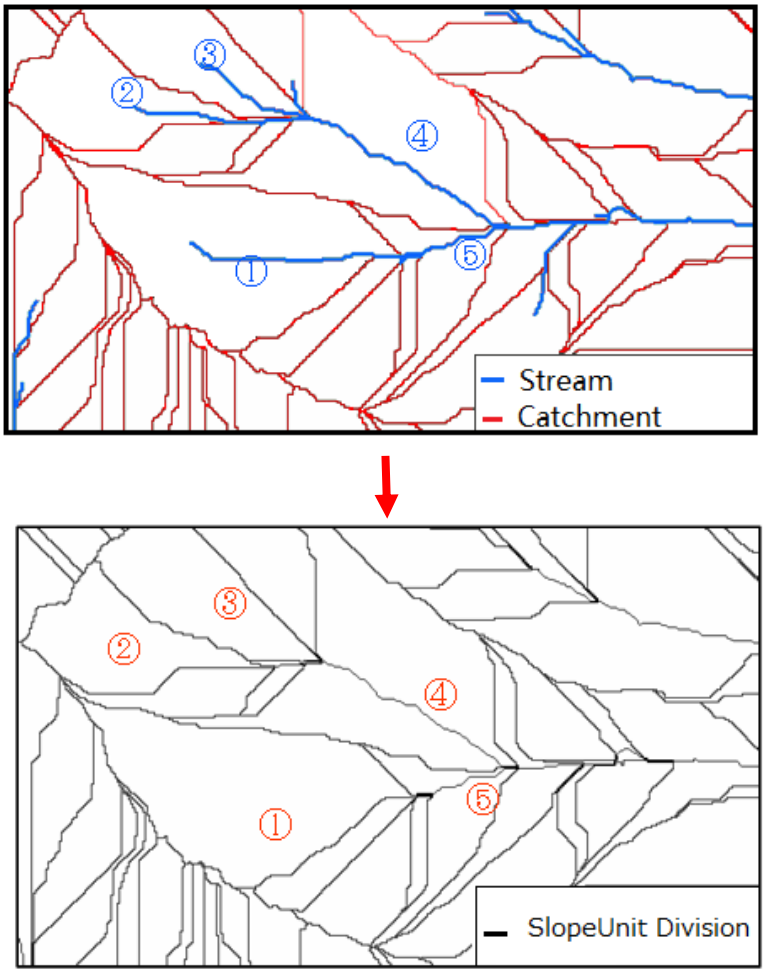

Fig 3.23. Slope unit identification

Therefore, the problem of inaccurate division in hill top areas is avoided, and the problem of bad intersections is improved. Regarding the improper division of slope units, in this process implements reasonable partitions, which is important in the analysis of 2-D stability analysis, which will be performed in the next chapter.

3.5 COMPARISON

To validate the improvements of the new method, an example area is selected and identified with the same number of slope units in both the new method and the existing method. The results are shown in Fig 3.24.

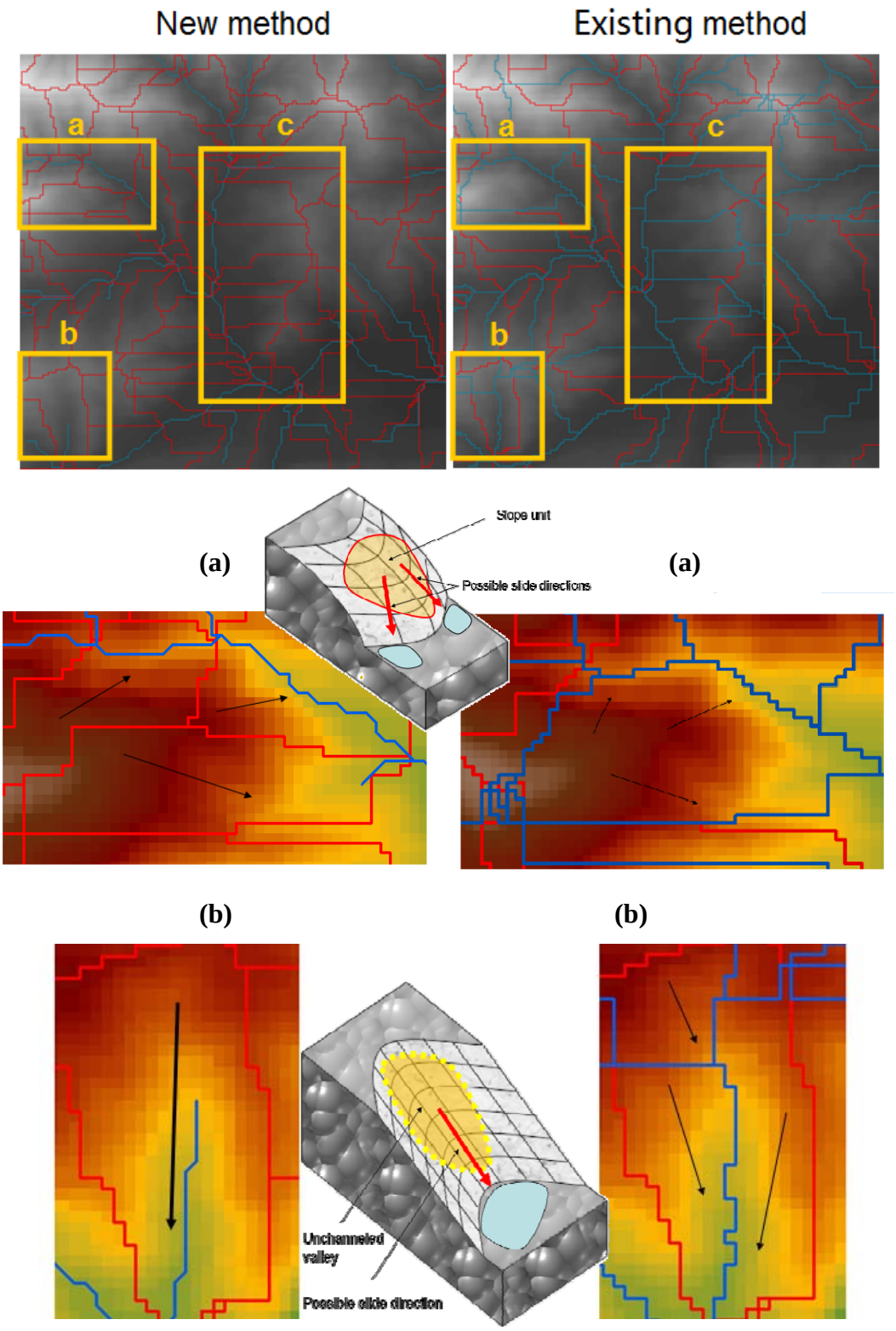

Fig 3.24. Comparison of slope unit identification methods

In Fig 3.24(a), three different possible slide directions are not distinguished in the common method, but they are divided into three slope units in the new method. In addition, many small pieces of slope units in the common method do not appear in the new method.

On the other hand, as shown in in Fig 3.24(b), the three different possible slide directions detected in the common method are actually revised along the drainage channel if the slide has a relatively large scale, compared with the whole slope unit. Thus, the new method keeps the origin of the flow in one slope unit.

In case of a wide hillside as shown at Fig 3.24(c), the new method divides the area into convex slope units while the existing method divides into concave slope units. The new one provides reasonable slope units partition to detect possible slope slide directions.

It can be concluded that the proposed method for identifying slope units is rational and matches the possible slide directions better than the common method does.

3.6 SUMMARY

The GIS utilities of the topography process is introduced, and the problems encountered in the common method of identifying slope units are discussed and classified as follows: 1) inaccurate division at hill top area; 2) mismatched valley lines and ridge lines; 3) undetected multiple possible slide direction; and 4) erroneous division of flow origin area.

A new identification method is proposed to solve the above problems. The method includes the following processes: 1) preparing topography data; 2) detecting stream lines; 3) detecting catchments; and 4) dividing slope units.

Finally, the improvements of the new method are validated in a sample area. The results showed that the proposed method divides slopes rationally, and matches the possible slide directions better than the common method does.

REFERENCES

Ayalew L, Yamagishi H, 2005, The application of GIS-based logistic regression for

landslide susceptibility mapping in the Kakuda-Yahiko Mountains, central Japan. In: Geomorphology, 65, p.15-31.

Bonham Carter G. F, 1994, Geographical Information Systems for Geoscientists: Modeling with GIS. Tarrytown, NY: Pergamon Press.

Carrara A, Cardinali M, Detti R, Guzzetti F, Pasqui V, Reichenbach P, 1991, GIS techniques and statistical models in evaluating landslide hazard. In: Earth Surface Processes and Landforms, 16, p.427-445.

Carrara A, Cardinali M, Guzzetti F, Reichenbach P, 1995, GIS technology in mapping landslide hazard, in: Geographical Information Systems in Assessing Natural Hazards, The Netherlands, p.135-176.

Carrara A, Crosta G. B, Frattini P, 2008, Comparing models of debris-flow susceptibility in the alpine environment, Geomorphology, 94, 353-378.

Dai F. C, Lee, C. E, Ngai Y. Y, 2002, Landslide risk assessment and management: an overview. In: Engineering Geology, 64, p.65-87.

David, R. M. 2002. In Arc Hydro: GIS for Water Resources, ESRI Press, Redlands, CA.

Guzzetti F, Carrara A, Cardinali M, Reichenbach P, 1999, Landslide hazard evaluation: a review of current techniques and their application in a multiscale studym, Central Italy. In: Geomorphology, 31(1-4), p.181-216.

Murat E, 2008, An Overview on the Landslide Susceptibility AssessmentTechniques. In: 1st WSEAS International Conference on environmental and geological science and engineering, Malta, September 11-13.

Safaei M, Omar H, Huat B. K, Yousof Z. B. M, Ghiasi V, 2001, Deterministic rainfall induced landslide approaches, advantage and limitation. In: Electronic Journal of Geotechnical Engineering, p.1619-1650.

Soeters R, van Westen C. J, 1996, Slope stability recognition, analysis, and zonation application of geographical information system to landslide hazard zonation. In: Turner, A.K., Schuster, R.L., (Eds.), Landslides: Investigation and Mitigation. Sp.-Rep. 247, Transportation Research Board, National Research Council. National Academy Press, Washington, D.C, p.129-177.

van Westen C. J, Terlien M.T.J, 1996, An approach towards deterministic landslide hazard analysis in GIS : a case study from Manizales, Colombia. In: Earth surface processes and landforms, 21(9), p.853-868.

Xie M, Esaki T, Zhou G, Mitani Y, 2002, Three-dimensional stability evaluation of landslides and asliding process simulation using a new Geographic Information Systems component. In: Environmental Geology, p.1-24.

CHAPTER 4

THE DEVELOPMENT OF A NEW MAPPING APPROACH FOR A LANDSLIDE HAZARD MAP

4.1 INTRODUCTION

After identifying slope units, the second step in predicting a landslide dam is the extraction of landslide prone slopes. As argued in chapter 1, a landslide hazard map is very useful in cutting the earthquake induced geo-disaster chain because the map shows the landslide prone slopes and the local government can take preventive measures to strengthen those slopes before an earthquake occurs. The landslide hazard map also shows whether the slopes with high susceptibility collapsed immediately after an earthquake. Then the landslide debris and loose deposits can be transferred at an early stage to avoid the occurrence of a landslide dam or debris flow.

In previous studies, a deterministic approach of infinite slope method is well received because it predicts the landslide through slope stability analysis. It can be easily implemented and managed in grid mapping units. The infinite slope method assumes that the slope is extended infinitely in all directions and slide occurs along a plane parallel to the face of the slope (Taylor, 1948). Therefore, the calculations can easily be performed in GIS by calculating the stability of each individual pixel or cell in grid cell division, and ignoring the influence of its neighbors (Van Westen

et al., 1997). Due to its simplicity, fast calculation, and easy programming, many researchers have selected this method to analyze the deformation and failure of slopes (Fukuzono, 1985; Michiue and Fujita, 1990; Masashi, 2012). It has become the most the most commonly used approach (Hammouri et al., 2008).

However, the infinite slope method cannot accommodate the complex data of geometry, stratum, and groundwater, which vary in space even along a short distance. In most cases, the method is used for a probabilistic analysis combined with Monte Carlo simulation. Furthermore, the scale of the landslide with slip surface and volume information cannot be obtained from a one-dimensional method. Knowledge of the latter is essential in studying the domino effect of disasters and predicting landslide-dam hazards.

On the other hand, as the most common type of numerical analysis in geotechnical engineering, analysis of stability usually takes the slip surface to be an arc and divides the sliding mass into slices (a two-dimensional [2D] model). Although it is not difficult to grasp, no studies produce a hazard map using a curved slip surface because the solution is needed to determine the cross sections of runout paths over a wide area. In addition, the 2D model is easily achieved in much powerful software for an individual slope stability analysis, but it is difficult to do so in GIS for landslide hazard mapping over a wide area.

Thus, this chapter aims to propose a new mapping approach for developing a landslide hazard map using the 2D model. First, a solution for slope cross section extracting is developed. Then, the 2D model is achieved in a GIS environment by applying a trial procedure involving many possible slip surfaces, and the trial slope surface with the lowest safety factor is deemed the governing or critical slip surface. In addition, the seismic force is considered in slope stability analysis. Finally, the GIS module of stability analysis using 2D model is developed. Practical applications show that the new hazard mapping method can carry out accurate stability analysis and predict possible slide scales and sliding mass volume.

4.2 A NEW MAPPING APPROACH USING 2D SLOPE STABILITY ANALYSIS

To achieve a hazard mapping of landslides using 2D stability analysis, first, a cross section will be extracted to represent a slope shape, and then the slip surface will be assumed several times to seek the critical slip surface with the minimum safety factor result. A solution for cross section extraction is developed within a GIS environment. Since the mapping approach is applied over extensive areas, the effectiveness of stability calculation is the fundamental problem for general utility.

This study chooses the Swedish method for safety factor completing and the slip surface is assumed as a circle shape searched with different positions of center point O and radii R. As the earthquake-induced landslide is the study target, seismic force will also be considered in the stability analysis.

4.2.1 EXTRACTION OF THE SLOPE CROSS SECTION

Following the proposed identification method of slope units in chapter 3, many concave slope units can be derived. A possible landslide is assumed to have a relatively large scale compared to the slope unit and can offer enough mass rushing down through the drainage. Therefore, the tendency of a landslide is to go along the flow line, from the top to the bottom.

As shown in Fig 4.1, the elevations within a slope unit range from the higher ridge barrier to the lower valley barrier. The longest drainage line that can be derived within a slope unit is a link between the highest point and lowest point. Therefore, by creating a linking line between the highest point and lowest point, a sample model of a 2D slope can be extracted from the Digital Elevation Model (DEM) for slope stability analysis.

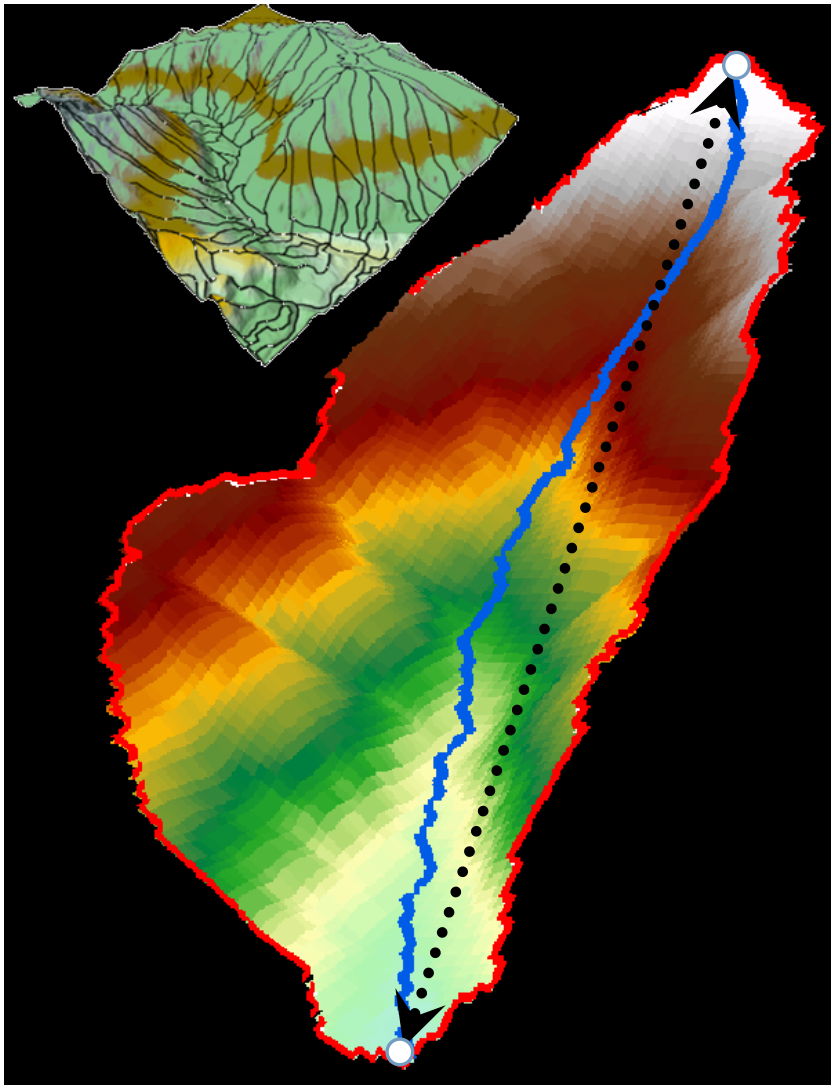

Fig 4.1. An approached slope from slope unit division.

Note: The blue line represents the longest drainage line; the black dotted arrow line represents the link between the highest point and the lowest point.

This study first states the elevations within each slope unit. Then, by recording the positions of the highest point and lowest point, the cross lines are created with pairs of points. A module is developed in GIS to achieve this procedure.

Since it is assumed as the approximate runout path, the path is extended by 10% and 20% of the total projected length at the top and bottom respectively, in order to include plenty of topography features (see Fig 4.2). Another module is developed in GIS to achieve this procedure.

Later, the Interpolate function of GIS is used to extract the elevation data into the cross line at a given step, such as 1m interval space. As shown in Fig 4.3, each point of the path line stores an elevation data.

Finally, the elevations of the points are arranged within an array to obtain the cross section of a possible landslide, this is essential to carry out 2D stability analysis.

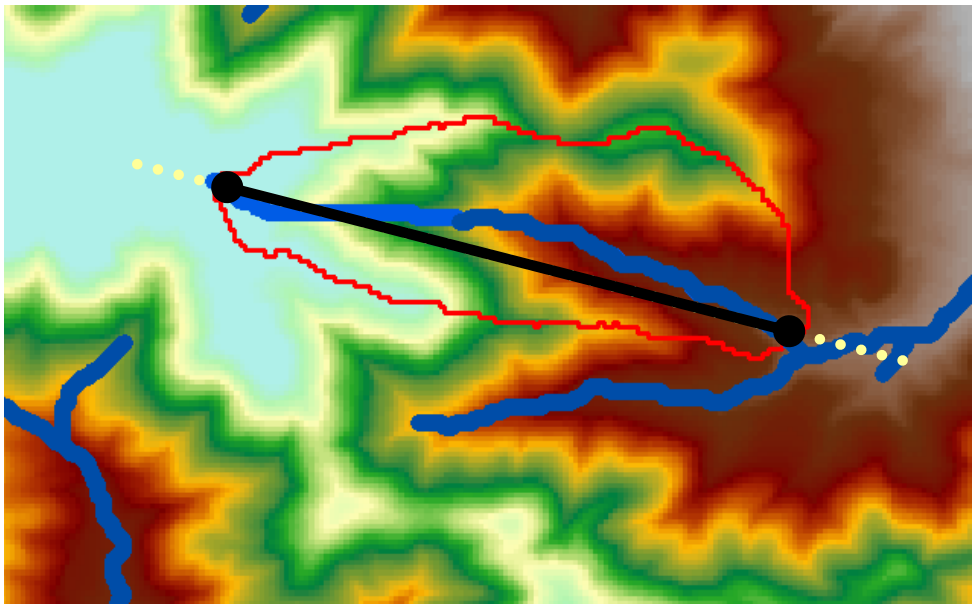

Fig 4.2. Extension of the approximate path by 10% and 20% of the total projected length at its top and bottom respectively.

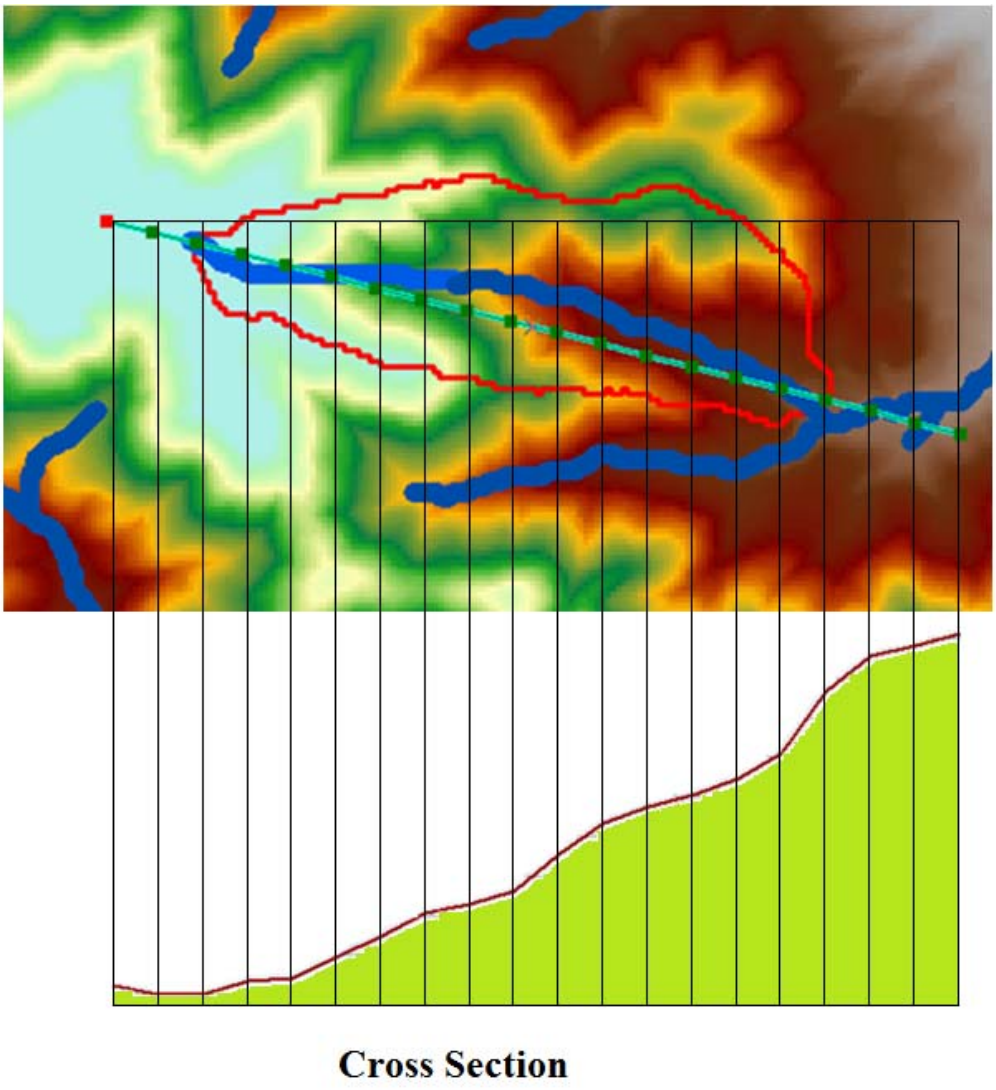

Fig 4.3. Interpolation of the elevation data into the approximate path from DEM and the obtained cross section of a prone slope.

4.2.2 2D SLOPE STABILITY ANALYSIS

Safety factor is one of the key components for the landslide hazard assessment, among which the method of slices is used to analyze the slope stability. In 2D slope stability analysis, vertical planes divide the soil mass above an assumed failure surface into a series of slices. Then, the forces acting on the slices are assessed to evaluate the safety factors of the trial failure surface.

Table 4.1. Method of 2D slope stability analysis.

Method	Factor of Safety (FS)		Interslice Force Assumption (H=horizontal, V=vertical)
	Force Equilibrium	Moment Equilibrium	
(1) Ordinary (Swedish or USBR)	-	Yes	Ignore both H and V
(2) Bishop's Simplified	-	Yes	V ignored, H considered
(3) Janbu's Simplified	Yes	-	V ignored, H considered
(4) Janbu's 'Generalized'	Yes	-	Both H and V considered
(5) Spencer	Yes	Yes	Both H and V considered
(6) Morgestern-Price	Yes	Yes	Both H and V considered
(7) Lowe-Karafiath	Yes	-	Both H and V considered
(8) Corps of Engineers	Yes	-	Both H and V considered

However, the problem is statically indeterminate and many different 2D methods have been developed for computing the factor of safety (see Table 4.1). Of all these 2D models, the Swedish method of slices, Bishop's Simplified method, Janbu's Simplified method, and Spencer's method are widely adopted and have become the most commonly used methods.

The differences in those methods are the assumptions on inter slice forces:

1) The Swedish Method ignores inter slice forces (V=H=0),

2) Bishop's Simplified Method assumes inter slice forces are horizontal (V=0, H>0),

3) Spencer's Method assumes all inter slice forces are parallel (V>0, H>0) with an unknown inclination that is computed through iterations.

2D methods are difficult to integrate with a GIS environment because its searching progress of slip surface is difficult to implement over a wide area within GIS. Especially for the nonlinear methods, the safety factor appears at both sides of the equation, so the regression calculation needs to be repeated several times. For this reason and because of its easy computing, the Swedish Slice Method is chosen for slope stability assessment. The slip surface is assumed as a circle shape with different positions of center point O and radii R. The analysis process is coded into a function, which is integrated within GIS platform using C# language.

4.2.3 SEARCHING FOR THE CRITICAL SLIP SURFACE

As we arrange the data in GIS, the cross section is stored as an array of n points of elevation at the same step as projected interval length d. The total projected length L = n*d. In this study, an enumeration algorithm was performed to get a series of trial slip surfaces with various centers of rotation O and radii R.

First, the slope surface is split into two equal parts. Then, 10 head points A are assembled from the upper part and 10 toe points B from the lower part through a simple enumeration algorithm as well as 10 length values of R according to the length of AB. By means of permutation and a combination of their sample groups, 1,000 different slip surfaces were derived for critical slip surface searching. To avoid local limit cycle, the projected distance between point A and B is set as > L/5.

If we take one assumed slip surface as example (Fig 4.4), the known conditions are position order x_{ao} of head point A, position order x_{bo} of toe point B, length r of radii R, and slope surface elevations array E[i] from top point 0 to bottom point n.

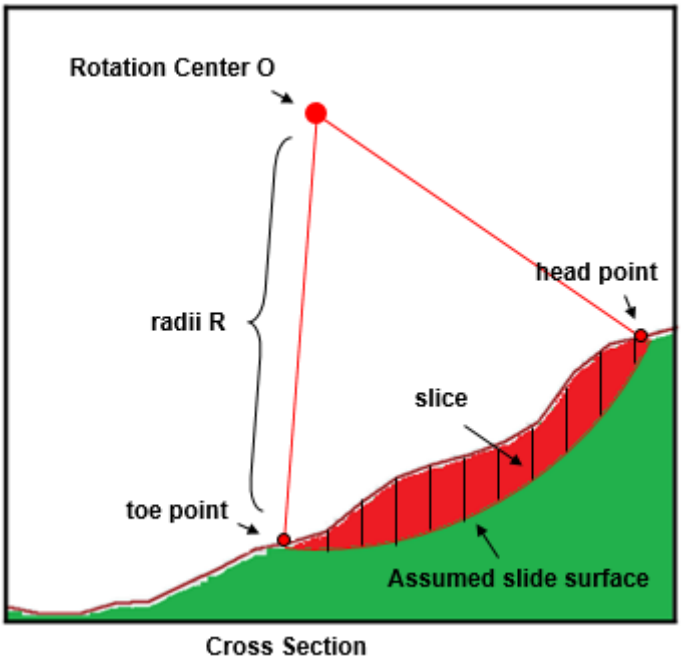

Fig 4.4. An assumed slip surface and sliding mass divided into a series of slices.

Then, the Swedish method is performed to calculate the safety factors of each assumed slide. The minimum safety factor is chosen as the final result, and the corresponding surface is deemed as the critical slip surface.

4.2.4 ASSESSMENT OF AN EARTHQUAKE-INDUCED LANDSLIDE

Earthquake-induced landslides are mainly due to the ground shaking and associated inertial forces. Seismic force with even a very small magnitude may trigger failure in slopes, which are perfectly stable otherwise. As we aim to propose an approach for earthquake-induced landslides in general utility, it is necessary to assess the stability of the slope under seismic conditions. The seismic slope stability is estimated using a pseudo-static approach in this study.

PSEUDO-STATIC COEFFICIENT

Pseudo-static analysis simulates the ground motion as a constant static horizontal force acting in a direction out of the face. The analysis represents the effects of an earthquake shaking by pseudo-static accelerations that produce inertial forces, "f_H" and "fv", which act through the centroid of the each slice. The magnitude of the pseudo-static force is the product of seismic coefficient "k_H" and the weight of the sliding block "W". The value of "k_H" may be taken as equal to the designed Peak Ground Acceleration (PGA), which is expressed as a fraction of the gravity acceleration. The horizontal pseudo-static force decreases the safety factor by increases the driving force and reducing the resisting force (for $\varphi>0$). The effect of vertical accelerations is usually neglected in pseudo-static analyses as the vertical pseudo-static force typically has been thought less influential than the factor of safety. Table 4.1 lists a recommendation for selecting a pseudo-static coefficient (Pyke, 1991).

Table 4.2. Pseudo-static coefficients recommendation (Pyke, 1991).

Magnitude	Recommended k_H
8.25	1/2 PGA
7.5	1/3 PGA
7.0	1/4 PGA
6.5	1/4 PGA

PEAK GROUND ACCELERATION

Peak ground acceleration is a measure of earthquake acceleration on the ground and an important input parameter for earthquake engineering. Systematic reviews by various authors put forward the development of attenuation relations for the peak ground acceleration (see for example, Boore and Joyner, 1982; Campbell, 1985; Joyner and Boore, 1988; Abrahamson and Letihiser, 1989; Fukushima and Tanaka, 1990). The general ground motion model (Bhushan, 2009) of the attenuation relation may be considered as follows:

$$\log(a) = f_1(M) + f_2(r, E) + f_3(r, M, E) + f_4(F) + \varepsilon \qquad (4.1)$$

Where:

a is the peak ground acceleration (horizontal or vertical);

$f_1(M)$ is a function of earthquake magnitude;

$f_2(r, E)$ is a function of earthquake-to-recording site distance and the tectonic environment;

$f_3(r, M, E)$ is a non-separable function of magnitude, distance, and tectonic environment;

$f_4(F)$ is a function of fault type;

and ε is a random variable representing uncertainty in log(a).

Within many attenuation relations, an equation provide by Fukushima (1995) is recommend by the National Institute for Land and Infrastructure Management, Japan. It is also used in this study and is outlined below:

$$\log A = 0.42M - \log(R + 0.012 * 10^{0.42M}) - 0.0033R + 1.22 \qquad (4.2)$$

Where:

A is the horizontal peak ground acceleration in cm/s^2;

M is earthquake magnitude;

and R is the fault-to-recording distance in km.

4.3 DEVELOPMENT OF GIS MODULES

To integrate within the GIS platform, we developed a GIS slope stability analysis module using C# language. All of the above mentioned mathematical models were dealt with in the ArcMap application.

As show in Fig 4.5, we developed an Assessment toolbar with many functions to manage geo-spatial data for hazard assessment. By simply clicking the corresponding buttons, a range of functions can be processed automatically as can be seen in the screenshot below.

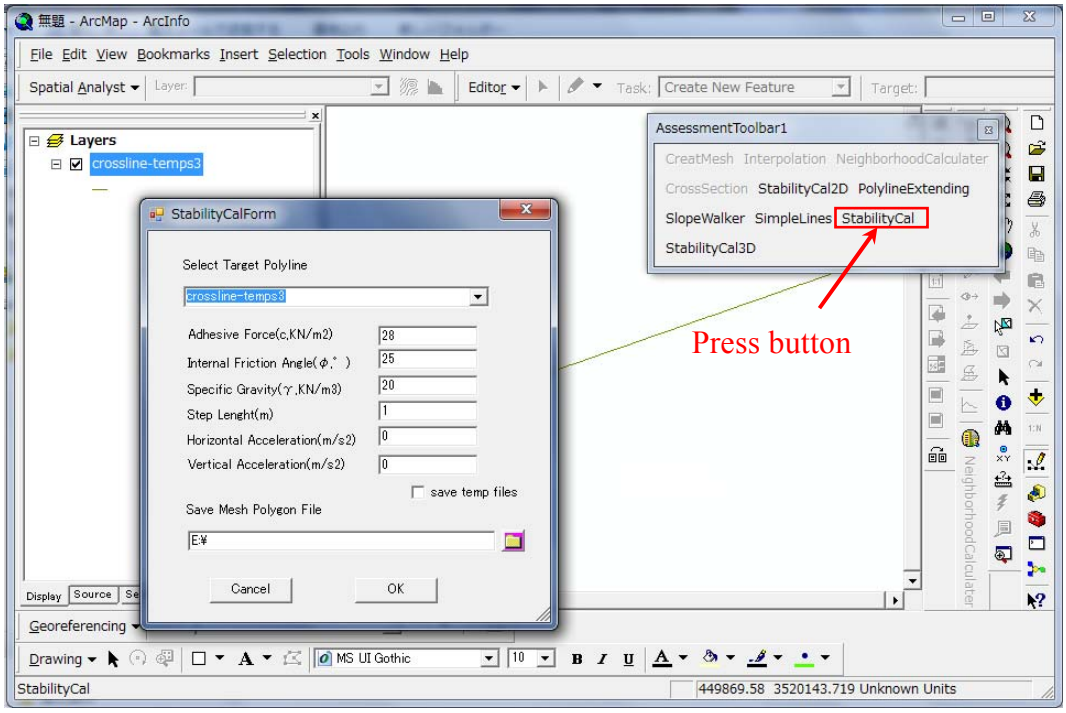

Fig 4.5. Assessment toolbar within the ArcMap application.

4.3.1 CROSS SECTION FUNCTION

This function is developed for the cross line extraction of each slope unit. As mentioned above, the cross line is defined as the link line of the highest point and the lowest point with one slope unit. It is therefore necessary to count the elevations of all the cells of a slope unit. Fig 4.6 shows the process of cross section extraction inherited from slope units division. The slope units division is first translated into raster data.

This function uses the derived raster data and DEM for elevation statistics. An array of declared slope unit recorders with index (grid codes) is used to store elevation and the position of the highest and lowest points. The value from the raster data of the catchment grid indicates the slope index, and the value from the raster of DEM represents the elevation. The algorithm counts each cell sequentially and updates the array with a new record. Later, a new polyline file is created according the positions of start/to points from the recorder array. Each polyline is assigned a corresponding slope index and the other recorded parameters.

Fig 4.6. The process of cross section extraction.

The parameter input form is shown in Fig 4.7, in which the target raster (DEM) and slope unit raster (catchment grid raster) is required.

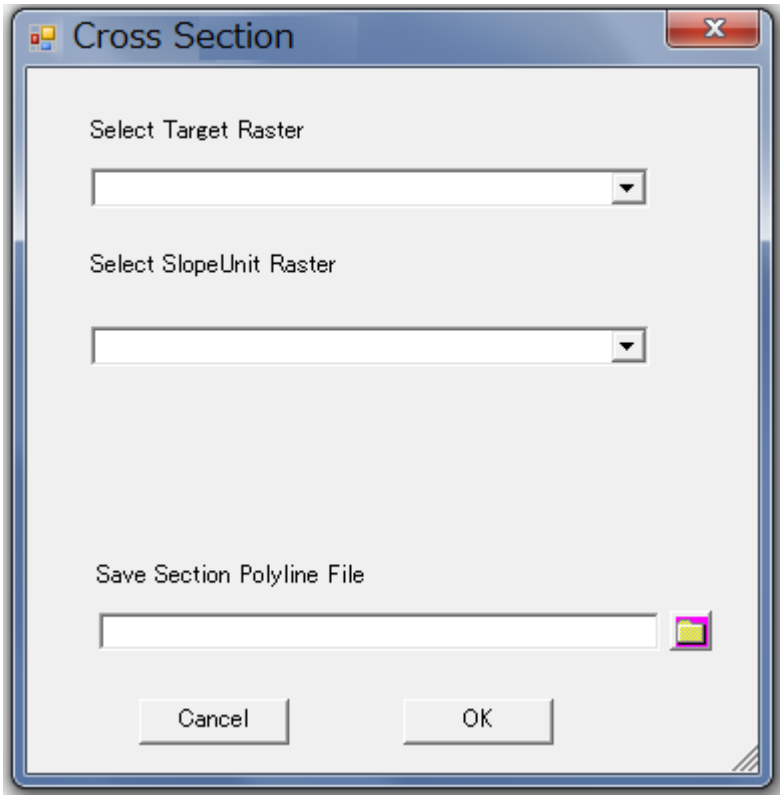

Fig 4.7. The input form of the Cross Section Function.

4.3.2 POLYLINE EXTENDING FUNCTION

To get plenty of topography features of a cross section, it is necessary to extend the cross line by 10% and 20% of the total projected length at the top and bottom respectively. Thus, the polyline extending function is developed to enhance the ability of polyline processing.

This function first counts the total length of each polyline within vector data, and it detects the start/to direction. Then, it computes the updated point at a given distance. Finally, the derived new polylines are stored in a new vector file.

The parameter input form is shown in Fig 4.8, in which the target vector data of polyline is required. The extended direction can be chosen manually and the extended distance can be assigned by meters or by a percentage of the total length of the original polyline.

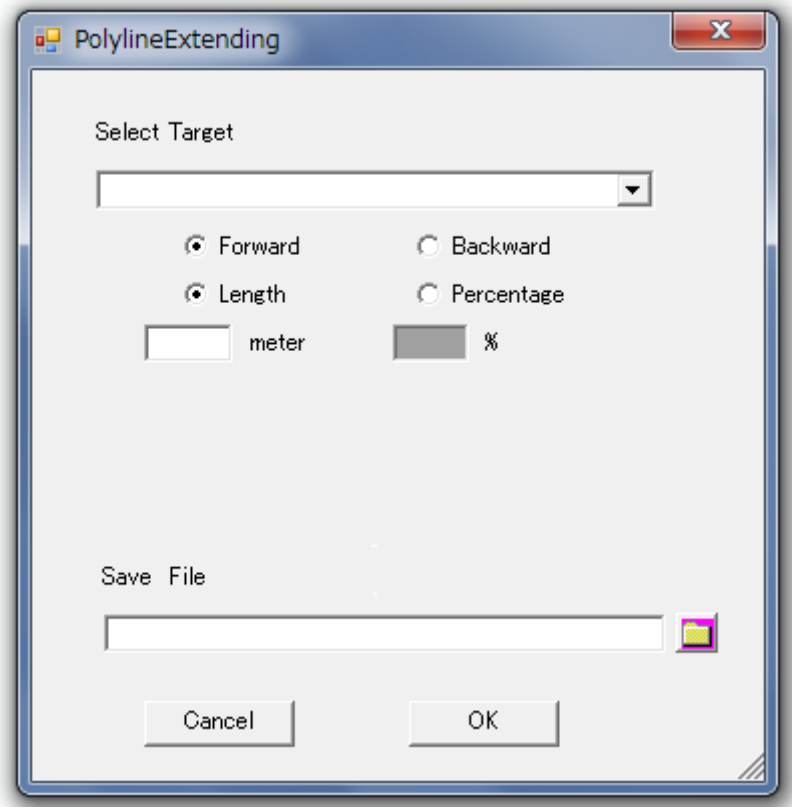

Fig 4.8. The input form of the Polyline Extending Function.

4.3.3 STABILITY CALCULATION FUNCTION

To obtain the critical slip surface with the minimum safety factor, this function contains two components: slip surface computing and stability computing.

SLIP SURFACE COMPUTING

As outlined above, an enumeration algorithm was performed to get a series of trial slip surfaces with various centers of rotation O and radii R. Then, the GIS module needs to compute the elevation of every trail slip surface to get ready for slope stability analysis.

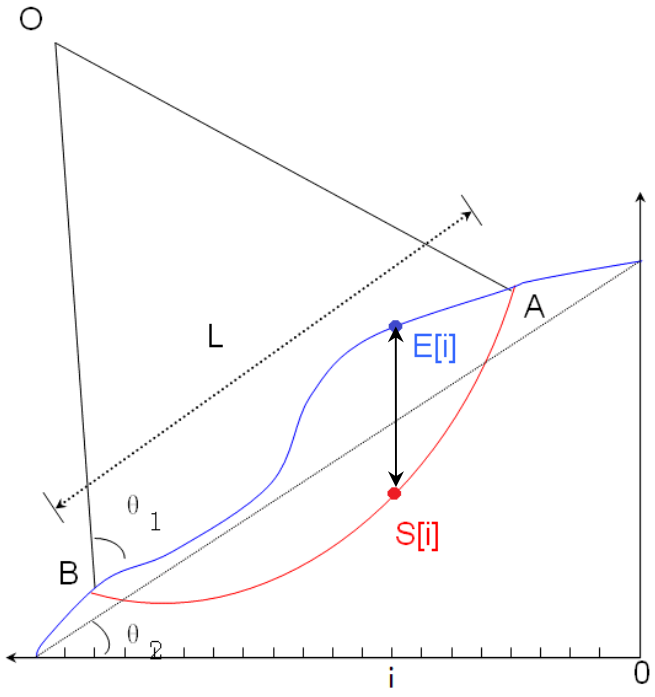

Fig 4.9. An assumed slip surface.

Note: E[i] is the elevation array of slope surface and S[i] is of the slip surface.

From the known conditions of one assumed slip surface (x_{ao}, x_{bo}, r, E[i]), as shown in Fig 4.9, the elevation of y_a and y_b of A and B can be derived as:

$$y_a = E[x_{ao}] \tag{4.3}$$

$$y_b = E[x_{ao}] \tag{4.4}$$

By defining the pixel cell length as l_P, the real positions of point A, B is:

$$x_a = x_{ao} * l_P \tag{4.5}$$

$$x_b = x_{bo} * l_p \tag{4.6}$$

Thus, the length L of line AB can be derived by:

$$L = \sqrt{(x_a - x_b)^2 + (y_a - y_b)^2} \tag{4.7}$$

Here, we define angle θ_1, θ_2 as:

$$\theta_1 = \arccos((L / 2) / r) \tag{4.8}$$

$$\theta_2 = \arctan2(y2 - y1, x2 - x1) \tag{4.9}$$

Thus, the position x_o, y_o of center point O can be derived by:

$$x_o = x_a * l_P + r * \cos(\theta_1 + \theta_2) \tag{4.10}$$

$$y_o = y_a + r * \sin(\theta_1 + \theta_2) \quad (4.11)$$

Finally, the slip surface elevation array S[i] can be derived by:

$$S[i] = y_o - \sqrt{r^2 - (i * l_P - x_o)^2} \quad (4.12)$$

SLOPE STABILITY COMPUTING USING THE SWEDISH METHOD

The Swedish solution (Fellenius, 1927 and 1936) is the earliest solution for the method of slices, which is included in the syllabus of many soil mechanics courses and many design codes for practicing engineers. Turnbull and Hvorslev (1967) first suggested it to analyze slope stability in the 1960s. The following equation for Fs is commonly found in the textbooks and literature on soil mechanics for analyzing slope stability using the Swedish solution:

$$Fs_{2D} = \frac{\sum_{i=1}^{n} [(W_i \cos\alpha_i - \mu_i l_i) \tan\varphi_i + c_i l_i]}{\sum_{i=1}^{n} (W_i \sin\alpha_i)} \quad (4.13)$$

Where:

n denotes the number of slices;

W_i denotes the weight of i^{th} slice;

α_i denotes the inclination of the base of i^{th} slice to the horizontal direction;

μ_i denotes total water pressure at the base of i^{th} slice;

l_i denotes the length of the base of i^{th} slice;

φ_i denotes the angle of internal friction at the base of of i^{th} slice;

c_i denotes the cohesion at the base of i^{th} slice;

and l_i is the length of the sliding surface of each slice.

While we deal with the homogeneous assumed slope, the equation of the safety factor can be simplified as:

$$Fs_{2D} = \frac{\sum_{i=1}^{n} W_i \cos\alpha_i \tan\varphi_i + \sum_{i=1}^{n} c_i l_i}{\sum_{i=1}^{n} (W_i \sin\alpha_i)} \quad (4.14)$$

The term Wi can be derived by:

$$Wi = (E[i] - S[i]) * \gamma * l_P * w \quad (4.15)$$

Where:

γ denotes the unit weight in kN/m^3;

and w denotes the thickness of the cross section in m.

Bishop (1955) demonstrated that conservative results might be obtained because the effective normal stress at the base of the slices may decrease to a negative value with an increasing inclination or water pressure. Whitman and Bailey (1967) presented that the discrepancy of the computed results can be as high as 60%. Duncan and Wright (1980) compared the minimum safety factor calculated by different methods of slices and showed that the differences between the Swedish method and other rigorous methods of slices can be as high as 50%.

However, in a wide area assessment, the 2D models will be simple enough to calculate and easy to manage. Most of other rigorous methods make the safety equation nonlinear, which means FS appearances on both sides of the equation. Thus, a regression algorithm is required to solve the equation, which relies on computing power and is extremely time costly if we apply it to slopes over an enormous area. Therefore, the Swedish method is still a recommended solution and we insist on using it for general utility.

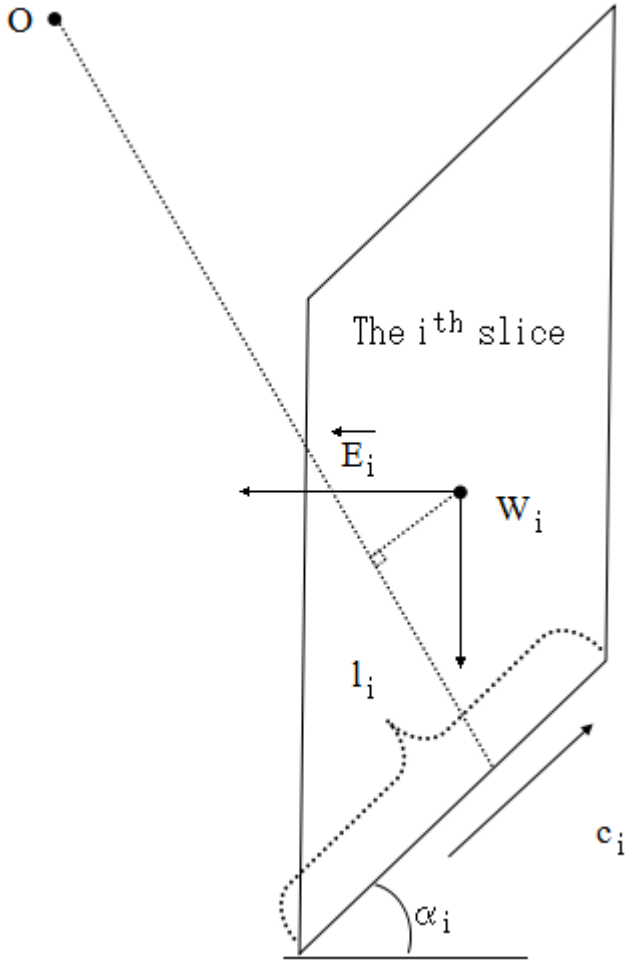

Fig 4.10. The ith slice ignoring water pressure.

SLOPE STABILITY COMPUTING UNDER SEISMIC CONDITIONS

By using befitting c coefficient and attenuation relation of PGA, we can derive a pseudo-static force at any slope unit. Thus, an improved Swedish Slice Method can be used to include the seismic force in slope stability analysis. It involves a force moment vector at each slice as shown in Fig 4.10. The equation can be improved as follows:

$$Fs_{2D} = \frac{\sum_{i=1}^{n} W_i \cos\alpha_i \tan\varphi_i + \sum_{i=1}^{n} c_i l_i}{\sum_{i=1}^{n} (W_i \sin\alpha_i) + \sum_{i=1}^{n} E_i} \tag{4.16}$$

As the moment forces rotated center point O, the union of all the slices'

pseudo-static force can be derived by:

$$E_i = k_H W_i \frac{r\cos\varphi_i - (E[i] - s[i])/2}{r} \qquad (4.17)$$

The k_H may be taken as equal to the designed Peak Ground Acceleration (PGA), which is expressed as a fraction of the gravity acceleration:

$k_H = k*PGA/9.8$ (4.18)

Here, k is the pseudo-static coefficient as mentioned above.

THE INPUT FORM OF STABILITY CALCULATION

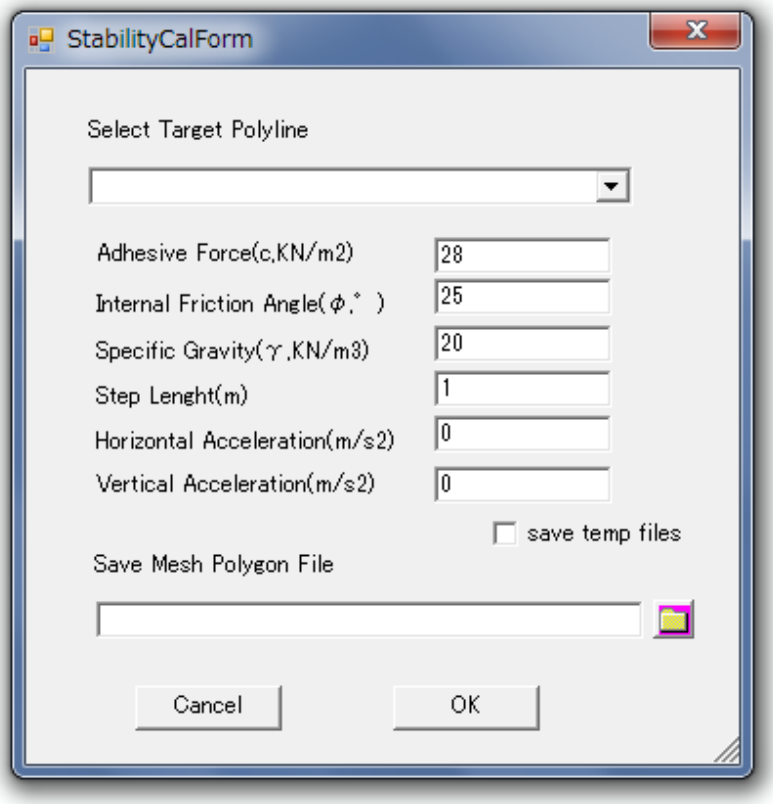

Fig 4.11. The input form for Stability Calculation in the ArcMap application.

Fig 4.11 shows the input form for Stability Calculation in the ArcMap application. The required parameters include vector data of cross line, adhesive force, internal friction angle, unit weight, step length, pseudo-static force of horizontal acceleration, and vertical acceleration.

To emphasize, the parameters of adhesive force, internal friction angle, unit

weight, pseudo-static force of horizontal acceleration, and vertical acceleration can be read directly from the attributes of each cross line if a different condition is specified at each slope and 0 is entered in the textbox.

4.3.4 ACCURACY VERIFYING

To verify the computing results of stability calculation, a regular slope as shown in Fig 4.12 is used to give a comparison. The computation is carried out between the developed GIS module and the commercial software called SLOPE/W.

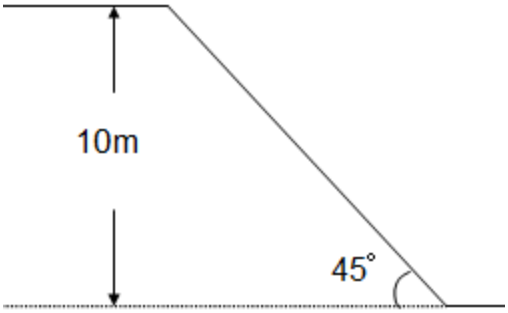

Fig 4.12. A regular slope model.

From Fig 4.13, it can be seen that the safety factor computed from the developed GIS module is a little bit smaller than that in the SLOPE/W software. However, it can be concluded that the results computed from the developed GIS module are reliable and can be used to indicate the possibility of slope failure.

Developed GIS module SLOPE/W

Group 1:

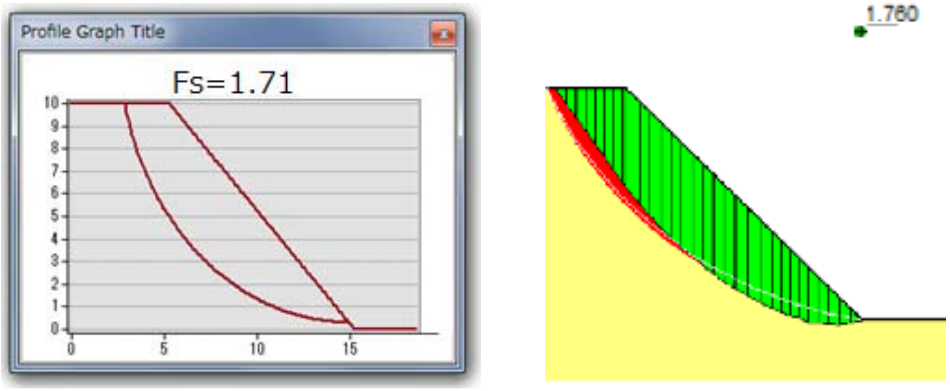

Group 2:

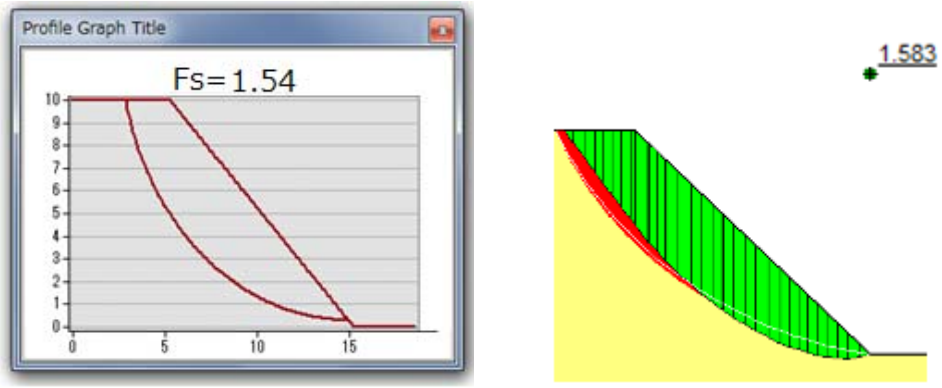

Fig 4.13. A comparison of stability computing between the developed GIS module and SLOPE/W.

Note: Attributes used for group 1: γ=24kN/m3, c=24kN/m2, φ=35°.

Attributes used for group 2: γ=22kN/m3, c=20kN/m2, φ=32°.

4.4 APPLICATION

4.4.1 INTRODUCTION

The 2008 Wenchuan earthquake triggered more than 50,000 landslides of various types in the mountainous terrain in the Sichuan Province, China, throughout an area of about 50,000km^2 (Fan, 2012). According to the statistics, the 21st deadliest earthquake of all time resulted in 20,000 people dying instantly (Yin et al., 2009), and 69,195 deaths and 18,392 missing people were reported in the aftermath. The most affected area of the earthquake extended from Wenchuan County to the

north and east, along the three main faults in Longmenshan. The hardest hit regions were Wenchuan, Beichuan, Mianzhu, Shifang, Qingchuan, Mao xian, An xian, Dujiangyan, Pingwu, and Pengzhou.

In this section, we implement the proposed hazard assessment approach in order to make an earthquake induced landslide hazard map using the 2D stability approach.

4.4.1 STUDY AREA

Our study area is located in Beichuan County, 180 km away from the northern part of Chengdu and northeast of the earthquake's epicenter, with eastern longitude of 103º44′to 104º42′, and northern latitude of 31º14′to 32º14′. This area is in the transitional belt between the Sichuan Basin and the Western Sichuan Plateau and it is mostly mountainous. The tectonics and strata system are very complex, a wide variety of sedimentary, metamorphic rock, unconsolidated sedimentary deposits, and exposed strata of Cambrian, Silurian, Devonian, Carboniferous, Triassic, Jurassic age, and Quaternary loose deposits are wildly outcropped. As shown in Fig 4.14, this area has high seismic shaking levels and it is located at the main fault rupture zone. The Yingxiu-Beichuan fault, which ruptured in the Wenchuan earthquake, runs through the southeastern portion of the study area. Many and various kinds of landslides occurred here as a result of the Wenchuan earthquake. Therefore, this area is suitable to show the effectiveness and practicality of the proposed approach in this study.

This area has abundant rainfall each year. The average annual rainfall is 1,399 mm, the maximum annual rainfall is 2,340 mm (1967), the daily maximum rainfall is 101 mm, and the hourly maximum rainfall is 32 mm. The rainfall concentrated from June to September, accounting for 71~76% of the whole year, the maximum record reaches to 90% (1981).

The Tongkou (Jinxing) River is a tributary of the PeiJiang River, which originates in the northwest mountains and runs through the county territory. It is 47.9 km long and has a drainage area of 455.80 km^2 in Beichuan County. The river head is 203 m, the average slope is 4.2%, the average annual runoff is 102.7 m^3/s, the average annual runoff volume is 3,257 billion m3, the average annual sediment

runoff is 40~50 million T, and the basin average annual erosion modulus is 7,072, 61T / km^2 • a.

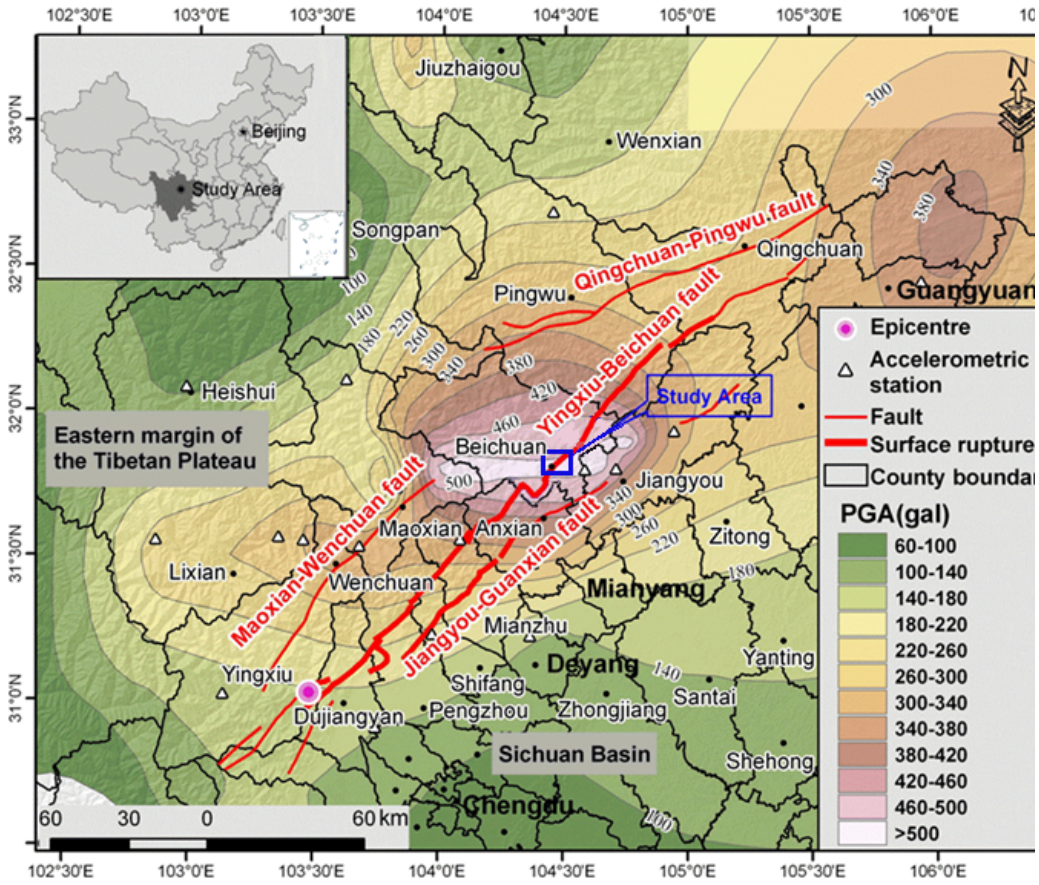

Fig 4.14. The study area and PGA distribution of the Wenchuan earthquake

The devastating Wenchuan earthquake occurred on the NE-trending Longmenshan thrust fault zone (LTFZ) at a focal depth of 14-19 km. The LTFZ separates the Sichuan basin from the steep and heavily dissected eastern margin of the Tibetan Plateau in China. The LTFZ consists of three major sub-parallel faults: the Wenchuan-Maowen (WMF), Yingxiu-Beichuan (YBF), and Pengguan faults (PF) (see Fig 2.1). The coseismic rupture initiated near Yingxiu town (31.06°N, 103.33°E) and propagated unilaterally towards the northeast, generating a 240-km-long surface rupture along the Yingxiu Beichuan fault, and a 72-km-long rupture along the Pengguan fault (Xu X et al., 2009; Lin et al., 2009; Shen et al., 2009).

The basic data utilized in this study included a DEM with a resolution of 10 m,

and a satellite image with a resolution of 2.5 m.

4.4.2 METHODOLOGIES

Based on the previous study of 2D slope stability assessment, a new mapping approach for landslide hazard map is proposed in this chapter, using a two-dimensional limit equilibrium model and integrating it with GIS environment. The proposed approach adopts the following procedures (Fig 4.15).

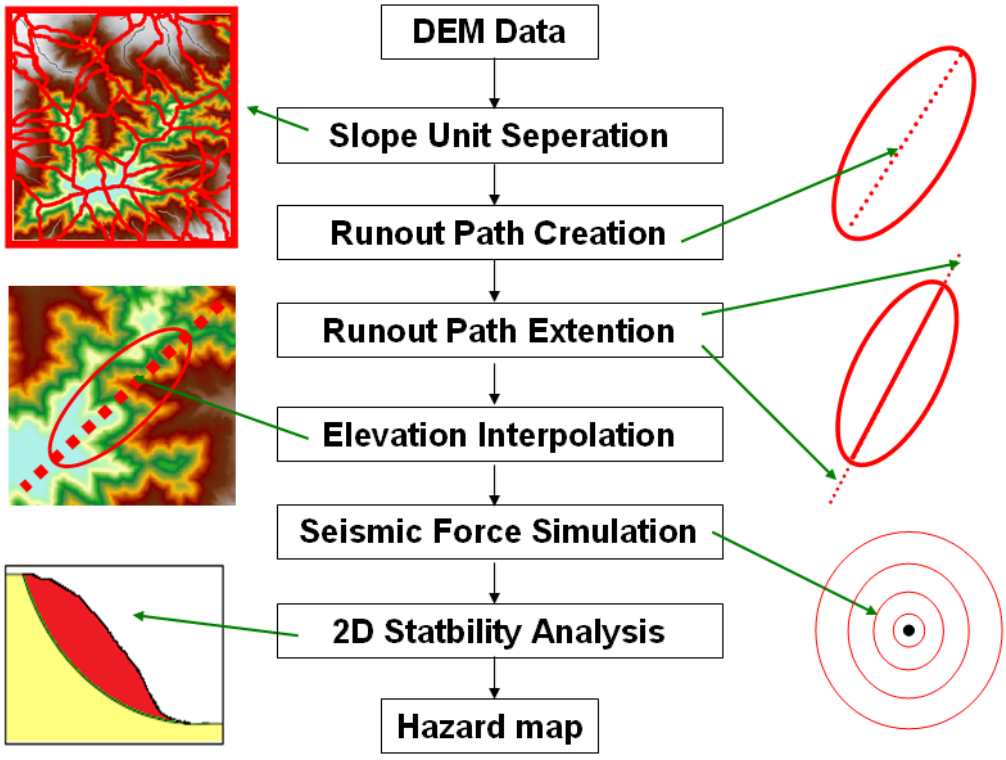

Fig 4.15. The process of the proposed new mapping approach.

1. Separate the digital elevation map into slope units to obtain approached slopes with geomorphology and hydrology data;

2. Link the highest point to the lowest point to obtain the approximate runout path;

3. Extend runout path line in order to get plenty of topography features;

4. Interpolate the elevation data into the path line at a certain step to obtain the

cross section of a prone slope;

5. Simulate ground motion by attenuation relation equation, and then select proper seismic coefficient to derive suitable pseudo-static force for slope stability analysis;

6. Employ an enumeration of circle assumed slip surface with slope stability analysis of the Swedish Slice Method. The minimum safety factor is adopted to describe slope susceptibility and its corresponding slip surface is recorded for future study. This step can be enclosed into a GIS module for general utility.

4.4.3 RESULTS AND DISCUSSION

Following the procedures of the proposed slope units identification method, we first divide the whole area into 10,186 slope units as shown in Fig 4.16. The plain area with an inclination of < 15°is excluded from the slope unit identification.

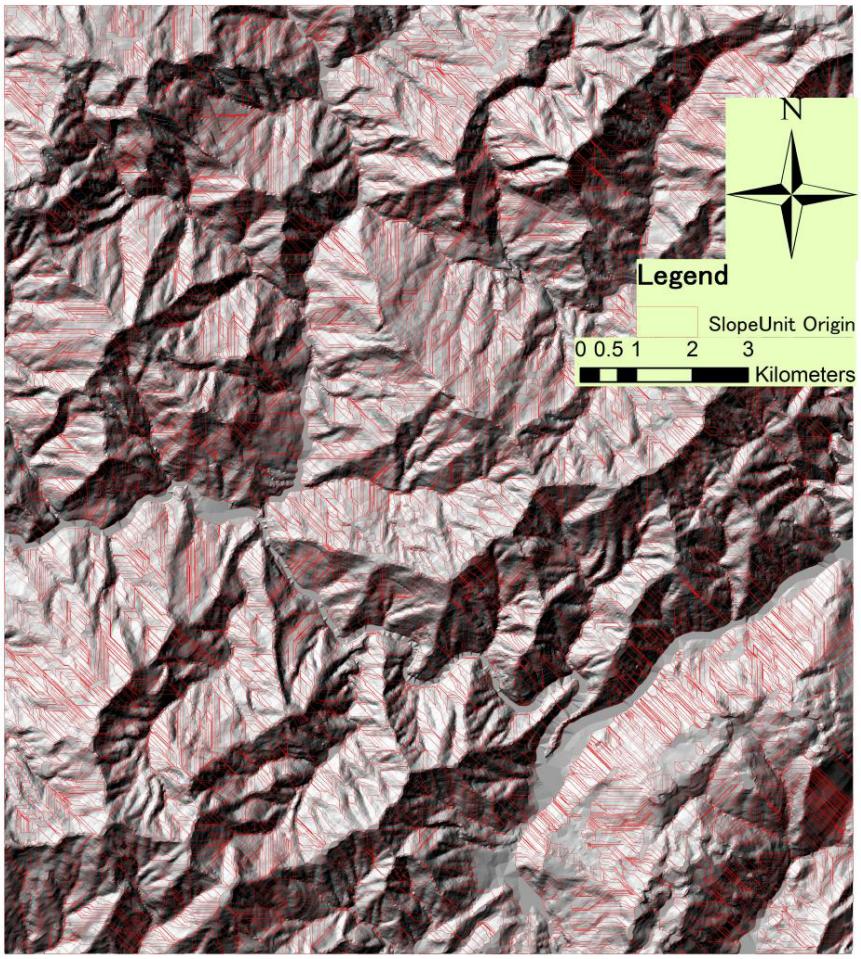

Fig 4.16. Slope unit division of study area.

Second, the highest point is linked to the lowest at each slope unit to obtain the approximate runout path as shown in Fig 4.17. Fig 4.18 shows the extent of the runout path lines.

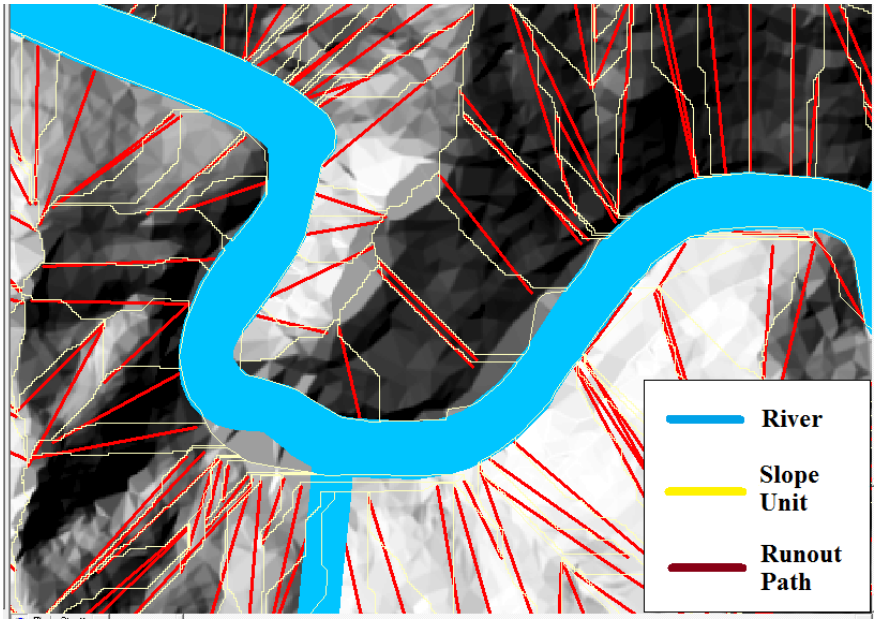

Fig 4.17. The approximate runout path of slope unit.

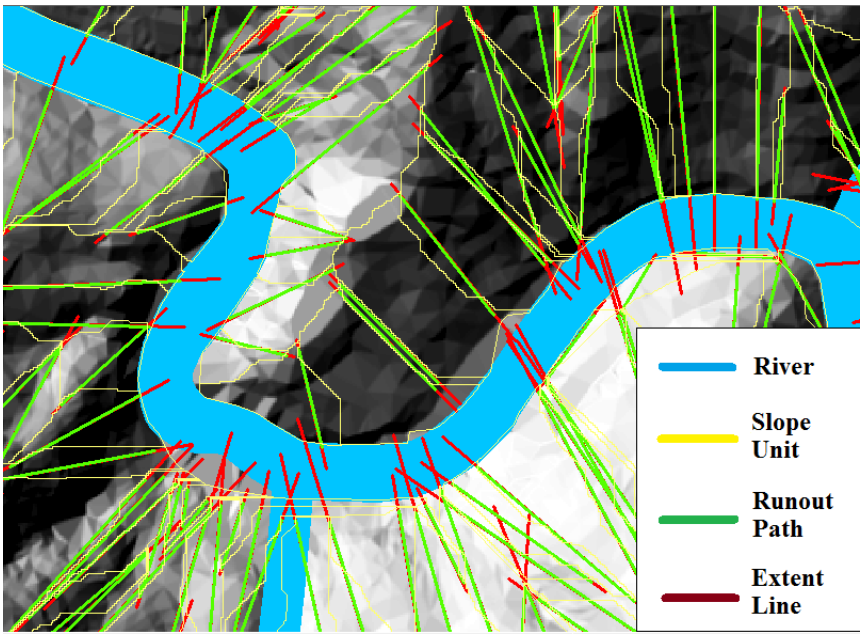

Fig 4.18. The extended approximate runout path of slope unit.

The third step is to interpolate the elevation data into the path line of each slope unit at 4 m steps to obtain the cross section of every prone slope. Based on the calculation of the fault-to-slope unit distance, the seismic motion is translated to the pseudo-static force using the equation of attenuation relation provided by Fukushima (1995). Magnitude is assumed as Wenchuan Earthquake (Ms = 8.0), accordingly, pseudo-static coefficients are set to 1/3. The results range from 151.67 to 221.27 cm/s2, as shown in Fig 4.19.

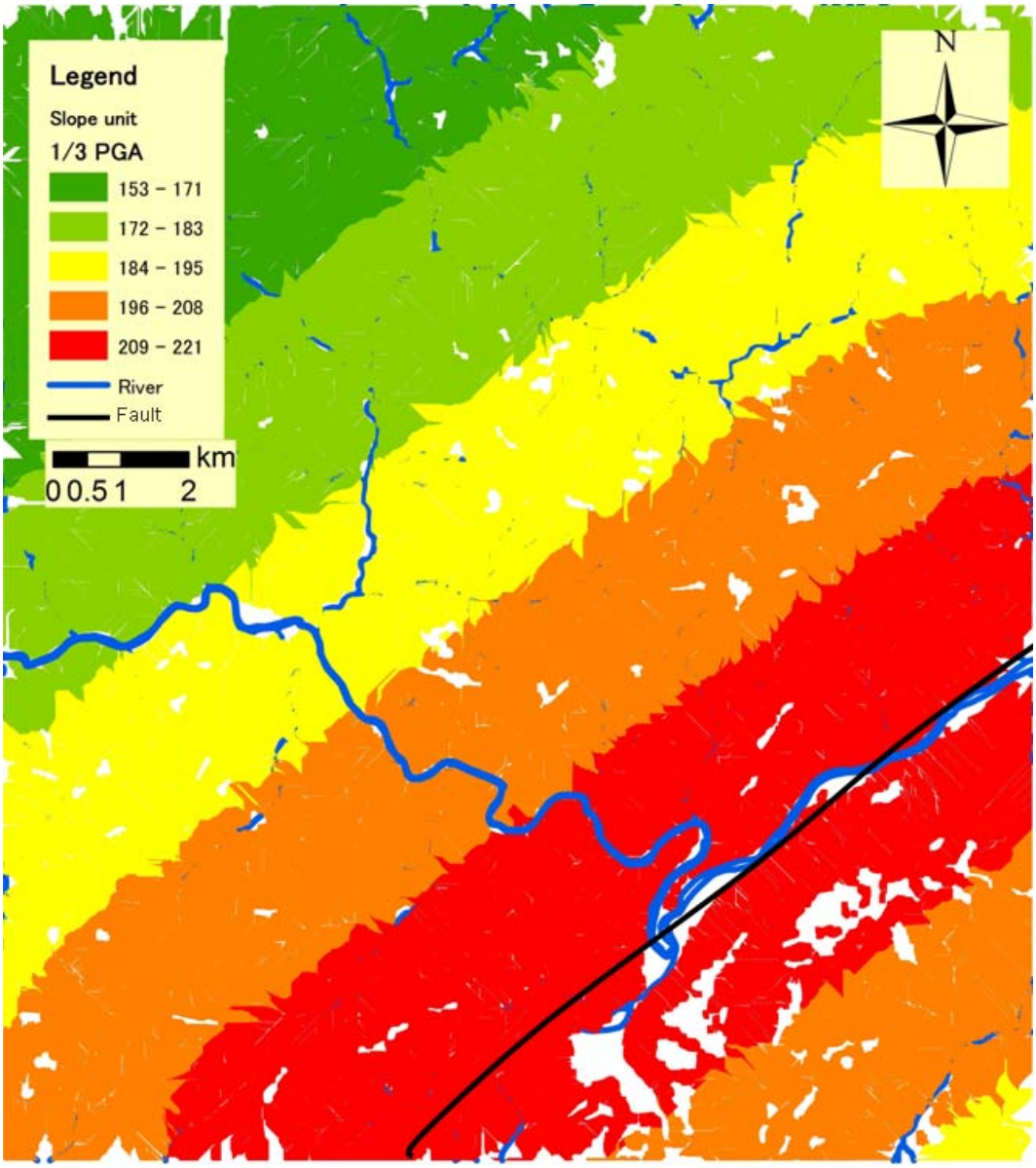

Fig 4.19. The safety factors from 2D slope stability analysis under seismic conditions.

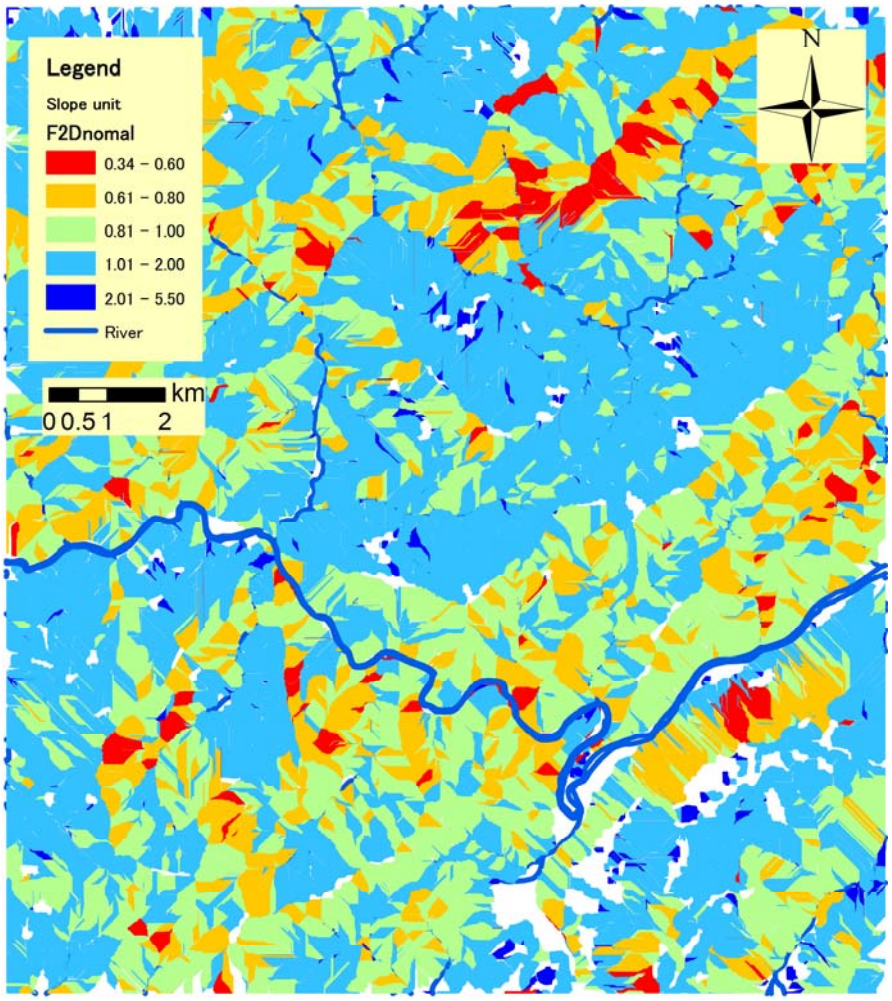

Fig 4.20. The safety factors from 2D slope stability analysis under seismic conditions.

The fourth step is to validate the 2D slope stability without seismic conditions. According to the field investigation at the Tangjiashan landslide, the following parameters, which are the averages of remaining weathered rock, were performed in the safety factor calculation: the soil unit weight is γ=22kN/m3, the cohesion strength of slope material is c=20kN/m2 and the internal friction angle of slope material is φ=32°.

The results are shown in Fig 4.20. The mean value of safety factors is 1.14, ranging from 0.34 to 5.55. The safety factor from the Swedish Slice Method is usually considered as 0.7 ~ 0.95 of the actual results. As we solved the problem in homogeneous soil conditions and the actual slope has a more complex structure of

rocks and strata, the outcome is not beyond what is expected.

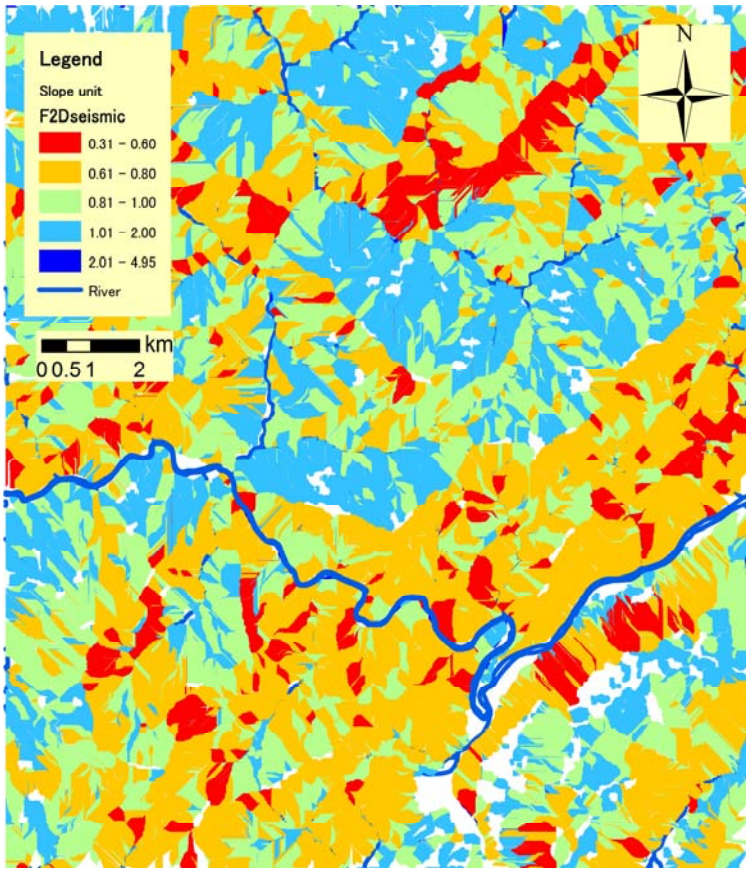

Fig 4.21. The safety factors from 2D slope stability analysis under seismic conditions.

The fifth step is to validate the 2D slope stability under seismic conditions. The results are shown in Fig 4.21. The mean value of safety factors is 0.88, with a range from 0.31 to 4.95. The safety factors decrease about 20.8% in mean from 2D safety factors.

Fig 4.22 gives a comparison of safety factors distribution with and without seismic conditions. It can be seen that 1,855 slope units have a high risk (SF < 0.8) of landslide without seismic force, accounting for 18.4% of the total slopes; while 4,395 slope units have a high risk of landslide with seismic force, accounting for 43.5% of the total slopes.

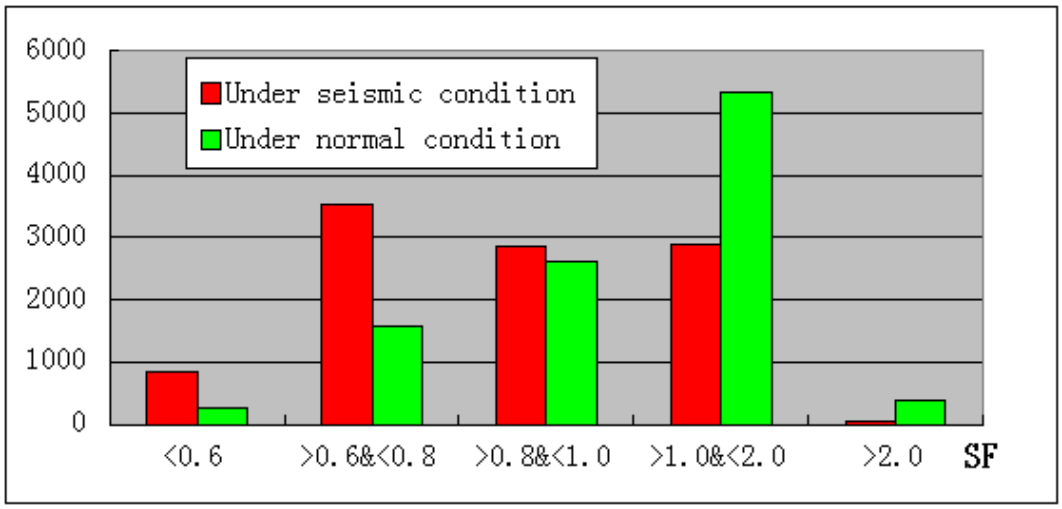

Fig 4.22. Comparison of safety factors distribution with and without seismic conditions.

4.5 SUMMARIES

This study first proposed a new hazard mapping method based on the well-known Swedish Method, a 2D limit equilibrium analysis method with a circular slip mode. The slope shape was extracted from DEM and critical slip surface searching progress was performed. The assessment of earthquake-induced landslides was also coded into a GIS module to achieve generalized utilities.

Then, the above procedures were all coded into a GIS module and grouped into an assessment tool kit. With the help of developed tools, the 2D slope stability analysis can be easily performed and managed.

Finally, the proposed hazard mapping method was implemented at Tongkou River area. The results highlight dangerous landslide-prone slopes.

REFERENCES

Abrahamson N. A, Litehiser J. J, 1989, Attenuation of vertical peak acceleration. Bulletin of the Seismological Society of America, 79(3), p.549-580.

Bishop A.W, 1955, The use of the slip circle in the stability analysis of slopes. In: Géotechnique, 5, p.7-17.

Bhushan P. B, 2009, Fundamentals of Soil Dynamics and Earthquake Engineering Paperback.

Boore D. M, Joyner W. B, 1982, The empirical prediction of ground motion. In: Bulletin of the Seismological Society of America, 72, p.43-60.

Campbell K. W, 1985, Strong motion attenuation relations: A ten-year perspective. In: Earthquake Spectra, 1(4), p.759-804.

Duncan J.M, Wright S.G, 1980, The accuracy of equilibrium methods of slope stability analysis. In: Engineering Geology, 16, p.5-17.

Fan X, van Westen C. J, Xu Q, Görüm, T, Dai, F, 2012, Analysis of landslide dams induced by the 2008 Wenchuan earthquake. In: Journal of Asian Earth Sciences, 57, p.25-37.

Fellenius W, 1927, Erdstatische Berechnungen mit Reibung und Kohäsion (Adhäsion) und unter Annahme kreiszylindrischer Gleitflächen, Ernst & Sohn, Berlin.

Fellenius W, 1936, Calculations of the stability of earth dams. Transaction of the 2nd Congress on Large Dams, 4, Washington, D.C.

Fukuzono T, 1985, A new method for predicting the failure time of a slope. In: Procs 4th Int. Conf. and Field Workshop on landslides, Tokyo, p.145-150.

Fukushima Y, Tanaka T, 1990, A new attenuation relation for peak horizontal acceleration of strong earthquake ground motion in Japan. In :Bulletin of the Seismological Society of America, 80(4), p.757-783.

Fukushima Y, Gariel J. C, Tanaka R, 1995, Site-dependent attenuation relations of seismic motion parameters at depth using borehole data. In: Bulletin of the Seismological Society of America, 85(6), p.1790-1804.

Hammouri N. A, Husein Malkawi A. I, Yamin M. M. A, 2008, Stability analysis of slopes using the finite elemnet method and limiting equilibrium approach. In: Bulletin of Engeering Geology and the Environment, 67(4), p.471-478.

Joyner W. B, Boore D. M, 1988, Measurement, characterisation, and prediction of strong ground motion. In: Proc. Eartheq. Engg. and Soil Dyn. II GT Div/ASCE , Utah, p.43-102.

Lin A, Ren Z, Jia D, Wu X, 2009, Co-seismic thrusting rupture and slip distribution produced by the 2008 Mw 7.9 Wenchuan earthquake, China. In: Tectonophysics, 471(3-4), p.203-215.

Masashi S, 2012, Development of forest road design and strip road networks

arrangement support techniques using LiDAR data. In: Bulletin of the Utsunomiya University Forests, 48, p.71-110.

Michiue M, Fujita M, 1990, Method for Predicting Slope Failure. In: Journal of Natural Disaster Science, 12(1), p.49-62.

Pyke R, 1991, Selection of Seismic Coefficients for Use in Pseudo-Static Slope Stablility Analyses. Http://www.tagasoft.com/TAGAsoft/Discussion/articl2_html, Engineering Protal Ltd.

Shen Z. K, Sun J, Zhang P, Wan Y, Wang M, Burgmann R, Zeng Y, Gan W, Liao H, Wang Q, 2009, Slip maxima at fault junctions and rupturing of barriers during the 2008 Wenchuan earthquake. In: Nature Geoscience, 2(10), p.718-724.

Taylor D. W, 1948, Fundamentals of soil mechanics, Wiley, Hoboken, NJ.

Turnbull W. J, Hvorslev M. J, 1967, Special problems in slope stability. In: Journal of the Soil Mechanics and Foundations Division, ASCE, 93(4), p.499-528.

Whitman R.V, Bailey W.A, 1967, Use of computers for slope stability analysis. In: Journal of the Soil Mechanics and Foundations Division, ASCE, 93, p.75-498.

van Westen C. J, Rengers N, Terlien M. T. J, Soeters R, 1997, Prediction of the occurrence of slope instability phenomena through GIS-based hazard zonation. In: Geol. Rndsch, 86, p.404-414.

Xu Q, Fan X. M, Huang R. Q, Westen C, 2009, Landslide dams triggered by the Wenchuan Earthquake, Sichuan Province, south west China. In: Bulletin of Engineering Geology and the Environment, 68(3), p.373-386.

Yin Y, Wang F, Sun P, 2009, Landslide hazards triggered by the 2008 Wenchuan earthquake, Sichuan, China. In: Landslides, 6(2), p.139-152.

CHAPTER 5

DEVELOPMENT OF A NEW MAPPING METHOD USING 3D SLOPE STABILITY ANALYSIS

5.1 INTRODUCTION

To predict a landslide dam, the third step is estimating the slide scale and possible slide volume. As discussed in Chapters 1 and 2, the deposit volume plays a key role in landslide dam formation, but it is difficult to make a prediction. However, the slide mass can offer relevant data. Some previous studies have highlighted a statistical relation between slide volume and slope topography (Larsen et al., 2010), while others have proposed a new mapping method using 3D slope stability analysis to estimate the possible slide situation (Xie, 2002). This study recommends the latter method because past landslide records are not available in many cases.

On the other hand, although a mapping method using 2D stability analysis was proposed in Chapter 4, the 3D methods can accommodate more complex data of geometry, stratum, and groundwater, which leads to a better understanding of the spatial distribution of the slip body. Moreover, the safety factor of the 2D model is conservative because the sheer resistance along the two sides of slip mass is neglected. Therefore, a 3D model is preferred in natural slope stability analysis.

For a 3D stability analysis, a semi-ellipsoid slip model is generally used. The key issue is how to determine the ellipsoid parameters to obtain the minimum slope

safety factor. The existing 3D method applies Monte Carlo simulation to determine the parameters. Because running the 3D limit equilibrium analysis with Monte Carlo simulation to achieve an acceptable minimum safety factor is extremely time-consuming, the existing method is unadaptable in hazard mapping. Therefore, a new method for determining the parameters of an ellipsoid is proposed based on the 2D limit equilibrium analysis with the Swedish method.

In this chapter, the existing 3D method is introduced, as are its service restrictions. Then, a new mapping method using improved 3D slope stability analysis is proposed. The circular slip determined in 2D analysis is used to estimate the lengths of two axes of a tri-axial ellipsoid; the other axial length is estimated directly from the slope shape. Finally, the GIS module of the 3D limit equilibrium analysis is developed using the new approach of determining ellipsoid parameters. Practical applications show that the new hazard mapping method based on the new approach for 3D limit equilibrium analysis can greatly reduce the processing time.

5.2 THE EXISTING 3D STABILITY MAPPING METHOD

As all slope failures have a three-dimensional (3D) geometry, it is reasonable to use a 3D model for slope stability analysis. A large number of 3D methods have been proposed since the late 1960s (Hovland, 1977; Hungr, 1987; Hungr et al., 1989; Lam and Fredlund, 1993; Leshchisky and Huang. 1992). As shown in Table 5.1, Duncan summarized a list of the existing studies, most of which have used a column-based approach and can be considered a direct extension of corresponding 2D methods. For example, the 3D Janbu method keeps the same assumption as the 2D simplified Janbu method and extends the slice unit into column unit. These methods either neglect inter-column forces or make assumptions for the 3D safety factor calculation. Because of the complex algorithms, iteration procedures, and the third dimension of data management, 3D deterministic model applications are very difficult to achieve in landslide mapping.

Table 5.1. Methods of Analyzing 3D Slope Stability (Duncan, 1996).

Authors	Method	Strength	Geometry of slope/slip surface	3-D effects found
Anagnosti (1969)	Extended Morgenstern and Price	c, ϕ	Unrestricted/unrestricted	F, = 1.5 F2 in one case
Baligh and Azzouz (1975)	Extended circular arc	ϕ=0	Simple slopes/surfaces of revolution	F, > F2
Giger and Krizek (1975)	Upper bound theory of perfect plasticity	c, ϕ	Slopes with cornersllog spiral	F, > F2
Giger and Krizek (1976)	Upper bound theory of perfect plasticity	c, ϕ	Slopes with cornersllog spiral (with loads on top of slope)	F, > F2
Baligh et al. (1977)	Extended circular arc	ϕ=0	Simple loaded slopes/surfaces of revolution	F, > F2
Hovland (1977)	Extended ordinary method of slices	c, ϕ	Unrestricted/unrestricted	F, < F2 for some cases
Azzouz et al. (1981)	Extended Swedish circle	ϕ=0	Four real embankments/surfaces of revolution	F, = 1.07 F2 to 1.3 F2
Chen and Chameau (1982)	Extended Spencer, and finite element	c, ϕ	Unrestricted/unrestricted	FEM
Chen and Chameau (1983)	Extended Spencer	c, ϕ	Unrestricted/unrestricted	F, < F2 for some cases
Azzouz and Baligh (1983)	Extended Swedish circle	ϕ=0	Same as Baligh and Azzouz with loads on top	F, > F2
Dennhardt and Forster (1985)	Assumed on slip surface	c, ϕ	Slopes with loads/unrestricted	F, > F2
Leshchinsky et al. (1985)	Limit equilibrium and variational analysis	c, ϕ	Unrestricted	F, > F2
Ugai (1985)	Limit equilibrium and variational analysis	ϕ=0	Vertical slopes/cylindrical	F, > F2
Leshchinsky and Baker (1986)	Limit equilibrium and variational analysis	c, ϕ	Slopes constrained in 3rd dimension/unrestricted	F, > F2 for c > 0, F, = F2 for c=O
Baker and Leshchinsky (1987)	Limit equilibrium and variational analysis	c, ϕ	Conical heaps/unrestricted	F, > F2
Cavounidis (1987)	Limit equilibrium	c, ϕ	Unrestricted/unrestricted	F, must be > F2

Authors	Method	Strength	Geometry of slope/slip surface	3-D effects found
Hungr (1987)	Extended Bishop's modified	c, ϕ	Unrestricted/surfaces of revolution	F, > F2
Gens et al. (1988)	Extended Swedish circle	ϕ=0	Simple slopes/surfaces of revolution	F, > F2
Leshchinsky and Mullet (1988)	Limit equilibrium and variational analysis	c,ϕ	Vertical slopes with corners/unrestricted	F, > F2
Ugai (1988)	Extended ordinary method of slices, Bishop's modified, Janbu, and Spencer	c, ϕ	Unrestricted/unrestricted	F, > F2, except for OMS
Xing (1988)	Limit equilibrium	c, ϕ	Unrestricted/ellipsoidal	F, > F2
Michalowski (1989)	Kinematical theorem of limit plasticity	c, ϕ	Unrestricted/unrestricted	F, > F2
Seed et al. (1990)	Ad hoc 2D and 3D	c, ϕ	One particular case, the Kettleman Hills failure	F, < F2
Leshchinsky and Huang (1992)	Limit equilibrium and variational analysis	c. ϕ	Unrestricted/unrestricted	F, > F2

By combining GIS grid-based data with a column-based 3D ellipsoid slip model, the existing method (Xie, 2003) chooses Hovland's method for calculating the safety factor because it has the easiest data managing of its conventional slide assumption and the easiest computing of its linear equation.

To detect 3D critical slips, the search of the slip surface is performed by minimizing the 3D safety factor using the Monte Carlo random simulation method. The basic slip surface is assumed to be the lower part of an ellipsoid slip, and the critical slip will be changed according to different strengths of strata and conditions of the discontinuous surface. The object of this change is to minimize the 3D safety factor. The flowchart is shown in Fig 5.1.

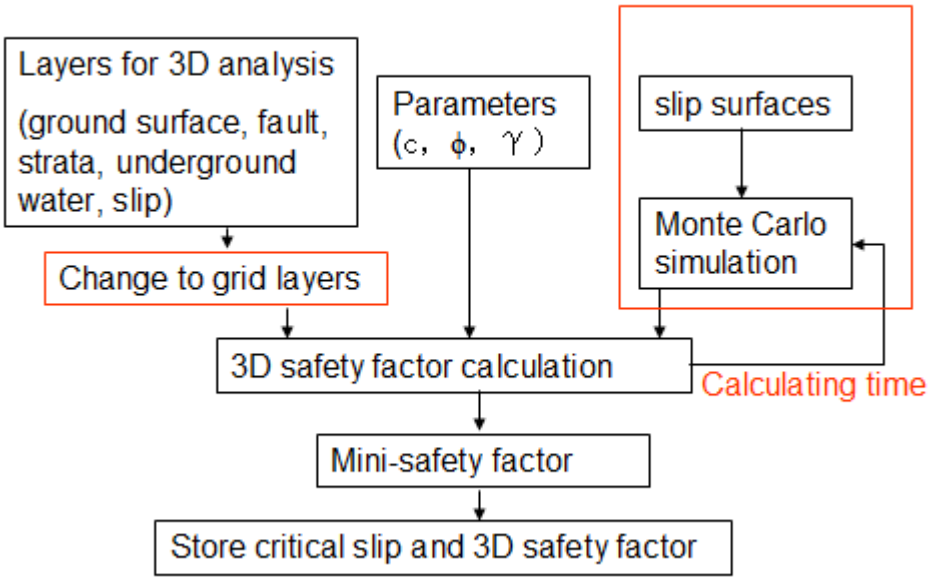

Fig 5.1. The flowchart of 3D slope stability analysis from Xie (2004).

In this method, five parameters of slip surface are applied from Monte Carlo simulation, which makes the critical slip searching extremely time costly. Furthermore, if one parameter were simulated 10 times to get a "true" result, the total slip surface would be simulated 100,000 times. The possibility of a "true" series of parameters is so low that it results in a gross underestimation of the probability of "low-probability" events. Therefore, the Monte Carlo simulation is not suitable to carry out this assessment over an extensive area.

On the other hand, the DEM is fairly large as a whole but rough in detail, so it is also time costly to manage the entire map in each slope analysis. Moreover, without pre-treatment, the rough topography data may cause inaccuracies in the safety factor calculation, for example, a 30 m based ASTER GDEM can comprise a small landslide in only one or fewer than 10 pixels.

In conclusion, the existing method is not suitable for wide area landslide mapping because of its low efficiency. Thus, a new mapping approach is proposed for 3D slope stability analysis in the next section.

5.3 A NEW MAPPING APPROACH USING 3D SLOPE STABILITY ANALYSIS

The flowchart of the new mapping method proposed is shown in Fig 5.2. The improvements when compared to existing method include: 1) increase a conversion progress to extract an elevation matrix for slip surface searching; and 2) estimate the parameters of the ellipsoid slip body using 2D analysis results instead of Monte Carlo simulation.

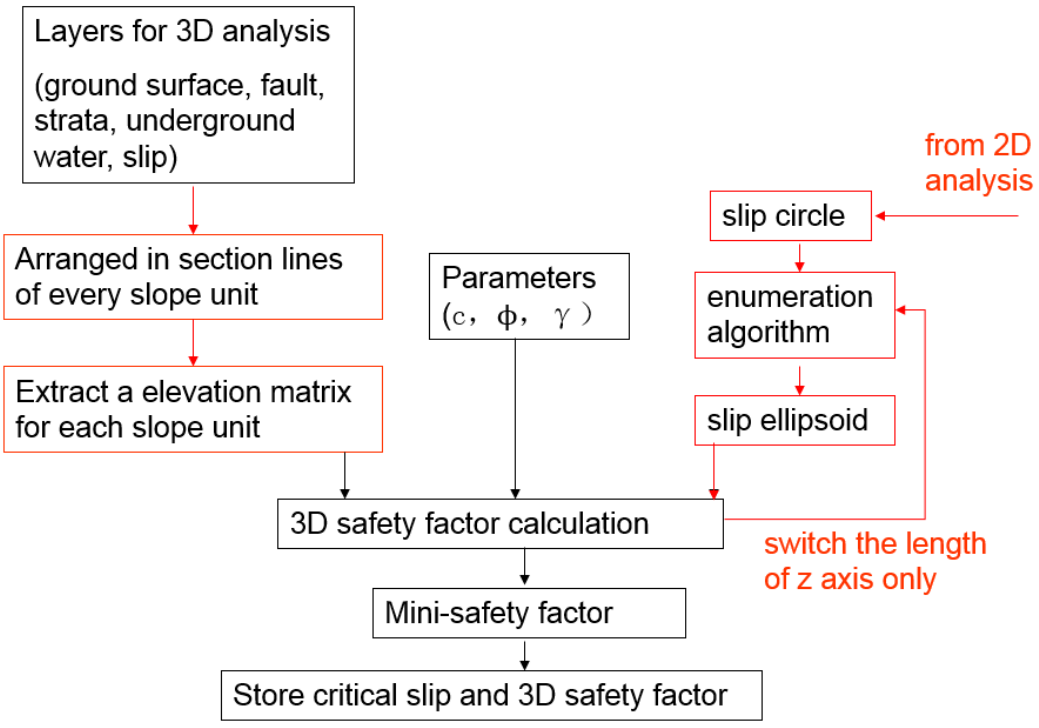

Fig 5.2. A flowchart of the improved new 3D slope stability analysis.

The contents of this method can be grouped into three parts:

- Data preparation
- Slip surface search
- Safety factor calculation

5.3.1 ELEVATION MATRIX EXTRACTION WITH COORDINATE CHANGE (DATA PREPARING)

In many places, the valid DEM is not detailed enough for landslide assessment, such as the 30 m based ASTER GDEM. It is inaccurate to imply a small slip surface search without any treatment. Traditional data management dominates the elevations in pixels, and that is what 3D analysis has used for grid-column division in other studies (see Fig 5.3). Fig 5.4 shows an example of 30 m based DEM with a landslide vertical projected ellipse. The elevation data of each pixel is treated at the center of the pixel square. The projected ellipse of the landslide is quite big scaled with about 120 m in length and 70 m in width, although it can only involve seven pixels as the grid-column for stability analysis. On the other hand, the DEM is fairly large as a whole but rough in detail, so it is also time costly to manage the entire map for each slope analysis.

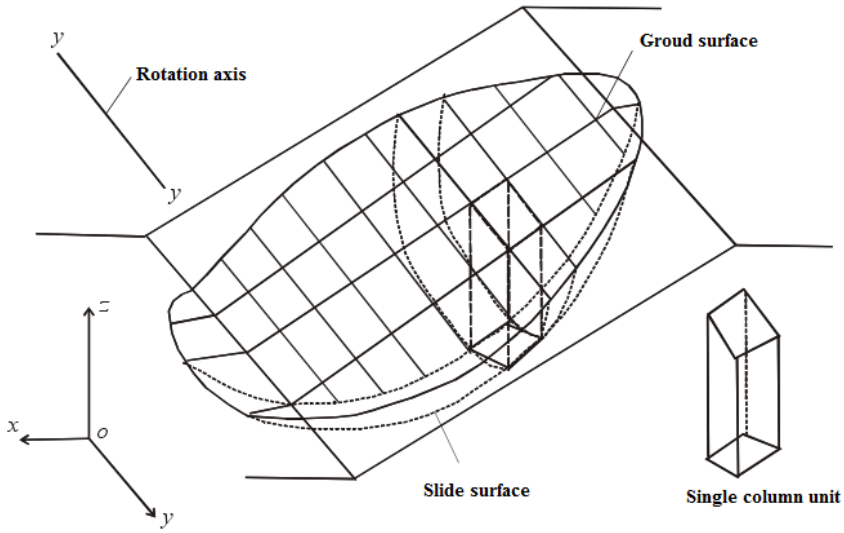

Fig 5.3. A column division example of a slide body in the 3D model.

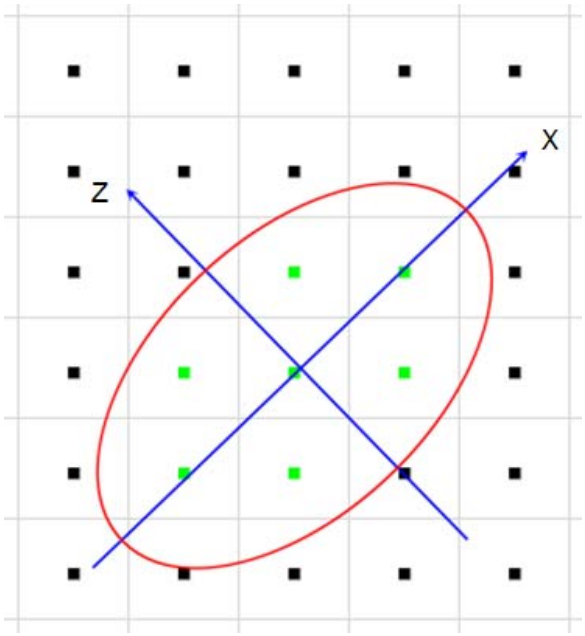

Fig 5.4. An example of a 30 m based DEM with a landslide vertical projected ellipse (red ellipse).

Since this study uses the parameters derived from the 2D mapping approach, the position of the landslide is stored in each cross line's attributes list. Therefore, we built an conversion function before the stability calculation process, which interpolates a matrix E[i, j] of ground surface from DEM, as shown in Fig 5.5. A given length 10 m of step is used to restrict grid-column width for computing, which can be set manually, and each extract elevation is calculated by a bilinear algorism. The matrix is arranged in a 2r × 4r square, and the coordinate origin position is settled at the vertical projected head point of ellipsoid slide body. r is the radii length derived from the 2D mapping approach. Thus, the following stability calculation is not based on the world coordinates of DEM, but uses its own coordinates.

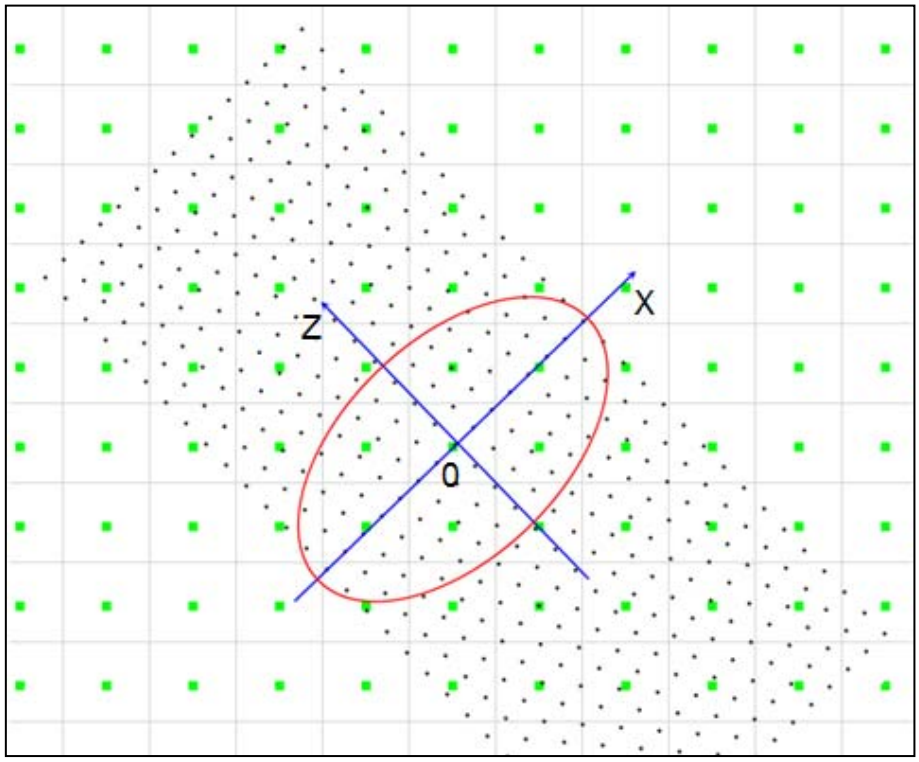

Fig 5.5. Interpolation of an elevation matrix (black dots) from DEM.

5.3.2 DETERMINE ELLIPSOID SLIP BODY (SLIP SURFACE SEARCHING)

To assume an ellipsoid slip surface, it is necessary to determine the parameters of the positions x_o, y_o, z_o of the ellipsoid center O, the Lengths x, y, z of the X, Y, Z axes, and the angles of aspect θas and inclination θin (see Fig 5.6). In the previous study, except for θas and θin, which are detected from the slope unit directly and y_o, which is extracted from the ground surface, all the other five parameters are uncertainty data derived from the Monte Carlo simulation.

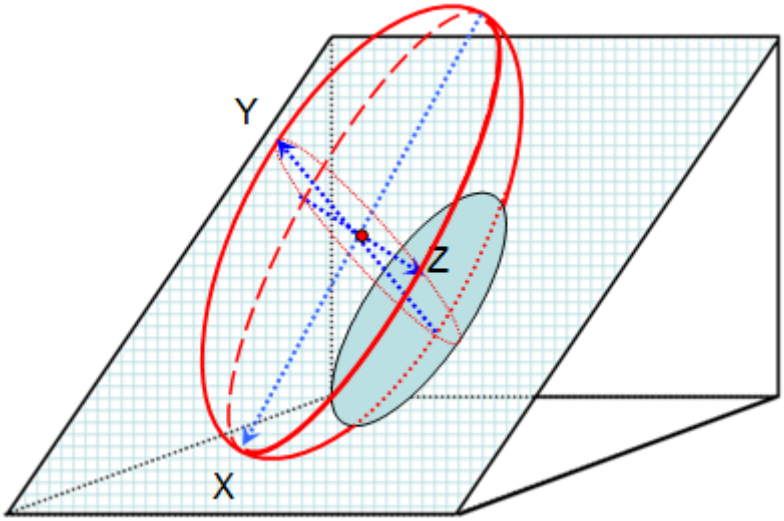

Fig 5.6. An example of ellipsoid assumed slip surface.

In contrast, this study can derive the position x_o, y_o of radii O, and Lengths r of x, y axis of circle from the 2D mapping approach. The length of the z axis is the only unknown remaining. Then, we simply choose 10 different lengths r_Z through enumeration algorism to determine the slip surface.

If we take one ellipsoid assumed slip surface as an example (Fig 4.5), the elevation matrix $S_{3\text{-}D}[i, j]$ of the slip surface can be derived by:

$$S_{3D}[i, j] = y_o - \sqrt{r^2(1 - \frac{z^2}{r_Z}) - x^2} \tag{5.1}$$

i, j is the position order of concerned grid-column in X and Y axis direction of the extracted matrix E[i, j] and term z, x is:

$$x = i * l_p \tag{5.2}$$

$$z = j * l_p \tag{5.3}$$

l_p is the pixel length. As the initial slice surface is assumed as the lower part of an ellipsoid slip, the grid-column shall be excluded when $S_{3\text{-}D}[i, j] < E[i, j]$, thus:

$$S_{3D}[i, j] = \begin{cases} E[i, j] & S_{3D}[i, j] > E[i, j] \\ S_{3D}[i, j] & S_{3D}[i, j] > E[i, j] \end{cases} \tag{5.4}$$

5.3.3 The Hovland method (Safety factor calculating)

In this research, a column-based 3D limit equilibrium model, revised Hovland

model, was used to calculate the safety factor of each slope unit. By assuming the vertical sides of each pixel column are frictionless, which means no side forces on the vertical sides of the pixel columns, or with their influence canceled out, the 3-D safety factor can be expressed as follows:

$$SF_{3D} = \frac{\sum_j \sum_i (cA_{i,j} + W_{i,j} \cos\theta_{XY\,i,j} \tan\phi)}{\sum_j \sum_i (W_{i,j} \sin\theta_{XY\,i,j} + E_{i,j})} \quad (5.5)$$

where:

$W_{i,j}$ denotes the weight of the i^{th}, j^{th} grid-column;

$A_{i,j}$ denotes the area of the slip surface of the i^{th}, j^{th} grid-column;

c denotes cohesion;

ϕ denotes the friction angle;

$\theta_{XYi,j}$ denotes the incline angle projected at plane XY of the i^{th}, j^{th} grid-column;

and $E_{i,j}$ denotes the moment forces of the i^{th}, j^{th} grid-column.

Using the extracted matrix E[i, j], term Wi,j can be derived as:

$$W_{i,j} = (E[i,j] - S[i,j]) * \gamma * l_p * w \quad (5.6)$$

Where:

γ denotes the unit weight in kN/m^3,

and w denotes the thickness of cross section in m.

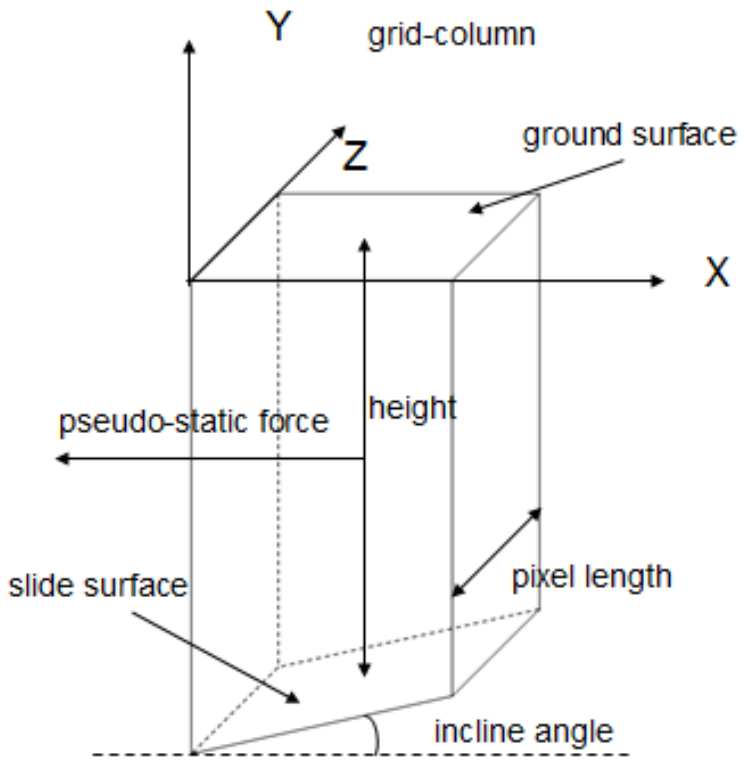

Fig 5.7. Picture of a one grid-column ignoring water pressure.

From Fig 5.6, the following equations can be derived for:

$$A_{i,j} = l_p^2 \times \cos\theta_{i,j} \tag{5.7}$$

As we already have the slip surface, some parameters can be derived directly with the GIS Spatial Analysis tool. Therefore, we calculate the incline angle $\theta_{i,j}$ of each grid-column by a neighbor calculation function, which uses a plane to the elevation values of a 3 x 3 cell neighborhood around the processing cell.

All the resistant and sliding forces should refer to the possible sliding direction. The main dip direction of the slope unit is assumed to be the possible sliding direction. Thus, term $\theta_{XYi,j}$ means the slide incline angle projected at plane XY, and can be derived by:

$$\theta_{XYi,j} = \arctan\frac{x}{y_o - S[i,j]} \tag{5.8}$$

As the slices' pseudo-static force act through the centroid of the each slice and rotated axis Z, the moment forces $E_{i,j}$ can be derived by:

$$E_{i,j} = k_H W_{i,j} \frac{\sqrt{r^2 - z^2}\cos\theta_{XY\,i,j} - (E[i,j] - S[i,j])/2}{\sqrt{r^2 - z^2}} \quad (5.9)$$

The k_H may be taken as equal to the designed Peak Ground Acceleration (PGA), which is expressed as a fraction of the gravity acceleration:

$k_H = k*PGA/9.8$ (5.10)

Here, k is the pseudo-static coefficient as mentioned in Chapter 4.

5.4 DEVELOPMENT OF GIS MODULES AND ACCURACY VERIFICATION

To integrate within the GIS platform, we developed a GIS 3D slope stability analysis module using C# language. All of the above mathematical models were achieved and implied with in ArcMap application.

As shown in Fig 4.5, we developed an Assessment toolbar. By simply clicking the corresponding buttons, the input form for 3D stability calculation will displace as depicted in Fig 5.8. The required parameters include vector data of cross line, raster data of DEM, adhesive force, internal friction angle, unit weight, step length, pseudo-static force of horizontal acceleration, and vertical acceleration.

To emphasize, the parameters of adhesive force, internal friction angle, unit weight, pseudo-static force of horizontal acceleration, and vertical acceleration can be read directly from the attributes of each cross line, if a different condition is specified at each slope and 0 is entered in the text-box.

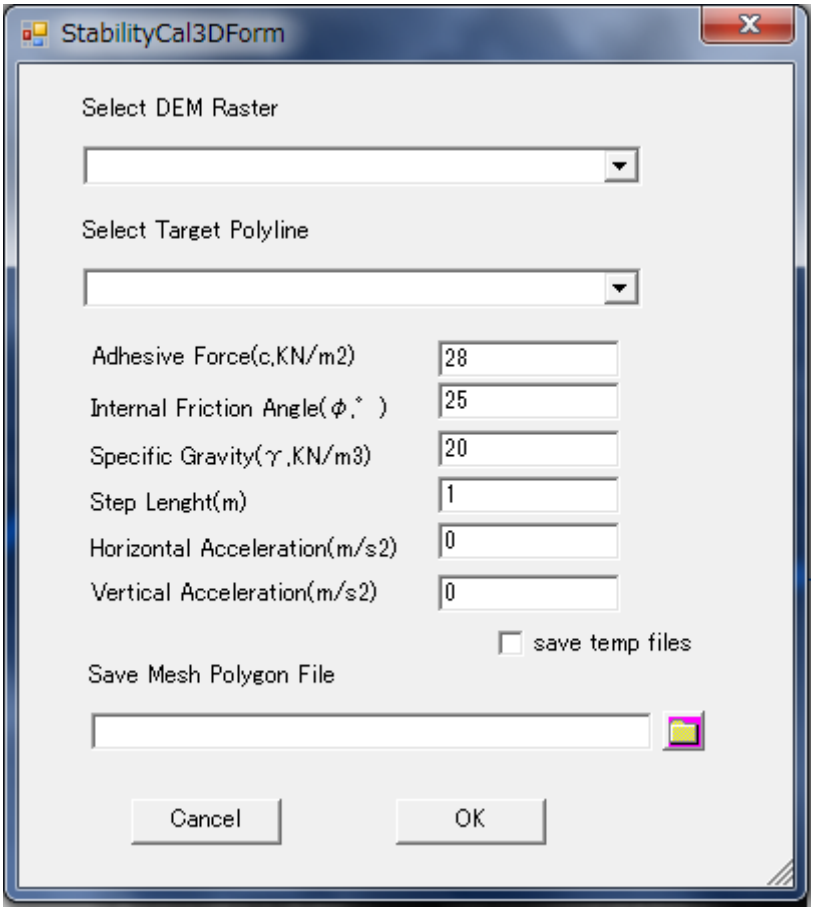

Fig 5.8. The input form for 3D stability calculation in the ArcMap application.

To verify the accuracy of developed GIS module, an example from Zhang (1988) is chosen and modeled in GIS (Fig 5.9). The given result of the Hovland method is SF=2.12, while the developed GIS module presents SF=2.63. Considering the different searching process of slip surface, this is an acceptable accurate result for slope stability analysis.

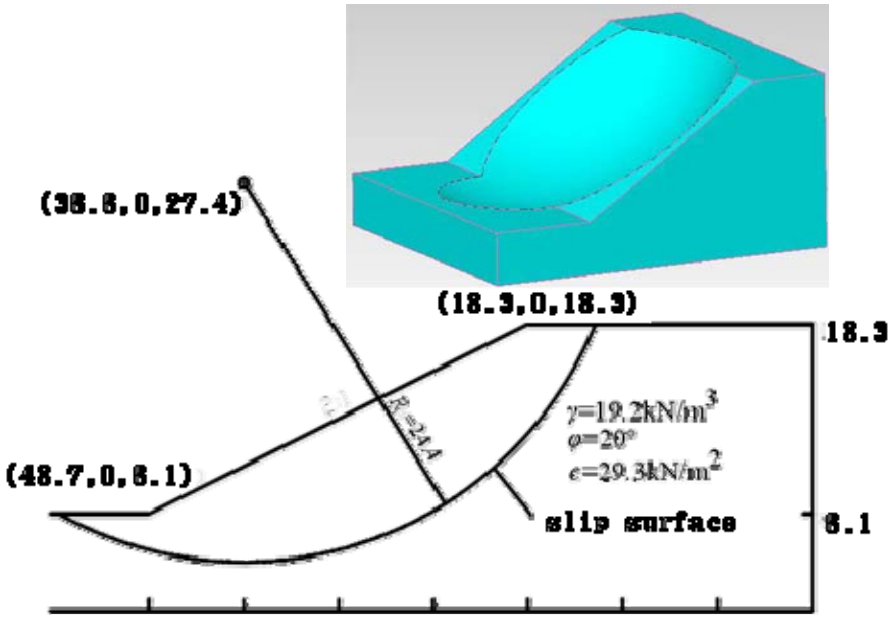

Fig 5.9. An example of a slope for accuracy verifying (Zhang, 1988).

5.5 APPLICATION AND COMPARISON

This chapter uses the same target area as in Chapter 4, which is a 15×12 km^2 square field in the basin of the Tongkou River.

5.5.1 METHODOLOGIES

Based on the 2D stability assessment of landslide, a new mapping approach is proposed in this chapter adopting 3D slope stability analysis, which consists of the following procedures (see Fig 5.10):

1. Separate the digital elevation map into slope units to get approached slopes with geomorphology and hydrology data;

2. Link the highest point to the lowest point to obtain the approximate runout path.

3. Extend the runout path line to obtain plenty of topography features;

4. Interpolate the elevation data into the path line at a certain step to obtain the cross section of a prone slope;

5. Simulate ground motion by attenuation relation equation, and then select proper seismic coefficients to derive suitable pseudo-static force for slope stability

analysis;

6. Employ an enumeration of circle assumed slip surface with slope stability analysis of the Swedish Slice Method. The minimum safety factor is adopted to describe slope susceptibility and its corresponding slip surface is recorded for future study;

7. Employ an enumeration of ellipsoid assumed slip surface with the Hovland Model based on the determinate position of radii O, and Lengths of x, y axes, which are obtained from a previous slope stability analysis of the Swedish Slice Method. The minimum safety factor is adopted to describe slope susceptibility and its corresponding slip surface and slide body are recorded for future study.

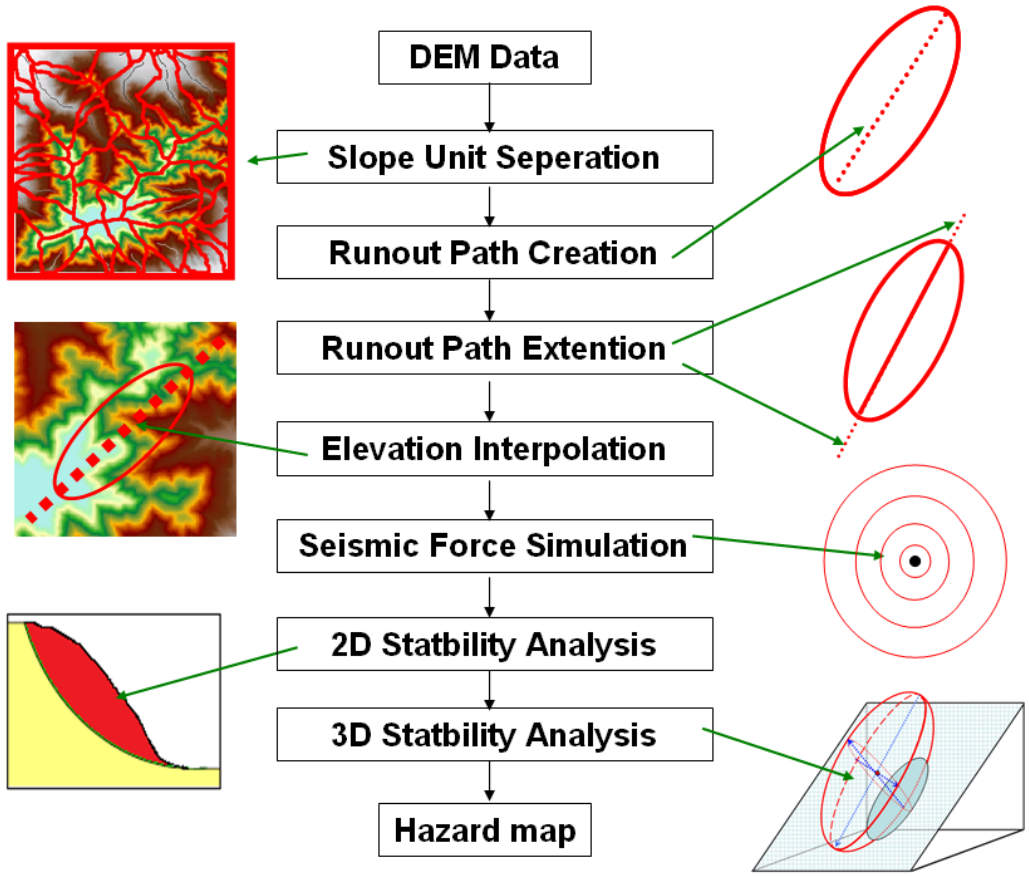

Fig 5.10. The framework of a new mapping approach adopting 3D slope stability analysis.

5.5.2 RESULTS AND DISCUSSION

To give a comparison of 3D slope stability analysis with and without seismic conditions, both hazard-mapping methods are processed following the procedures of the proposed approach.

The results without seismic condition are shown in Fig 5.11. The mean value of safety factors is 1.14, ranging from 0.34 to 5.55. The mean value of safety factors is 1.30, ranging from 0.31 to 7.25. The safety factors increase about 11.9% in mean from the 2D safety factors.

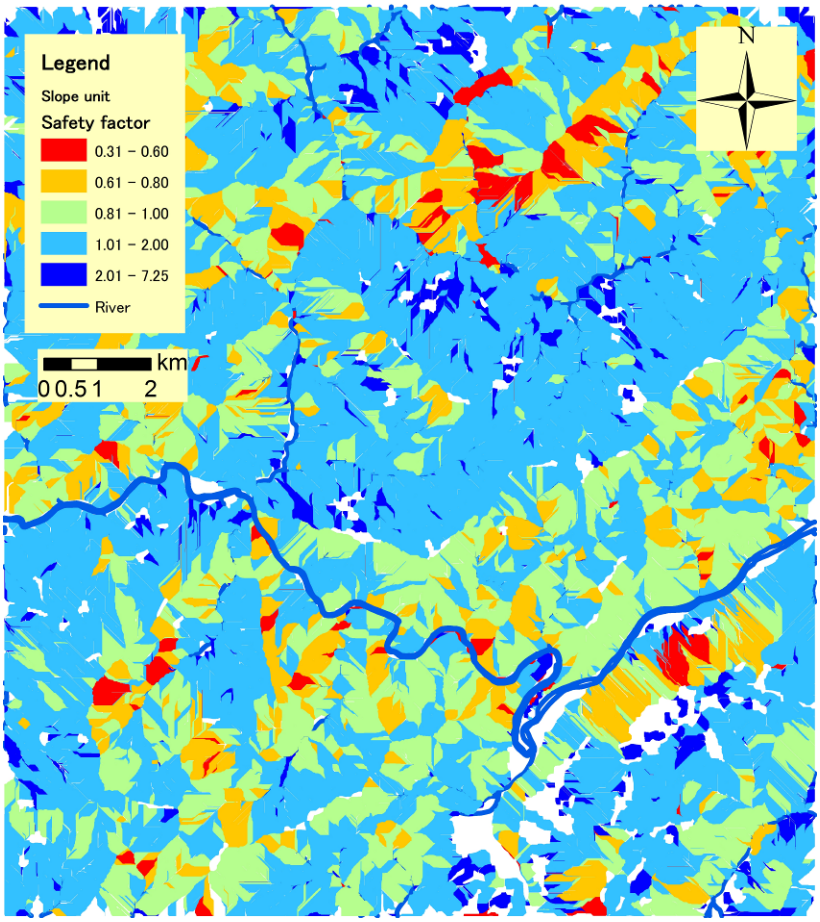

Fig 5.11. The safety factors from 3D slope stability analysis without seismic conditions.

The results with seismic conditions are shown in Fig 5.12. The mean value of safety factors is 0.96, ranging from 0.29 to 5.45. The safety factors increase about

8.5% in mean from 2D safety factors with seismic conditions and decrease about 22.7.% in mean from 3D safety factors without seismic conditions.

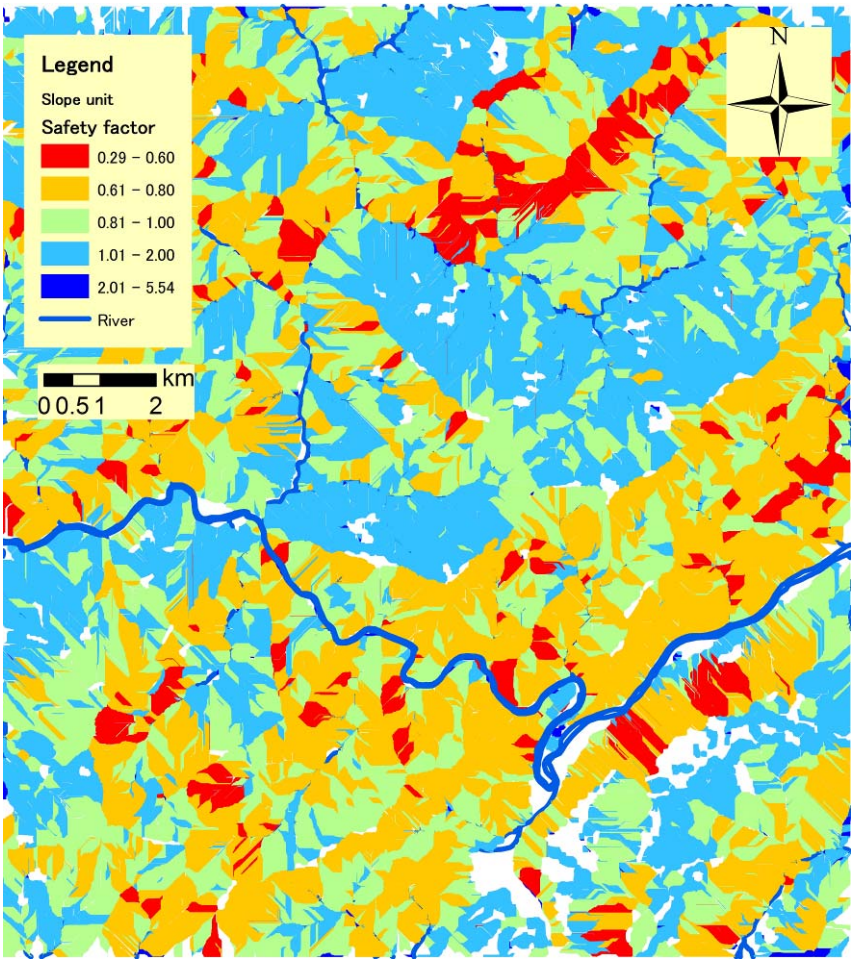

Fig 5.12. The safety factors from 3D slope stability analysis with seismic conditions.

Fig 5.13 gives a comparison of safety factors distribution with and without seismic conditions. It can be seen that 1,396 slope units have a high risk (SF < 0.8) of landslide without seismic conditions, accounting for 13.9% of the total slopes; while 3,495 slope units have a high risk of landslide with seismic conditions, accounting for 34.8% of the total slopes.

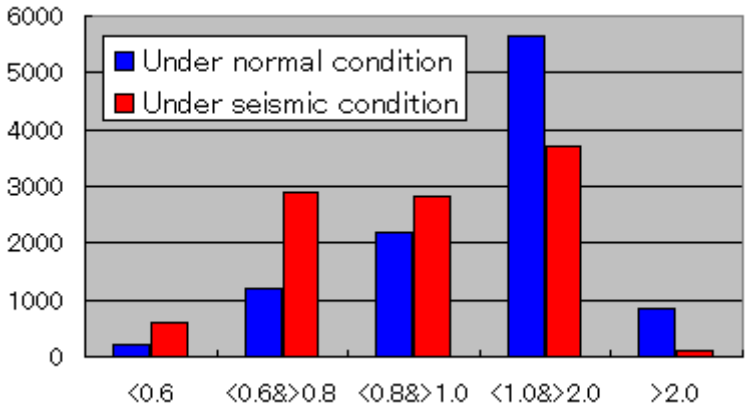

Fig 5.13. Comparison of safety factors distribution with and without seismic conditions.

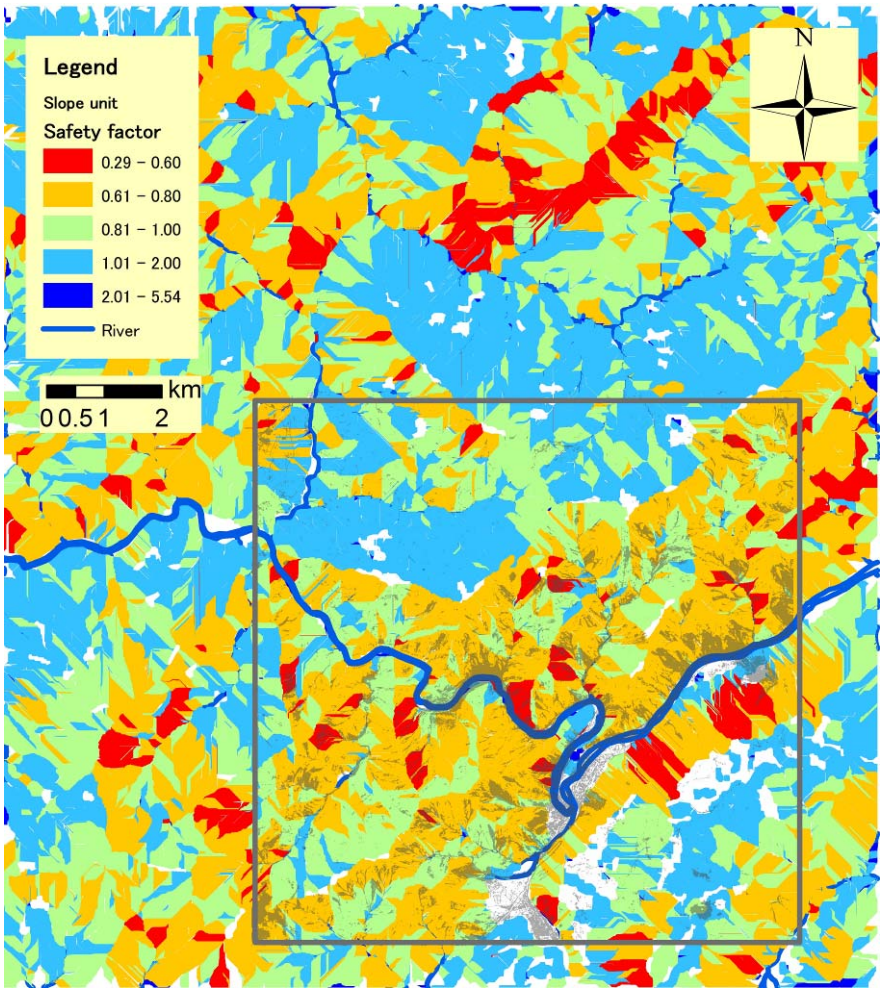

Fig 5.14. Safety factors distribution covered with satellite image (displacement area in green).

To verify the accuracy of the results, a displacement distribution map extracted from a satellite image is overlaid above the safety factor distribution map derived from the 3D stability analysis with seismic conditions. From the layered map of Fig 5.14, we can see most of the displacement takes place at the high-risk area (SF < 0.8). Therefore, we can conclude that the safety factors derived from the 3D stability analysis represent the tendency of landslide occurrence.

5.6 SUMMARIES

This chapter first introduced an existing hazard mapping method based on the Hovland method, a 3D limit equilibrium analysis method with an ellipsoid slip mode. This method applies Monte Carlo simulation to determine the parameters and this resulted in inefficiency and limitations.

A new mapping approach is proposed to determine the parameters of an ellipsoid. It is based on the 2D limit equilibrium analysis with the Swedish method. The improvements include an increase in the conversion progress to extract an elevation matrix for slip surface searching; and the ability to estimate the parameters of an ellipsoid slip body using 2D analysis results instead of Monte Carlo simulation.

The above procedures were all coded into a GIS module and grouped into an assessment tool kit. With the help of developed tools, the 3D slope stability analysis can be easily performed and managed.

Finally, the proposed hazard mapping method was implemented at Tongkou River area. The results represent the tendency of landslide occurrence and show a higher effectiveness than the existing method.

REFERENCES

Anagnosti P, 1969, Three dimensional stability of fill dams. In: Proceedings of the 7th International Conference on Soil Mechanics and Foundation Engineering, Mexico, 2, 275-280.

Azzouz A. S, BaUgh, M. M, and Ladd, C. C, 1981, Three dimensional stability analysis of four embankment failures. In: Proceedings of the 10th International Conference on Soil Mechanics and Foundation Engineering, Stockholm, 3,

p.343-346.

Azzouz A. S, Baligh M. M, 1983, Loaded areas on cohesive slopes. In: Journal of the Geotechnical Engineering Division, ASCE, 109(5), p.724-729.

Baker R, Leshchinsky D, 1987, Stability analysis of conical heaps. In: Soils and Found, 27(4), p.99-110.

Baligh M. M, Azzouz A. S, 1975, End effects on stability of cohesive slopes. In: Journal of the Geotechnical Engineering Division, ASCE, 101(11), p.1105-1117.

Baligh M. M, Azzouz A. S, Ladd C. C, 1977, Line loads on cohesive slopes. In: Proceedings of the 9th International Conference on Soil Mechanics and Foundation Engineering, Tokyo, 2, p.1317.

Bishop A. W, 1955, The use of the slip circle in the stability analysis of slopes. In: Geotechnique, London, 5(1), p.7-17.

Cavounidis S, 1987, On the ratio of factors of safety in slope stability analysis. In: Geotechnique, London, 37(2), p.207-210.

Chen R. H, Chameau J. L, 1982, Three dimensional slope stability analysis. In: Proceedings of the 4th International Conference on Numerical Methods, in Geomech, 2, p.671-677.

Chen R. H. Chameau J. L, 1983, Three-dimensional limit equilibrium analysis of slopes. In: Giotechnique, London, 33(1), p.31-40.

Dennhardt M, Forster W, 1985, Problems of three dimensional slope stability. In: P Proceedings of the 11th International Conference on Soil Mechanics and Foundation Engineering, San Francisco, 2, p.427-431.

Duncan J. M, 1996, State of the art: limit equilibrium and finite-element analysis of slopes. In: Geotechnical engineering, ASCE, 122(7), p.577-597.

Giger M. W, Krizek R. J, 1976, Stability of vertical corner cut with concentrated surcharge load. In: Journal of Geotechnical Engineering, ASCE, 102(1), p.31-40.

Gens A, Hutchinson J. N, Cavounidis S, 1988, Three dimensional analyses of slides in cohesive soils. In: Geotechnique, London, 38(1), p.1-23.

Hovland H. J, 1977, Three-dimensional slope stability analysis method. In: Journal of Geotechnical Engineering, ASCE, 103(9), p.971-986.

Hungr O, 1987, An extension of bishop's simplified method of slope stability analysis to three dimensions. In: Geotechnique, 37(1), p.113-117.

Hungr O, Salgado F. M, Byrne R. M, 1989, Evaluation of a three-dimensional method of slope stability analysis. In: Canadian Geotechnical Journal, 26, p.679-686.

Larsen I. J, Montgomery D. R, Korup O, 2010, Landslide erosion controlled by hillslope material. In: Nature Geoscience, 3(4), p.247-251.

Lam L, Fredlund D. G, 1993, A general limit equilibrium model for three-dimensional slope stability analysis. In: Canadian Geotechnical Journal, 30(6), p.905-919.

Leshchinsky D, Baker R, Silver M. L, 1985, Three dimensional analysis of slope stability. In: International Journal for Numerical and Analytical Methods in Geomechanics, 9(2), p.199-223.

Leshchinsky D, Baker R, 1986, Three-dimensional slope stability and effects. In: Soils and Found, 26(4), p.98-110.

Leshchinsky D, Mullet T. L, 1988, Design charts for vertical cuts. In: Journal of Geotechnical Engineering, ASCE, 114(3), p.337-344.

Leshchisky D, Huang C. C, 1992, generalized three dimensional slope stability analysis. In: Journal of Geotechnical Engineering, 118(11), p.1748-1763.

Michalowski R. L, 1989, Three dimensional analysis oflocally loaded slopes. In: Geotechnique, London, 39(1), p.27-38.

Seed R. B, Mitchell J. K, Seed H. B, 1990, Kettlemen Hills waste landfill slope failure, II: stability analysis. In: Journal of Geotechnical Engineering. ASCE, 116(4), p.669-690.

Ugai K, 1985, Three-dimensional stability analysis of vertical cohesive slopes. In: Soils and Found. Tokyo, 25(3), p.41-48.

Ugai K, 1988, Three dimensional slope stability analysis by slice methods. In: Proceeding of 6th International Journal for Numerical and Analytical Methods in Geomechanics, 2, p.1369-1374.

Xie M, Esaki T, Zhou G, Mitani Y, 2002, Three-dimensional stability evaluation of landslides and asliding process simulation using a new Geographic Information Systems component. In: Environmental Geology, p.1-24.

Xing Z, 1988, Three dimensional stability analysis of concave slopes in plan view. In: Journal of Geotechnical Engineering, ASCE, 114(6), p.658-671.

Zhang X, 1988, Three-dimensional stability analysis of concave slope in plan view. In: Journal of Geotechnical Engineering, ASCE, , 114, p.658-671.

CHAPTER 6

DEVELOPMENT OF A PREDICTION SYSTEM FOR LANDSLIDE DAM HAZARD MAPPING

6.1 INTRODUCTION

To form a landslide dam, the slope first has to be prone to a landslide. Then, the slide has to have enough mass volume to block a river. Finally, the spatial relation must allow the slide mass to reach the river. The previous chapters discussed the slope units division, slope stability analysis, and the slide volume estimating. This chapter aims to extract the spatial landslide dam prone slopes with GIS tools, and then establish a prediction system for landslide dam hazard mapping based on the above assessment.

In the previous studies on earthquake-induced landslide-dams, research has mainly focused on the prediction method for the flood flow at the time of collapse and numerical simulations (Costa, 1998; Yoshino, 2011). Other research has focused on analyzing the geotechnical, sediment logical, and particle size distribution of dam materials by field investigation and laboratory tests (Weidinger et al., 2002; Casagli et al., 2003; Dunning and Armitage, 2011; Weidinger, 2011). However, there have been few studies on landslide dam hazard mapping, despite the fact that it is important for breaking the disaster chain. A few methods based on statistics have been developed for landslide-dam susceptibility assessment (Jibson et al., 2000; Guzzetti et al., 2005; Corominas and Moya, 2008; Lee et al., 2008; Owen et

al., 2008; van Westen et al., 2008). However, they have not provided any landslide-dam hazard maps.

Therefore, this study presents a practical prediction system to extract the dangerous slopes based on an assumption that the landslide-dams are only formed when a large amount of landslide deposits directly rush into a river with moderate or high velocities. The extractions were based on slope unit division and consist of five filters: (1) Buffer filter; (2) Aspect filter; (3) Blockage filter; (4) Stability filter; and (5) Volume filter.

Then, the prediction method was used to extract slopes that have the potential to collapse and form landslide-dams in the catchment of the Tongkou River after the 2008 Wenchuan earthquake. Results show that the proposed method is effective and efficient.

6.2 HAZARD MAPPING METHOD

To extract the dangerous slopes that are thought to be prone to earthquake-induced landslide-dams, it was first necessary to identify slope units for analysis. The method proposed in Chapter 3 was used to meet this requirement, and then five filters were proposed for validation. A flow chart of the proposed prediction system is shown in Fig 6.1, including the following steps:

I) Slope units identification. All the slopes are identified based on the slope unit tool in GfIS, which we developed for the target area.

II) Buffer filter. The slopes along a stream are extracted for a certain distance from the riverbanks.

III) Aspect filter. A slope that could

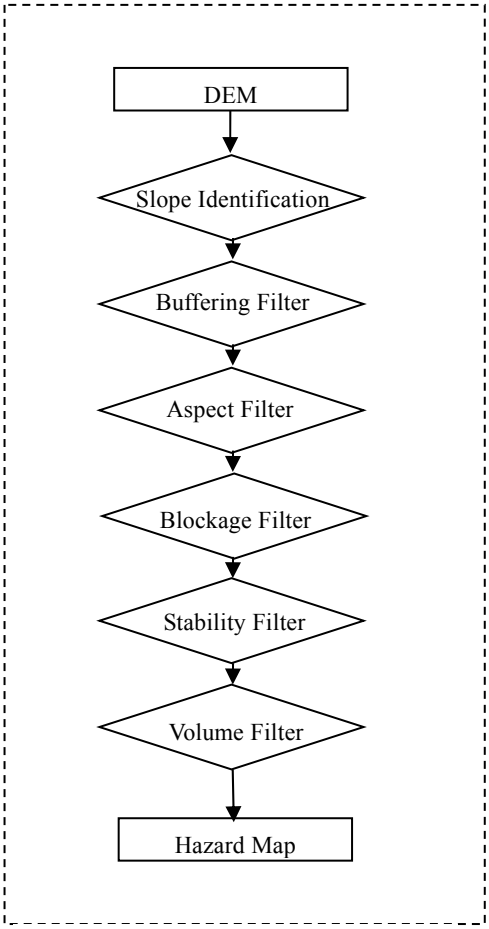

Fig 6.1. A flow chart of prediction system

not reach the river is excluded according to its direction to the river.

IV) Blockage filter. A slope that could not reach to the river is excluded according to the blockage height along the way to the river.

V) Stability filter. The slopes with low susceptibility are excluded by the index of safety factor calculated from the 2/3D Limit Equilibrium Analysis.

VI) Volume filter. The volume of slide mass calculated from Limit Equilibrium analysis is also considered to exclude low possibility slope for landslide dam formation.

VII) Production of the hazard map.

6.2.1 BUFFERING FILTER

To form a landslide-dam, the collapsed slope unit needs to be close enough to the river channel. Thus, a buffer filter is developed to extract those landslide-dam-prone slopes through a given distance D_r to the river.

GIS functions are used to make up this filter. First, the center point of each slope unit is calculated through PolygonToPoint tool. Then, the distance from the center point to the target river is derived by Near tool. Finally, by excluding the slope units with a center point that have a distance large than D_r, such as Slope unit 1 in Fig 6.2, the goal is achieved.

An example in Fig 6.3 shows the extracted center points in red, the slope units in green, and the river line in blue. The slope units with a distance < D_r are extracted as landslide-dam-prone slopes.

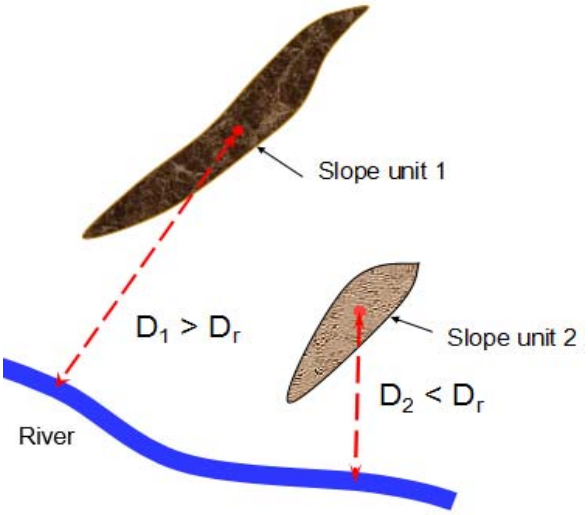

Fig 6.2. Distance from the center point of the slope unit to the dammed river.

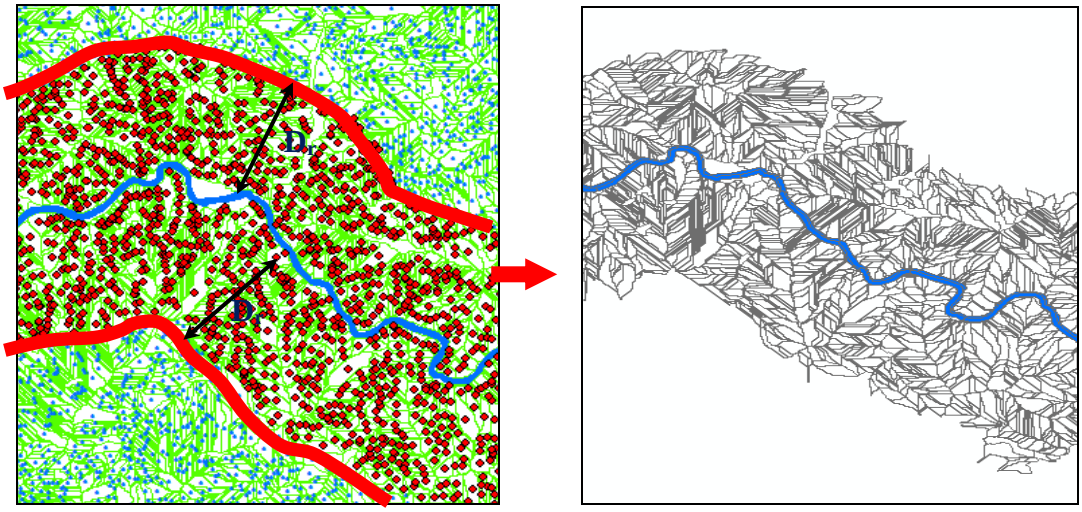

Fig 6.3. An example of the Buffering filter

6.2.2 ASPECT FILTER

To extract dangerous landslide-dams, it is necessary to consider whether the slide runouts can reach the valley or not. This could be done by extending a runout path towards the slide direction and then checking if it is conjoined with the stream lines. As highlighted in Chapter 4, the highest point was linked to the lowest point in each slope unit to obtain the approach runout path and direction (cross line). In this section, the derived cross lines are deemed as runout paths and extended a distance of D_r towards the downhill side. An example is shown in Fig 6.4, which

shows the extracted runout paths in red and the excluded runout paths in blue. Thus, we can judge if they reach the valley by intersecting with the river lines. Then, SpatialJoin tool of GIS was used here to obtain the spatial relationship between the extended lines and the stream lines. Finally, the aspect filter was achieved by excluding the runout paths that could not intersect with the river line. An example is shown in Fig 6.5 in which Slope unit 1 has an aspect that does not extend towards river, so it is excluded from landslide-dam-prone slopes.

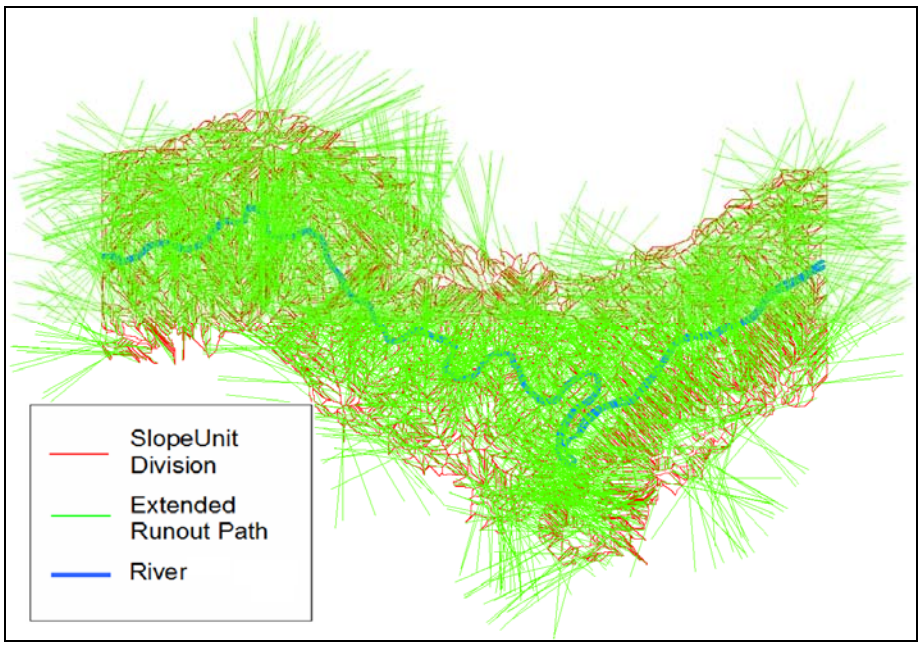

Fig 6.4. An example of an Aspect filter.

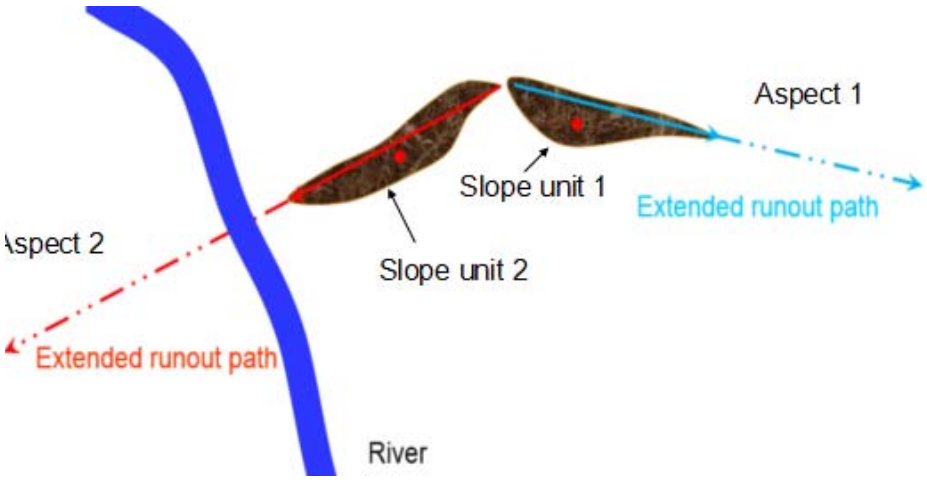

Fig 6.5. Extended runout paths and the dammed river.

6.2.3 BLOCKAGE FILTER

Another decisive factor of whether the slide runouts can reach the valley is the blockage height along the runout path towards river. Here, the blockage height is deemed a risen topography on the runout path, as shown in Fig 6.6. When it is high enough (> H_b), it is considered a hill along the runout path and the landslide deposits will be blocked in front of the blockage, or it is a slot sideward the runout path and the landslide deposits will be redirected along the slot so that they will not be able to reach the valley. In other words, the target slope unit is not a riverside slope. So the elevation of the extracted runout path is checked before it conjoins the river line.

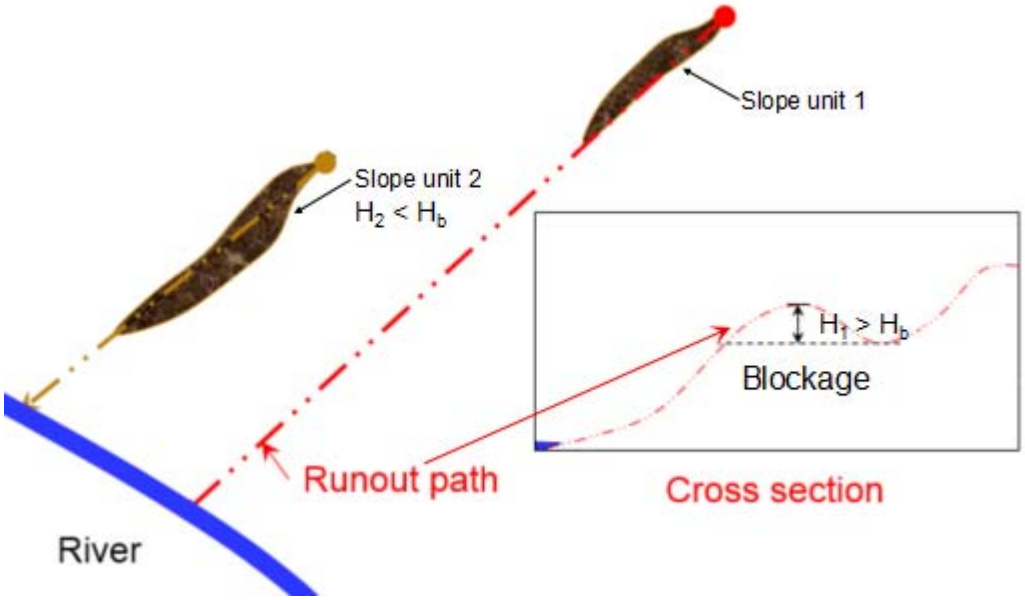

Fig 6.6. Slope unit and its blockage in cross section.

A GIS module is developed to make this filter. From the cross section in Fig 6.6, the slide direction can be deemed as starting from the higher elevation to the lower. Thus, the developed module counts the risen topographies along the slide direction and records the highest one. Any slope unit with a height > H_b is excluded from the landslide-dam-prone slopes, such as slope 1 in Fig 6.6.

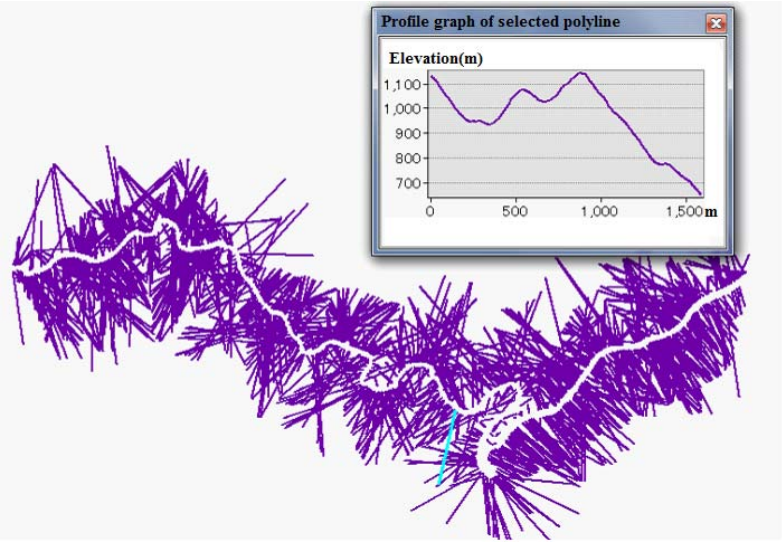

Fig 6.7. Slope unit and its blockage in cross section.

To employ this filter, the extended runout paths obtained above were first cut off by the two side lines of the river region using the Intersect tool of GIS. Secondly, the elevations were extracted along cut lines at a cross section shown in Fig 6.7. Thirdly, the developed module was executed to obtain the risen topography height. Finally, all the slopes with > H_b blockage were excluded because they cannot reach the river.

6.2.4 STABILITY FILTER

To extract dangerous landslide-dams, it is necessary to consider whether the slope is apt to slide under seismic conditions or not. As introduced in Chapters 4 and 5, this study has developed landslide hazards mapping methods using 2D or 3D slope stability analysis. Thus, the safety factor can be used as the fourth filter to exclude those stable slopes that cannot be landslide deposit providers.

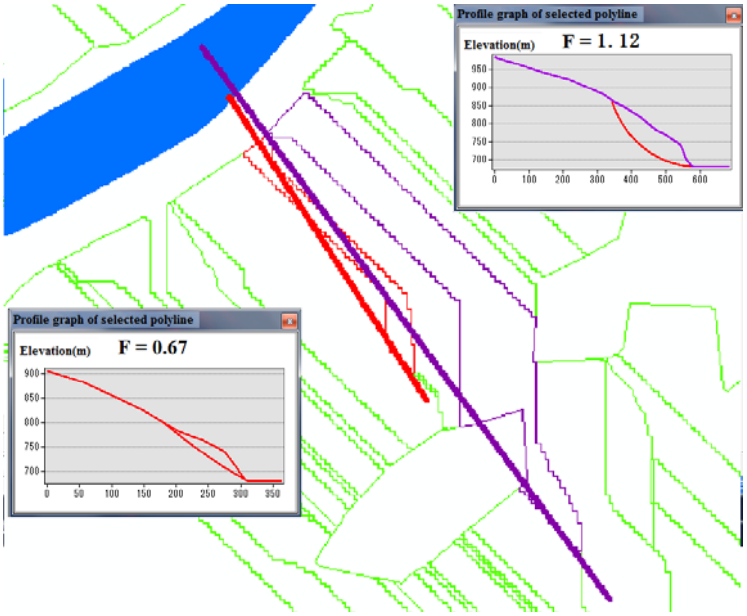

Fig 6.8. An example of a Stability filter.

Because 3D methods accommodate the most complex data of geometry, and the spatial distribution of slip body is better considered than in a 2D model, this study recommends the use of 3D safety factors to extract prone danger slopes. Following the proposed method, the 3D safety factors under seismic conditions can be derived. Then, the safety factors were used as a stability reference, so that slopes considered unlikely to collapse are excluded. Examples are shown in Fig 6.8, which shows a danger path with a SF = 0.67 in red and a stable path with a SF = 1.12 in purple.

6.2.5 VOLUME FILTER

Considering a channel blocking scenario, the scale of the landslide is a determining factor in the formation a river dam. As shown in Fig 6.9, a profile cross section from the Tangjiashan landslide is drawn with assumed landslide scales. It is very clear from the Fig that large-scale landslides have a significantly higher possibility of forming landslide-dams. The deposit volume can be derived by:

$$V_b = V_s - V_d \quad (6.1)$$

Where the V_s is the total slide mass volume and Vd is the deposit volume on the way.

If the minimum required block volume is V_r, when $V_b > V_r$, the landslide-dam takes place. By defining:

$$k_v = V_d / V_s \quad (6.2)$$

V_b can be represented as:

$$V_b = (1-k_v)\, V_s \quad (6.2)$$

V_s can be derived from 3D stability analysis. However, k is determined by the river condition and affected by the runout distance and the inclination of the ground. It is difficult to determine the variations at different slopes. As the DDA simulate can give a estimating of k_v, a verification of LDPS will be introduced in section 6.4.

As the 3D stability analysis has been implemented, the volume of slide body can be derived and deemed the landslide dam deposit volume. The 3D stability calculation tool was developed to be able to record the volume of each critical slide body in the corresponding polyline attribute table. Then, the volumes were used as a reference so that slopes considered as unlikely to collapse were excluded. Examples are shown in Fig 6.10, which shows a slope unit at high risk of landslide-dam formation with a $V_s = 5.9\times10^5$ in purple and a safe slope unit with a $V_s = 5.9\times10^5$ in red.

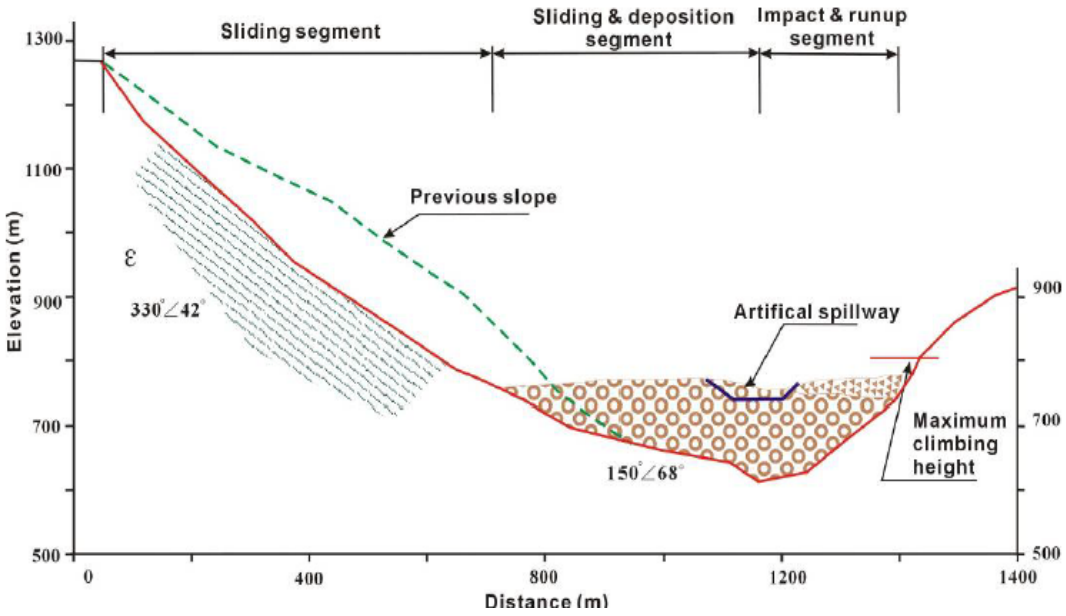

Fig 6.9. Profile of the Tangjianshan slide (Wu, 2011).

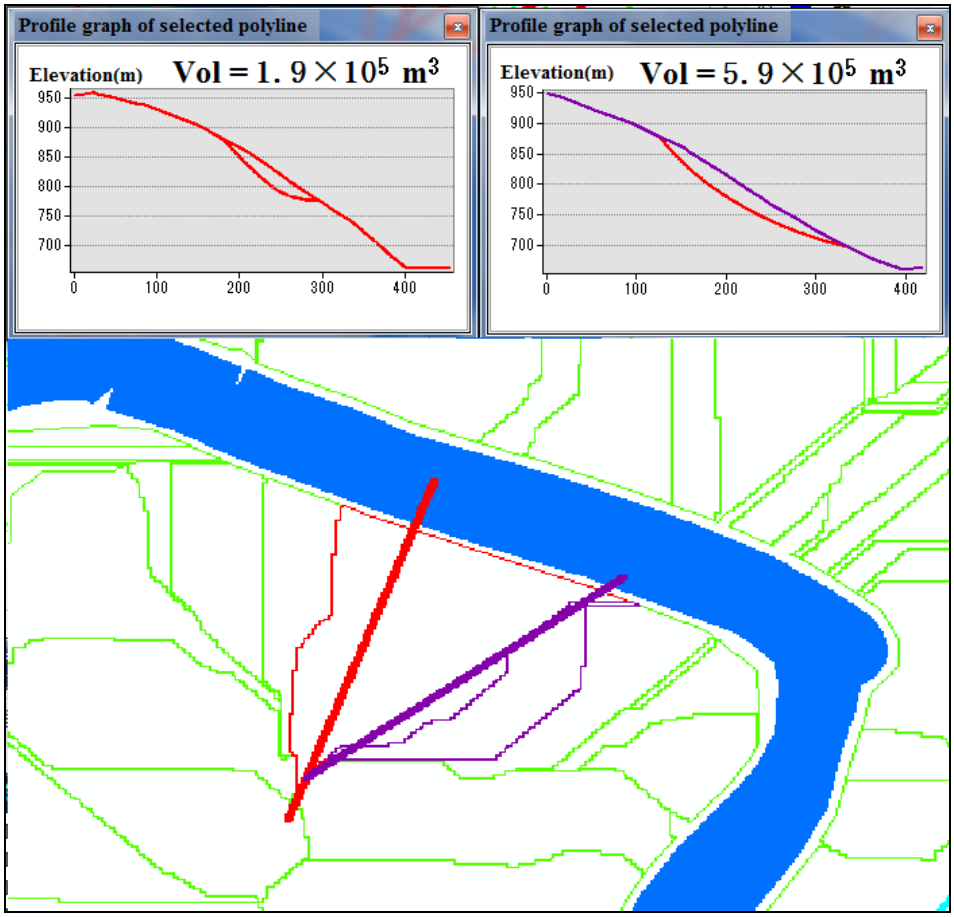

Fig 6.10. An example of a Volume filter.

6.3 LANDSLIDE DAM HAZARD MAP OF THE BASIN OF THE TONGKOU RIVER

This chapter uses the same target area as in the Chapter 5, which is a 15×12 km^2 square field in the basin of the Tongkou River.

6.3.1 STUDY AREA

A large number of the Wenchuan earthquake-induced landslides were able to be observed from satellite images. In addition, five large-scale landslide-dams were reported in this area, including the Tangjiashan Dam, the largest and most dangerous one induced by Wenchuan earthquake (Fig 6.11). The height of the dam varied from 82 to 124 m, the volume was estimated to be 2.04×10^7 m^3. The water storage capacity of landslide-dammed lake was estimated to be 3.15×10^8 m^3 and a submerged area of over 23 km long. Experts feared that aftershocks could shake the dam loose before the lake emptied, flooding communities downstream. Therefore,

thousands of soldiers worked for days to build an artificial spillway by excavation and blasting. The spillway had a positive effect on releasing the impounded water and more than 1 million people avoided being flooded. The basic data utilized in this study included a DEM with resolution of 10 m and a satellite image with resolution of 2.5 m.

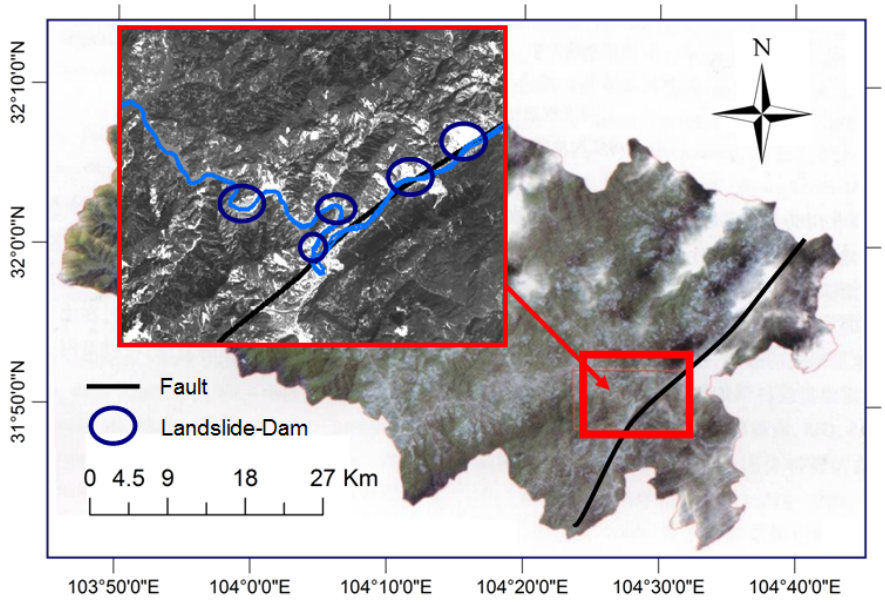

Fig 6.11. Spatial relation between the landslide-dam and the Longmenshan middle fracture zone.

6.3.2 Results and discussion

Slope identification and buffer filter

Following the slope units identification method, 10,186 slope units were identified.

According to the filed investigation at the seismic area after the Wenchuan earthquake, the longest runout distance was about 4.2 km observed from the Daguangbao landslide, but the distance from the center point of the collapsed slope to the dammed channel was about 1.2 km. Therefore, the buffer distance D_r from the center of slope unit to the potentially blocked channel is set at 2 km to include all potential sources slopes for river damming. There were 3,996 slope units extracted along the Tongkou River through the buffer filter, excluding 66.7% of

total slope units. The results are shown in Fig 6.12.

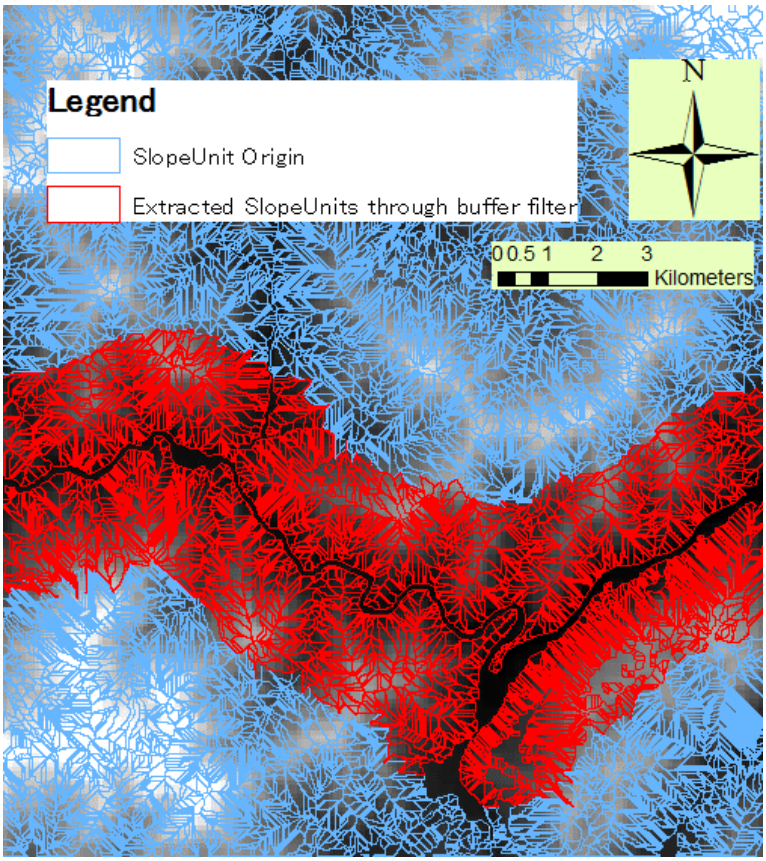

Fig 6.12. Extracted slope units through the buffer filter.

ASPECT FILTER

Then, the highest point was linked to the lowest point in each slope unit, and runout paths were extended 2 km towards the downhill side. Through the aspect filter, 1,596 slope units were extracted as potential risk areas from the remaining 3,996 slope units, thus excluding 53% of total slope units. The results are shown in Fig 6.13.

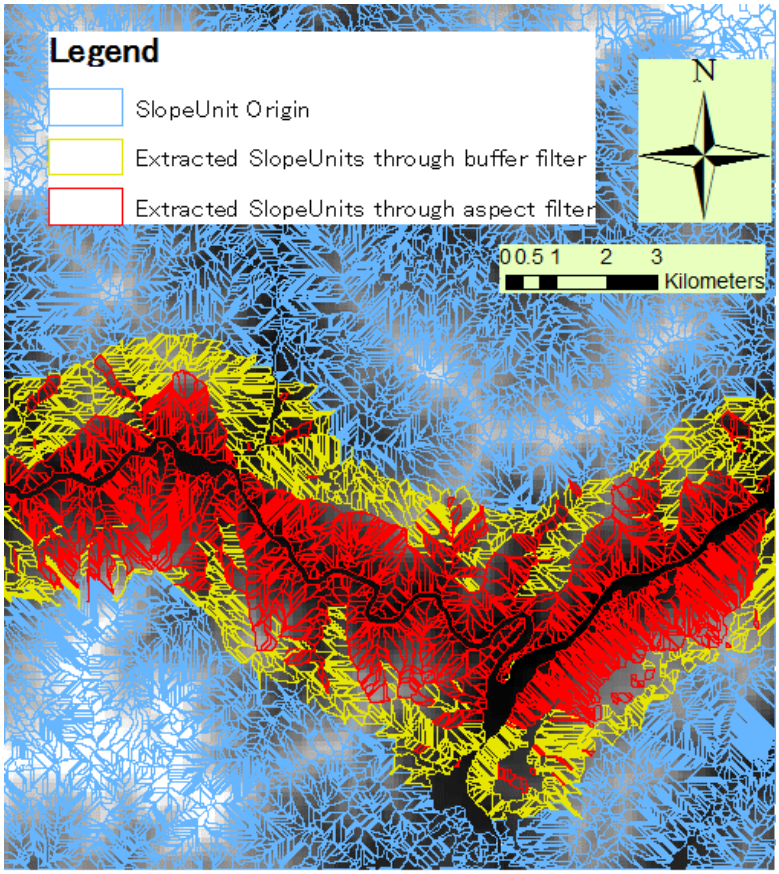

Fig 6.13. Extracted slope units through the aspect filter.

BLOCKAGE FILTER

The blockage height of each runout path was counted from the top towards the downhill direction with the SlopeWalker tool. This study tried many thresholds of H_b for impossible LDPS exclusions. By comparing the satellite image, 5 m satisfies the criteria that do not exclude any risk slopes. Therefore, 1,136 slope units were extracted as potential risk areas from the remaining 1,596 slope units, excluding 28.8% of total slope units. The results are shown in Fig 6.14.

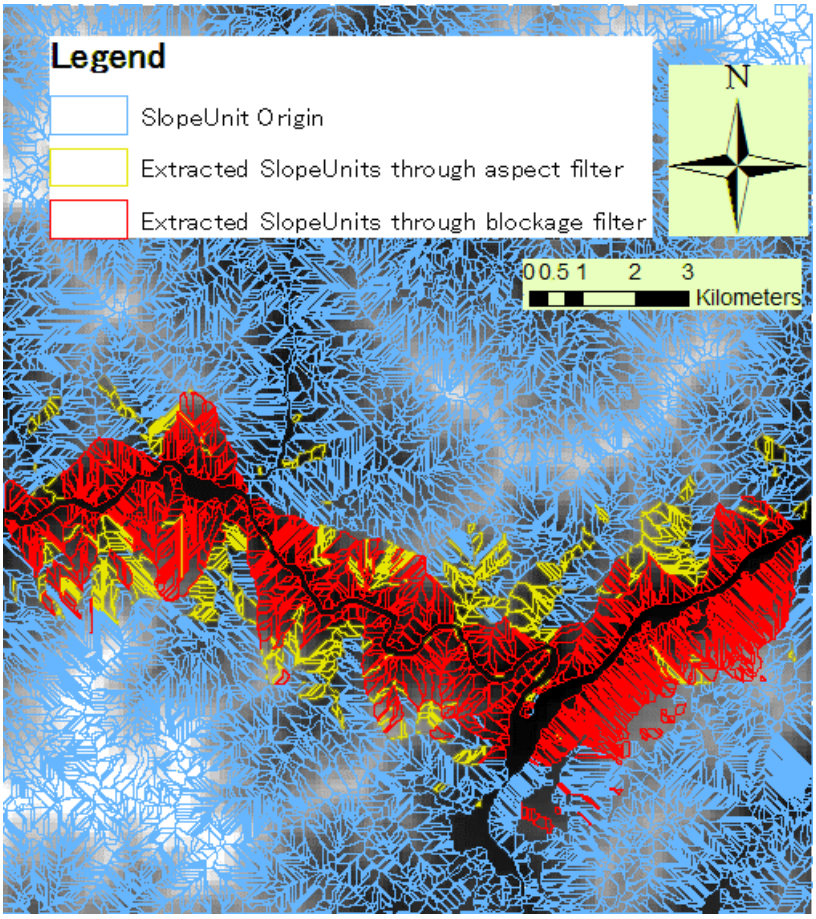

Fig 6.14. Extracted slope units through a blockage filter.

STABILITY FILTER

Before the stability calculation, each cross section line was extended by 10% and 20% of the total projected length at its top and bottom respectively. According to the field investigation at the Tangjiashan landslide, the following parameters, which are the averages of remaining weathered rock, were performed in the safety factor calculation: the soil unit weight is γ=22kN/m3, the cohesion strength of slope material is c=20kN/m2, and the internal friction angle of slope material is φ=32°. The results are shown in Fig 6.15.

It should be noted that the used soil material is predicted under an ideal assumption (the soils are homogeneous using parameters of weathered rock). If we consider satellite images, one could conclude that most landslide deposit areas shown in satellite images are within the slope units whose 3D safety factors are less than 0.8. The parameters of weathered rock are fairly weak and more apt to collapse

than actual material. Moreover, the Hovland method used does not consider the inter slice forces, so the safety factors are smaller than the reality. In this study, the slope units with a safety factor of more than 0.8 are excluded as impossible LDPS. As a result, 612 slope units were extracted as potential risk areas from the remaining 1,136, excluding 61.7% of total slope units (Fig 6.16).

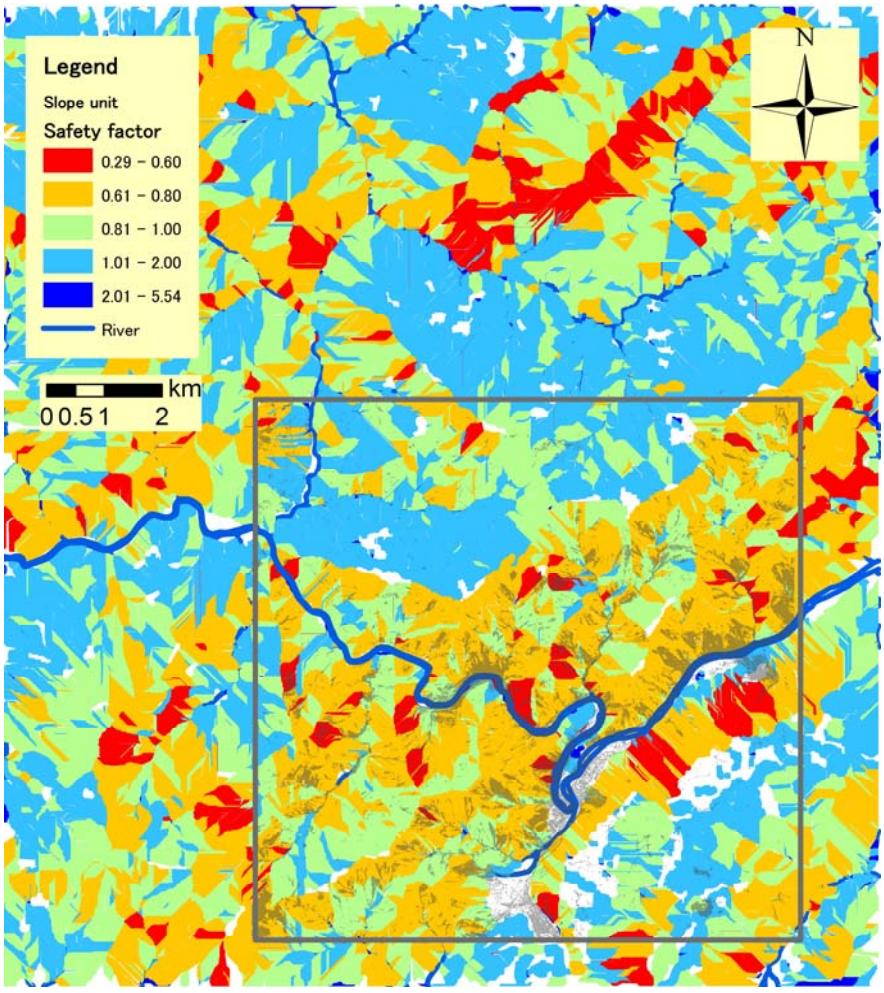

Fig 6.15. Safety factors distribution covered with satellite image (landslide deposit area in grey).

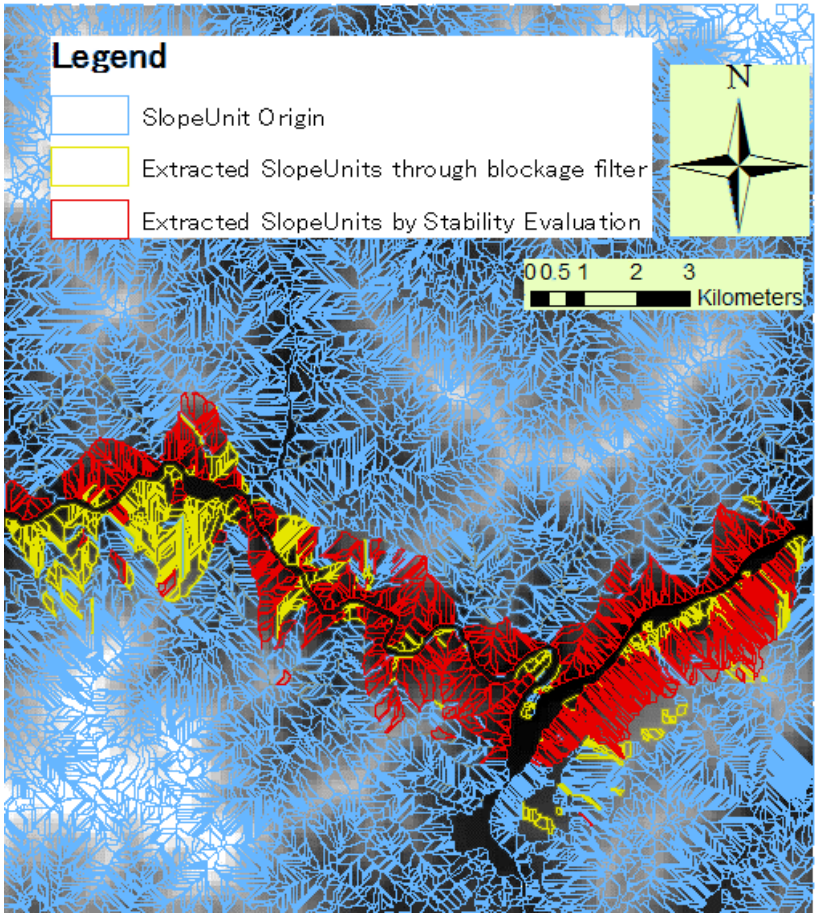

Fig 6.16. Extracted slope units by 3D stability filter (in red region).

VOLUME FILTER

As the program coded, the volume of critical slide body was recorded for each slope attribute table as in the previous step. A volume distribution map of the critical slide body of each slope unit is depicted in Fig 6.17 and it is covered with a satellite image (landslide deposit area in black). It can be seen that the slope units with little volume assumed are all small slope units and not covered with landslide deposit area.

Fan (2012) studied 65 landslide-dams that took place after the Wenchuan earthquake, and the smallest one had a volume > 5×10^5. Since there is no reference to determine the value of k_v for a variety landslides over a wide area, this study simply assumed $k_v = 0$ at present. Thus, slope units with volume < 5×10^5 are considered unable to block the valley entirely and were excluded from this study.

Therefore, 584 slope units were extracted as potential risk areas from the

remaining 612, excluding only 4.6% of total slope units. The final results are derived through volume filter, as shown in Fig 6.18.

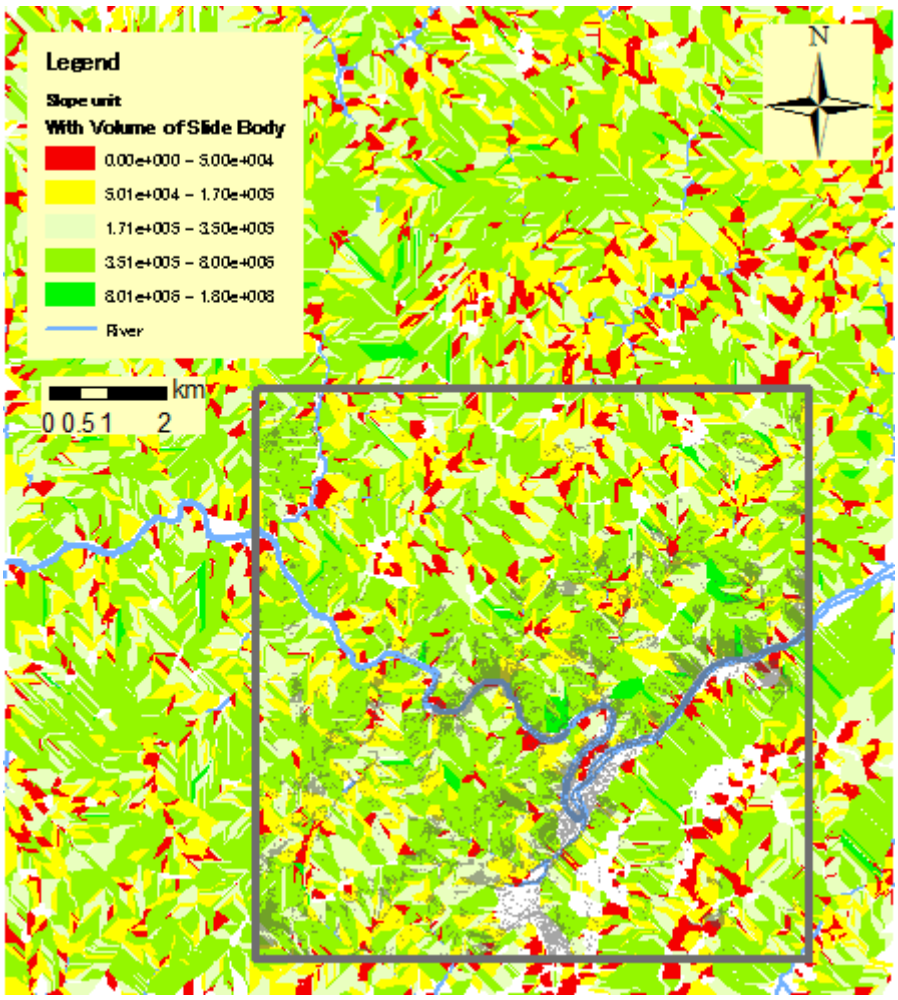

Fig 6.17. A volume distribution map of the critical slide body of each slope unit.

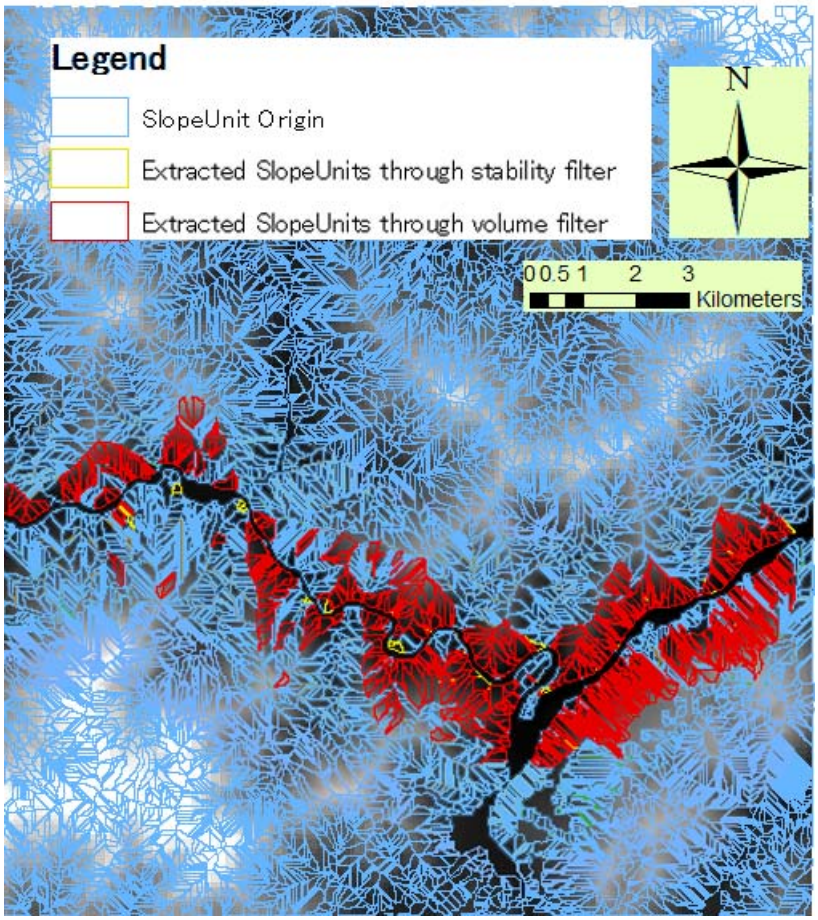

Fig 6.18. Extracted slope units by a volume filter (in red region).

HAZARD MAP

Finally, the hazard map for landslide dam was processed using the extracted slope units from all five filters. The results are ranked by the index of 3D safety factor, as shown in Fig 6.19.

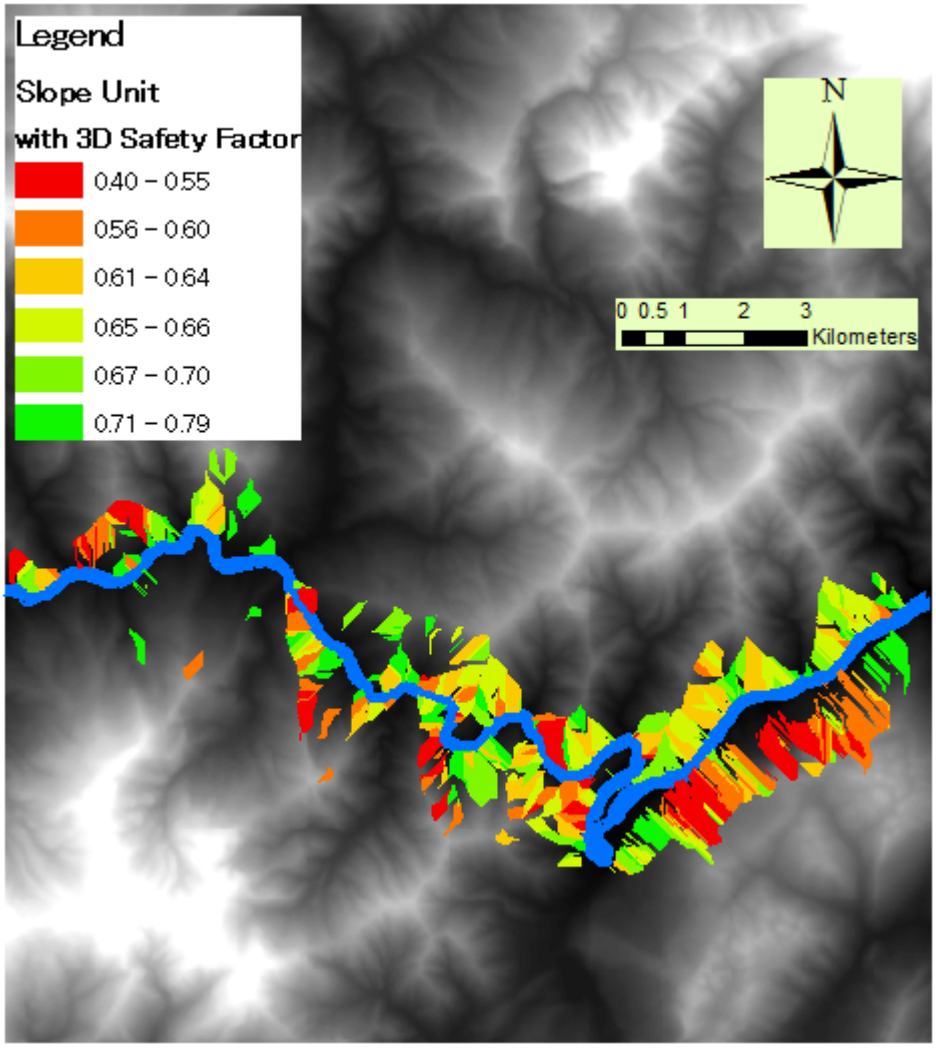

Fig 6.19. Landslide-dam hazard map ranked by 3D safety factors.

6.4 VERIFICATION OF LANDSLIDE-DAM PRONE AREA USING DDA SIMULATION

Because we can obtain the runout distance, distribution, and volume of debris from the DDA simulation, landslide-dam formation can be deduced based on river geometry and hydrology data together with the volume of the slide body. The effectiveness of the countermeasure using preventive structures can also be verified by discontinuous deformation analysis (DDA) simulation.

6.4.1 DISCONTINUOUS DEFORMATION ANALYSIS (DDA)

To predict landslide runout, many previous studies use the empirical relation between landslide volume and the tangent of the reach angle (defined as the ratio

between the vertical drop and the horizontal travel distance) (Heim, 1932; Scheidegger, 1973; Hsü, 1975). However, Corominas (1996) concluded that reach angle is dependent not only on landslide volume, but also on other factors, such as landslide type and topographic constraints along the runout path. In this study, the DDA method is used to deduce the landslide movement behavior.

The DDA method originated as a back-analysis algorithm to determine a best fit to a deformed configuration of a block system from field measured displacements and deformations (Goodman and Shi, 1985). It was later extended to perform the complete deformation analysis of a block system, where each block can move and deform independently, and the interaction between blocks is idealized by contact springs (Shi, 1988). Since DDA can be used for analyzing large deformation of materials with discontinuities and simulating rigid body movements in addition to stain-stress analysis, it is one of the most effective methods in disaster prevention.

Some utilizations of DDA in analyzing falls of single blocks and block assemblies have been described by Ohnishi et al. (1996), Koo and Chern (1998), Yang et al. (2004) and Ma et al. (2011). However, recent research has made many extensions and improvements on the original DDA and proposed using DDA to solve some practical problems in disaster prevention (Chen et al., 2010; Zheng et al., 2012; Zhang et al., 2013).

6.4.2 SLOPE MODELING AND VERIFICATION

In DDA simulation, the failure part of the slope, which will later become a landslide mass, must be discretized into an assemblage of blocks. It can be directly discretized according to discontinuities such as joints, faults, and cracks from the field investigation data in some cases. However, it is difficult to obtain such discontinuity data in most cases. Thus, sometimes it is necessary to discretize the failure part of the slope artificially based on appropriately assumed data.

It has been long recognized in rock mechanics that discontinuities (geological structures) significantly influence the response of rock masses to loadings and excavation (Goodman et al., 1968; Manfredini et al., 1975; Bandis et al., 1983).

Thus, the generated blocks should be as natural as possible. The random shape of a polygon is a better choice for cases that lack data.

The random shape of polygons can be obtained by the approach based on the Voronoi diagram (Aurenhammer, 1991) (Fig 6.20). The Voronoi diagram consists of the partitioning of a plane with n points into n convex polygons so that each polygon gives an area containing exactly one point of the n defined points and hedging the portion of the plane that is closer to its point than to any other. Using this unstructured mesh, it is possible to reduce the asymmetric effect obtained with a structured one (Fig 6.21).

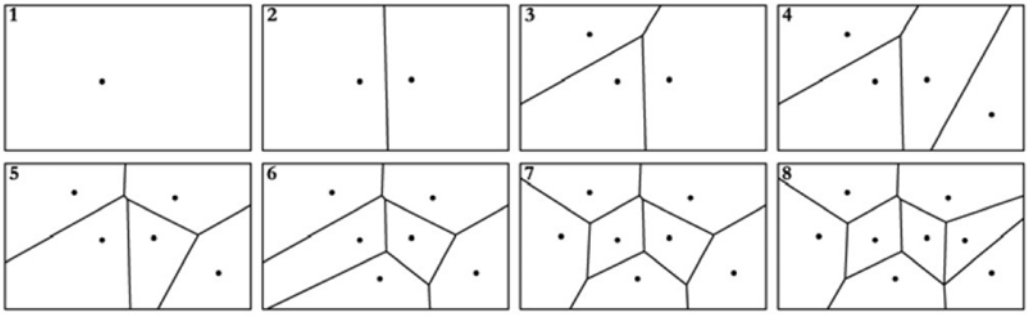

Fig 6.20. The Voronoi diagram

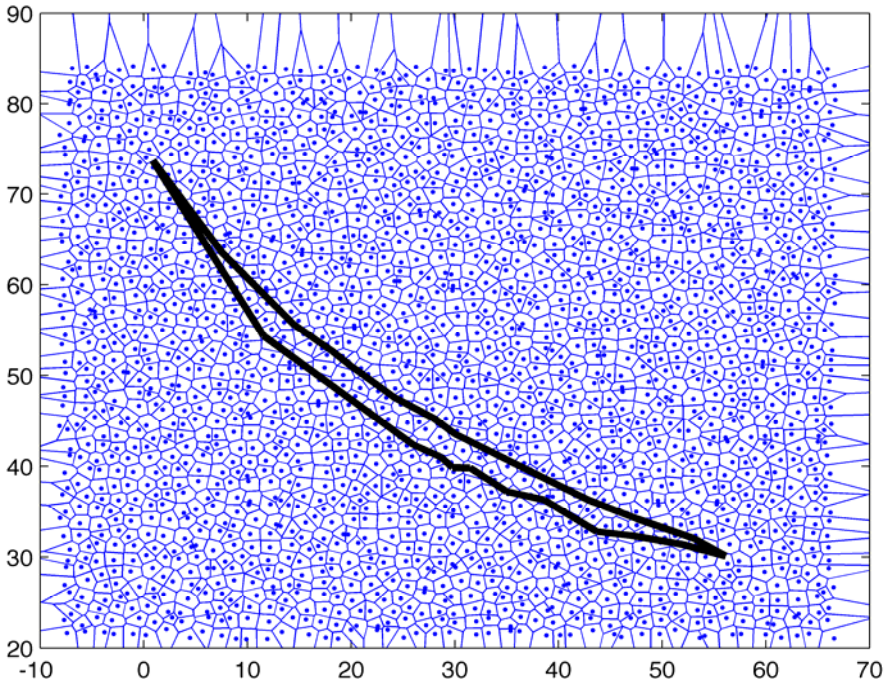

Fig 6.21. Discretization of landslide mass using the Voronoi diagram.

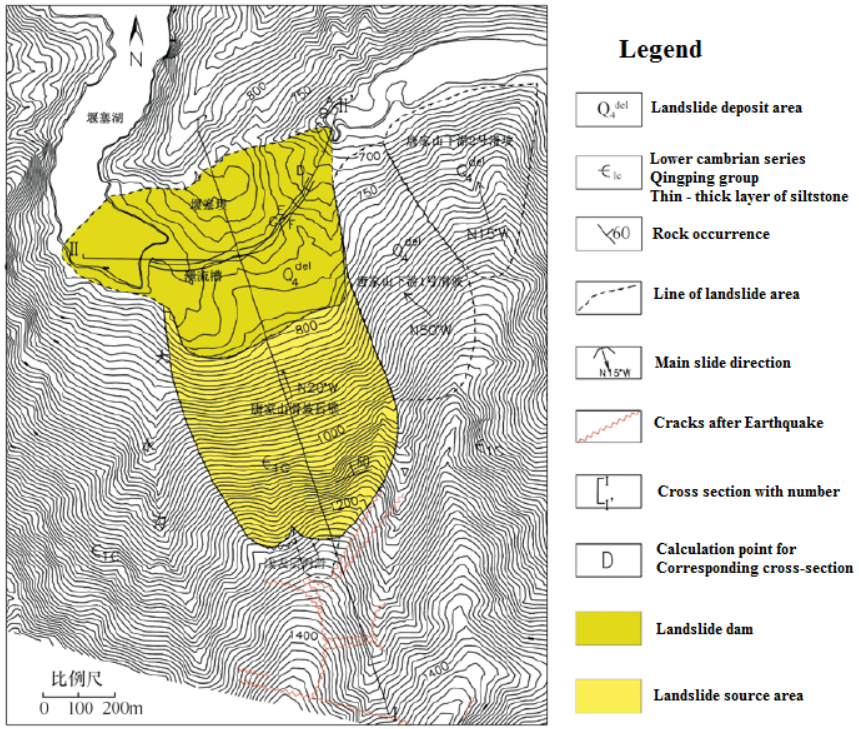

(a)Terrain of Tangjiashan landslide and its barrier dam , after earthquake(Q Xu, 2008)

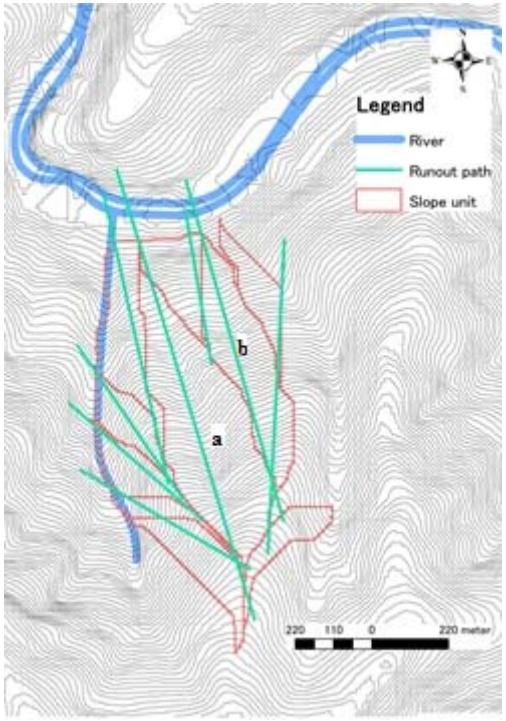

(b) Extacted runout path for stability analysis, before earthquake

Fig 6.22. Tangjiashan landslide and extracted runout paths for DDA simulation.

In this study, we chose the Tangjiashan landslide as a case study for DDA simulation, using the C code program created by Chen. The extracted runout paths are shown in Fig 6.22, marked as a and b. The results are shown as follows:

LANDSLIDE-A

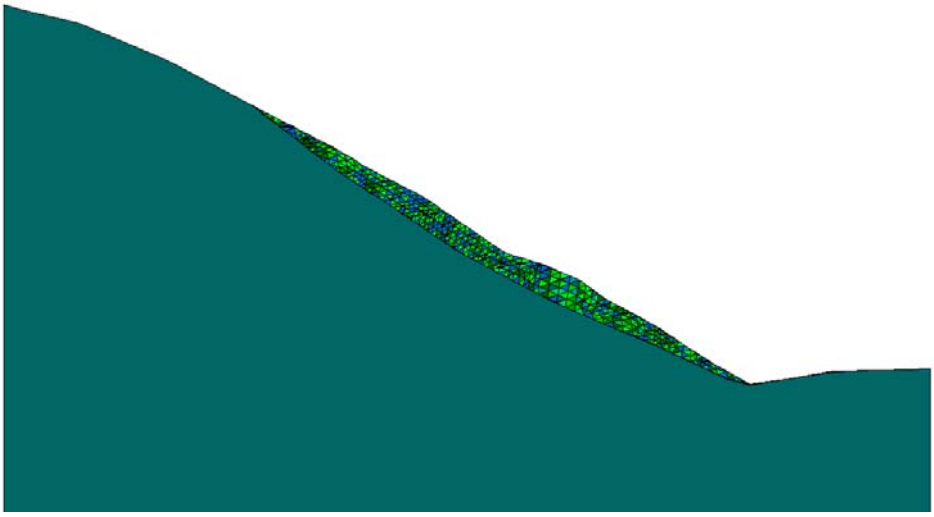

Fig 6.23. Landslide model of Landslide-a.

As shown in Fig 6.23, there were 523 blocks in Landslide-a. The bedrock was formed of one fixed block and the landslide body is divided into 522 blocks. The estimated slide volume from 3D stability analysis is 3,604,181 m^3 and the slide area from 2D stability analysis in this cross section is 24,858 m^2. The slide surface was found by slip circle method and the outline of this landslide came from the GIS data using the parameters shown in Table 6.1.

Table 6.1. Parameters used in the DDA modeling.

Parameter	Value
Unit weight (KN/m^3)	22
Young's modulus (kPa)	106
Poisson's ratio	0.2
Friction angle (°)	32
Cohesion （kPa）	20
Dynamic control parameter	1
Maximum displacement ratio	0.001
Time interval	Automatic
Contact spring stiffness （kN/m）	105
SOR value	1.3
Time steps	1100

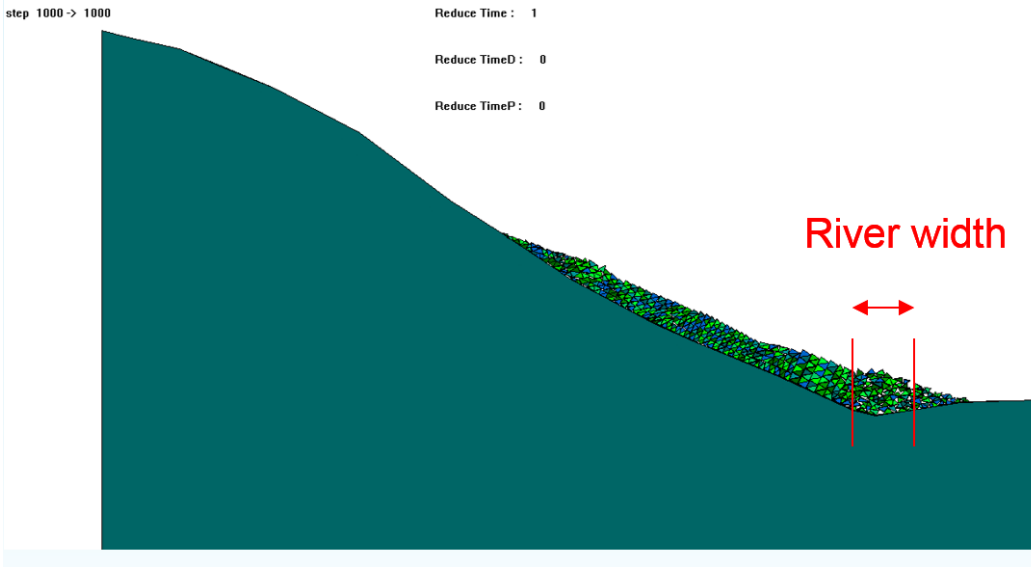

Fig 6.24. Deposit distribution pattern of Landslide-a.

The deposit distributions after 33s (1,000 steps) are shown in Fig 6.24. As the river width is 51 m, about 25% of the deposit area is located above the river area. Therefore, in this case, k_v is derived as 0.75. There is a very high possibility of a

landslide in this case.

LANDSLIDE-B

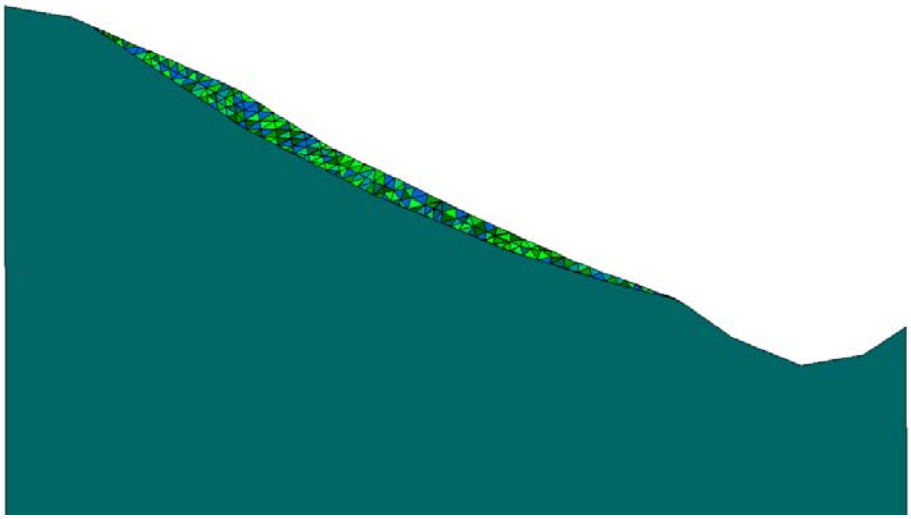

Fig 6.25. Landslide model of Landslide-b.

As shown in Fig 6.25, there were 237 blocks in this block system. The bedrock was formed of one fixed block and the landslide body is divided into 236 blocks. The estimated slide volume of Landslide-b is 3,604,181 m^3 and the slide area is 47,692 m^2. The deposit distributions after 112s (1,100 steps) are shown in Fig 6.26. About 5% of the deposit area is located above the river area. Therefore, in this case, k_v is derived as 0.95. Thus, the possibility of landslide-dam formation is very low in this case.

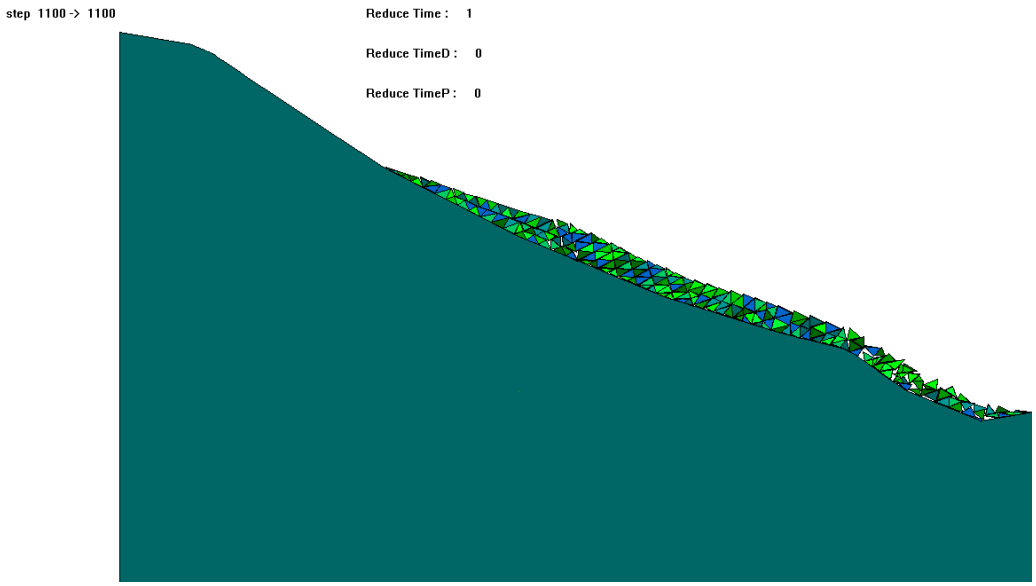

Fig 6.26. Deposit distribution pattern of Landslide-b.

6.5 SUMMARIES

In this chapter, we proposed a new prediction method to extract dangerous slopes as sources of landslide-dams. This prediction was based on GIS tools combining spatial statistics and Limit Equilibrium Analysis.

To extract the dangerous slopes, we first identified slope units for analysis.

Then five filters were proposed to meet the requirements. They are:

- Buffer filter
- Aspect filter
- Blockage filter
- Stability filter
- Volume filter

The final filtering result ranked with the safety factor makes the landslide hazard map.

This method was used to extract slopes that had the potential to collapse and form landslide-dams in the catchment area of the Tongkou River after the 2008 Wenchuan earthquake. Results show that the proposed method is effective and efficient.

In addition, DDA simulation is adopted to verify the potential LDPS after

filtering. The result proves that landslide-dam formation can be deduced based on river geometry and hydrology data together with the volume of the slide body.

REFERENCES

Aurenhammer F, 1991, Voronoi Diagrams - A survey of a fundamental geometric data structure. In: ACM Computing Surveys, 23(3), p.345-405.

Bandis S. C, Lumsden A. C, Barton, N.R, 1983, Fundamentals of rock joint deformation. In: International Journal of Rock Mechanics and Mining Science & Geomechanics Abstracts, 20(6), p.249-268.

Casagli N, Ermini L, Rosati G, 2003, Determining grain size distribution of the material composing landslide dams in the Northern Apennines: sampling and processing methods. In: Engineering Geology, 69(1-2), p.83-97.

Chen G. Q, Zen K, Zheng L, Jiang Z. S, 2010, A new model for long-distance movement of earthquake induced landslide. In: Proceedings of the 44th U.S. Symposium on Rock Mechanics, Salt Lake City, UT, USA.

Corominas J, 1996, The angle of reach as a mobility index for small and large landslides. In: Canadian Geotechnical Journal, 33, p.260-271.

Corominas J, Moya J, 2008, A review of assessing landslide frequency for hazard zoning purposes. In: Engineering Geology, 102(3-4), p.193-213.

Costa J, 1998, Floods from dam failure. In: Floods Geomorphology, p.436-439.

Dunning S. A, Armitage P, 2011, The grain-size distribution of rock-avalanche deposits. In: implications for natural dam stability, Natural and Artificial Rockslide Dams, Springer, p.479-498.

Goodman R. E, Taylor R. L, Brekke T. L, 1968, A model for the mechanics of jointed rock. In: Journal of the Soil Mechanics and Foundations Division ASCE, 94(SM3), p.637-659.

Goodman R. E, Shi G. H, 1985, Block theory and its application to rock engineering. In: Englewood Cliffs, New Jersey, Prentice-hall.

Guzzetti F, 2006. Landslide hazard and risk assement, UniversityBonn, Perugia.

Heim A, 1932, Gergsturz und Menschenleben(Landslides and Human Lives).

Translation by N. Skermer. Bitech Publishers Ltd, Vancouver, Canada.

Hsü K. J, 1975, Catastrophic debris streams (Sturzstroms) generated by rockfalls. In: Geological Society of America Bulletin, 86(1), p.129-40.

Jibson R. W, Harp E. L, Michael J. A, 2000, A method for producing digital probabilistic seismic landslide hazard maps. In: Engineering Geology, 58(3-4), p.271-289.

Koo C.Y, Chern, J.C, 1998, Modification of the DDA method for rigid block problems. In: International Journal of Rock Mechanics and Mining Science, 35(6), p.683-93.

Lee C. T, Huang C. C, Lee J. F, Pan K. L, Lin M. L, Dong J. J, 2008, Statistical approach to earthquake-induced landslide susceptibility. In: Engineering Geology, 100(1-2), p.43-58.

Ma G. C, Matsuyama H, Nishiyama S, Ohnishi Y, 2011, Practical studies on rockfall simulation by DDA. In: Journal of Rock Mechanics and Geotechnical Engineering, 3(1), p.57-63.

Manfredini G., Martinetti S, Ribacchi, R, 1975, Inadequacy of limiting equilibrium methods for rock slopes design. In: Design Methods in Rock Mechanics, Proceedings of the 16th Symposium on Rock Mechanics, University of Minnesota, Minneapolis, American Society of Civil Engineers, p.35-43.

Ohnishi Y, Yamamukai K, Chen G.Q, Application of DDA in rock fall analysis. In: Proceedings of 2nd North American Rock Mechanics Symposium, Montreal, Canada, p.2031-2037.

Owen L. A, Kamp U, Khattak G. A, Harp E. L, Keefer D. K, Bauer M. A, 2008, Landslides triggered by the 8 October 2005 Kashmir earthquake. In: Geomorphology, 94(1-2), p.1-9.

Scheidegger A, 1973, On the prediction of the reach and velocity of catastrophic landslides. In: Rock Mechanics 5, p.231-236.

Shi G. H, 1988, Discontinuous deformation Analysis. In: Ph.D. thesis, University of California, Berkeley, USA.

Weidinger J. T, Wang J, Ma N, 2002, The earthquake-triggered rock avalanche of Cui

Hua, Qin Ling Mountains, PR of China—the benefits of a lake-damming prehistoric natural disaster. In: Quaternary international, 93, p.207-214.

Weidinger J. T, 2011, Stability and Life Span of Landslide Dams in the Himalayas (India, Nepal) and the Qin Ling Mountains (China). In Evans, S. G., Hermanns, R. L., Strom, A., and Scarascia-Mugnozza, G., eds., Natural and Artificial Rockslide Dams, 133, Springer Berlin Heidelberg, p.243-277.

Van Westen C. J, Castellanos E, Kuriakose S. L, 2008, Spatial data for landslide susceptibility, hazard, and vulnerability assessment: An overview. In: Engineering Geology, 102(3-4), p.112-131.

Xu Q, Zhang S, Li W. L, van Asch Th. W. J, 2012, The 13 August 2010 catastrophic debris flows after the 2008 Wenchuan earthquake, China. In: Natural Hazards and Earth System Sciences, 12, p. 201-216.

Yang M, Fukawa T, Ohnishi Y, Nishiyama S, Miki S, Hirakawa Y, Mori S, 2004, The application of 3-dimensional DDA with a spherical rigid block for rockfall simulation. In: International Journal of Rock Mechanics and Mining Sciences, 41(S1), p.611-616.

Yoshino K, J Takahama, T Mizuyama, T Uchida, K Ogawa, 2011, Numerical simulation of landslide dam overtopping erosion process considering side bank collapse. In: Journal of the Japan Society of Erosion Control Engineering 63(6), p.52-58.

Zhang Y. B, Chen G. Q, Zheng L, Li Y, 2012, Numerical analysis of the largest landslide induced by the Wenchuan earthquake, May 12, 2008 using DDA. In: International Symposium on Earthquake-induced Landslides (IS-Kiryu), Kiryu, Japan.

Zheng L, Chen G. Q, Kasama K, Li Y. G, Zhang Y. B, 2012, Rockfall simulation with consideration of multi-blocks using 3D DDA and its application to countermeasures. In: Proceedings of 7th Asian Rock Mechanics Symposium (ARMS7), Seoul, Korea.

CHAPTER 7

SUMMARIES

A strong earthquake can induce a large number of landslides, and an extensive landslide can create a Landslide dam when debris flows into and stops a river. The water impounded by a landslide dam can create a dam reservoir, which may raise the surrounding groundwater and cause back-flooding (upstream flooding). Because of its loose nature and absence of a controlled spillway, a landslide dam can easily fail catastrophically and lead to debris flows or downstream flooding. Many reports show that the earthquake-induced landslide disaster chain can cause very serious damage. Therefore, it is important to focus attention on prediction of earthquake induced Landslide dams in order to break the earthquake-induced landslide disaster chain.

Hazard mapping is the first and also very important step for predicting landslide and landslide dam since it shows the location, possibility and dangerousness of potential landslides and landslide dams. However, there are very few studies on landslide dam hazard mapping method although several mapping methods have been developed for landslide. In addition, there are following issues unresolved in the existed landslide hazard mapping methods:

(1) How to identify slope mesh with sensed division;

(2) How to apply a higher accurate and effective stability

analysis method;

(3) How to estimate the landslide volume;

(4) How to analyze debris runout path and deposit distribution and judge if the river can be blocked.

For these reasons, this study aims at solving the above mentioned problems, and the objectives of this study are as follows:

(1) To propose a new approach for slope mesh identification;

(2) To develop a new landslide hazard mapping approach by using a higher accurate 2-D stability analysis method;

(3) To develop a new efficient landslide hazards mapping method using 3-D slope stability analysis;

(4) To develop a practical hazard mapping method for earthquake induced Landslide dam; and

(5) To verify Landslide dam prone area using DDA simulation.

The organization can be summarized as follows: 1) the new approach of slope mesh identification provides a suitable division of slopes for stability analysis; 2) the new landslide hazard mapping approach using 2-D stability analysis method offers the scale information with accurate safety factors; 3) another new approach using 3-D stability analysis determines the shape of an ellipsoid slide body based on 2-D analysis results and gives a prediction of slide volumes; 4) landslide dam hazard map is produced according to the derived safety factors and slide volumes, together with topography data and river conditions. In addition, discontinuous deformation analysis (DDA), a numerical simulation method, is applied to verify the final results.

The thesis consists of seven chapters.

Chapter 1 introduces a geo-disaster chain model from earthquake and gives a brief review of previous research on earthquake-induced disasters. It also describes the scope and objectives of the study.

Chapter 2 reviews the existing landslide hazard assessment methods and gives

a summary of issues that remain unresolved, such as slope unit identification, 2-D and 3-D slope stability analysis considering failure slip shapes, and Landslide dam prone hazard mapping.

Chapter 3 proposes a new slope unit identification approach. First, the problems of the existing method are analysed. Then, a new approach is proposed to solve the problems by (1) developing a method to detect stream lines and catchment areas instead of detecting valley lines and ridge lines, which is the major reason of mis-identification in the existing method; (2) identifying slope units by cutting catchment areas with stream lines. Finally, the improvement of identification accuracy is shown by using the new approach.

Chapter 4 develops a new hazard mapping method based on the well-known 2-D limit equilibrium analysis with a circular slip mode. The existing hazard mapping method is based on an infinite plane slip model (IPSM) because it is easy to implement in GIS. However, since most failure slip surfaces are not planes, a circular slip mode (CSM) is more popular than IPSM in geotechnical engineering because of its high accuracy and ability to accommodate the complex geometry, stratum and groundwater data. Also, the volume of a landslide can be estimated from CSM, which is necessary in Landslide dam hazard mapping. The issue is that IPSM is not easily incorporated into GIS. Therefore, a new hazard mapping method is developed based on the well-known Swedish Method, a 2-D limit equilibrium analysis method with a CSM. First, a method for automatic extraction of a cross slope section is proposed based on the topography of each slope. Then, a GIS module for evaluating slope safety factors based on the Swedish Method is developed using C#. Finally, practical applications have been made and it has been shown that the accuracy of the slope stability analysis improves and the hazard mapping can be completed quickly and effectively.

Chapter 5 develops a hazard mapping method based on 3-D limit equilibrium analysis. In order to estimate the volume of a landslide, a 3-D slope stability analysis is necessary. A semi-ellipsoid slip model is used in general. The key issue is how to determine the ellipsoid parameters to obtain the minimum slope safety factor. The

existing 3-D method applies Monte Carlo simulation to determine the parameters. Because running the 3-D limit equilibrium analysis with Monte Carlo simulation to achieve an acceptable minimum safety factor is extremely time-consuming, the existing method is unadaptable in hazard mapping. Therefore, a new method for determining the parameters of an ellipsoid is proposed based on the 2-D limit equilibrium analysis with the Swedish method. The circular slip determined in 2-D analysis is used to estimate the lengths of two axes of a tri-axial ellipsoid; the other axial length is estimated directly from the slope shape. The GIS module of the 3-D limit equilibrium analysis is developed using the new approach of determining ellipsoid parameters. Practical applications show that the new hazard mapping method based on the new approach for 3-D limit equilibrium analysis can greatly reduce the processing time.

Chapter 6 develops a prediction system of earthquake induced Landslide dams for Landslide dam hazard mapping based on GIS. To date, there have been few studies on Landslide dam hazard mapping, although it is important for breaking the disaster chain. The new approach of Landslide dam hazard mapping includes: (1) identifying the slope units; (2) extracting possible Landslide dam prone slopes (LDPS) using the river buffer filter; (3) excluding impossible LDPS using the aspect filter to exclude slopes that cannot reach a river based on their aspects towards the river; (4) excluding impossible LDPS using the blockage filter, by which a slope that could not reach the river is excluded based on the blockage height along its way to the river; (5) excluding impossible LDPS using the stability filter to exclude stable slopes based on slope stability analysis; (6) excluding impossible LDPS using the volume filter to exclude slopes with a small volume of slide mass. In addition, DDA, a numerical simulation method, is adopted to verify the potential LDPS after filtering. Because we can obtain the run out distance, distribution and volume of debris from the DDA simulation, Landslide dam formation can be deduced based on river geometry and hydrology data together with the volume of the slide body. The effectiveness of the countermeasure using preventive structures can also be verified by DDA simulation.

Chapter 7 summarizes the results and conclusions of the study. Also, problems are highlighted for future studies.